Task 7 - Landslide Scenario Assessment

Regionally consistent risk assessment for earthquakes and floods and selective landslide scenario analysis for strengthening financial resilience and accelerating risk reduction in Central Asia (SFRARR Central Asia disaster risk assessment)

FINAL VERSION

2 September 2022

RED – Risk Engineering + Development – Pavia, Italy

Revision History

Version	Date	State	Initials	Changes
r1d1	18/10/2021	Draft	UNESCO Chair	
r1d2	19/10/2021	Draft	OGS: SP	Document revision
r1d3	22/10/2021	Draft	RED: PB	Document revision
r1	9/11/2021	Approved	UNESCO Chair	Changes based on reviewers' Comments
r2d1	17/11/2021	Draft	UNESCO Chair	Changes based on reviewers' Comments
r2	14/02/2022	Approved	UNESCO Chair, RED: PC, GC	Changes based on reviewers' Comments
r3d1	16/03/2022	Draft	UNESCO Chair	Changes based on reviewers' Comments
r3	11/04/2022	Approved	UNESCO Chair, RED: PC, GC	Changes based on reviewers' Comments
r3d2	02/05/2022	Draft	UNESCO Chair, WB	Changes based on reviewers' Comments
r4	11/05/2022	Approved	UNESCO Chair, RED: PC, GC	Changes based on reviewers' Comments
	10/06/2022	Approved	WB	
r5	02/09/2022	Approved	RED: GC, PC	Appendix A – List of Acronyms

Technical Assignment number 1266456

RED Risk Engineering + Development

Executive Summary

With the goal of improving financial resilience and risk-informed investment planning, the European Union, in collaboration with the World Bank and the GFDRR, has started a program for "*Strengthening Financial Resilience and Accelerating Risk Reduction in Central Asia*" (SFRARR), aiming to advance disaster and climate resilience in Central Asia (from here after CA) countries, which includes Kazakhstan, Kyrgyz Republic, Tajikistan, Turkmenistan and Uzbekistan. The program includes several operational components, all contributing to the development of a comprehensive probabilistic risk assessment, consistent across multiple hazards and asset types of the target countries. Central Asia is an area characterized by complex tectonic and active deformation. The related seismic activity controls the earthquake hazard level that, due to the occurrence of secondary and tertiary effects, has also direct implications on the hazard related to mass movements (e.g., landslides). These phenomena, which include mudslides and debris flows in Central Asia, are causing an extensive number of casualties every year. Climatically, this region is characterized by strong rainfall gradient contrasts, due to the diversity of climate and vegetation zones. The region is drained by large, partly snow- and glacier-fed mountain rivers, which cross or terminate in arid forelands; therefore, it is affected by a significant river flood hazard, mainly in spring and summer seasons. The challenge posed by the combination of different hazards can only be tackled considering a multi-hazard approach harmonized among the different countries, in agreement with the requirements of the Sendai Framework for Disaster Risk Reduction, approved at the third UN World Conference on Disaster Risk Reduction in 2015. As a part of the proposed multi-hazard approach, within this project the most detailed landslide inventories covering both national and transboundary territories in Central Asia were collected, thanks to the availability of new global data, the academic network of the Consortium, and the contribution and resources from the local partners (scientists and practitioners) involved in the initiative promoted by the World Bank (see Table 1 for the complete list of involved scientific institutions from each partner country). These landslide inventories were used together with the available data and the knowledge of the scientific literature of the region to perform a regional scale landslide scenario assessment based on integrated geo-statistical methodological approach. The proposed approach represents an innovation in terms of resolution (from 30 to 70 m), extension of the analyzed area and different analyzed landslide effects (e.g., river damming potential) with respect to previous regional landslide susceptibility and hazard zonation models applied in Central Asia (e.g., Nadim et al., 2006; Havenith et al., 2015b; Stanley and Kirshbaum, 2017; Pittore et al., 2018). In detail, the adopted methodology is based on the following aspects:

- A reliable landslide susceptibility model was generated by means of the "Random Forest" machine learning algorithm, which is credited as one of the most advanced techniques in this field (Catani et al., 2013)
- For each studied country the landslide susceptibility distribution in the area covered by elements at risk, such as roads, railways, and buildings, was assessed using the data provided by the Consortium
- The river damming potential was also analyzed with a new tool developed in a GIS environment (Tacconi Stefanelli et al., 2020)

- Landslide scenarios were assessed in selected case studies representing of the major landslide problems and secondary/tertiary effects in Central Asia using open-source software, tools, and platforms.

Table 1. List of partner countries of the consortium and associated scientific institutions involved in the development of Landslide Scenario Assessment for CA.

Country	Scientific Institution	Local representative and support team
Kazakhstan	IS - Institute of Seismology under MoES of RoK	Dr. Natalya Silacheva Dr. Zhanar Raimbekova Dr. Murat Kasenov
Kyrgyz Republic	ISNASKR - Institute of Seismology of Kyrgyz Republic	Prof. Kanatbek Abdrakhmatov Dr. Anna Berezina Dr. Ruslan Umaraliev
Tajikistan	IWPHE - Institute of Water Problems, Hydropower Engineering and Ecology	Prof. Zainalobudin Kobuliev Dr. Mirzo Saidov Dr. Jovid Aminov
Turkmenistan	Various individual consultants	Dr. Japar Karaev Dr. Vladimir Belikov
Uzbekistan	ISASUz - Institute of Seismology Uzbekistan TSTU - Tashkent State Transport University	Prof. Vakhitkhan Ismailov Prof. Rustam Niyazov Dr. Ibragim Uralov Dr. Gany Bimurzaev Dr. Fazliddin Anorboev Dr. Zukhritdin Ergashev Dr. Kuvandyk Lesov

Index

Index of Figures

Index of Tables

1 Introduction

Geographically, Central Asia is a vast and diverse region including high mountain chains, deserts, and steppes. A large portion of the Central Asia countries, especially the southern and eastern borders, are occupied by the mountainous areas of Tien Shan, Trans-Alay Range, Pamir and Altaj, with peaks above 7000 m a.s.l (Strom, 2010) (Figure 1). These intraplate mountain systems formed in the Cenozoic between the Tarim Basin and the Kazakh Shield, as a result of the India-Asian collision (Molnar and Tapponier 1975, Abdrakhmatov et al., 1996, Havenith et al., 2006, Zubovich et al., 2010, Ullah et al., 2015) (Figure 2).

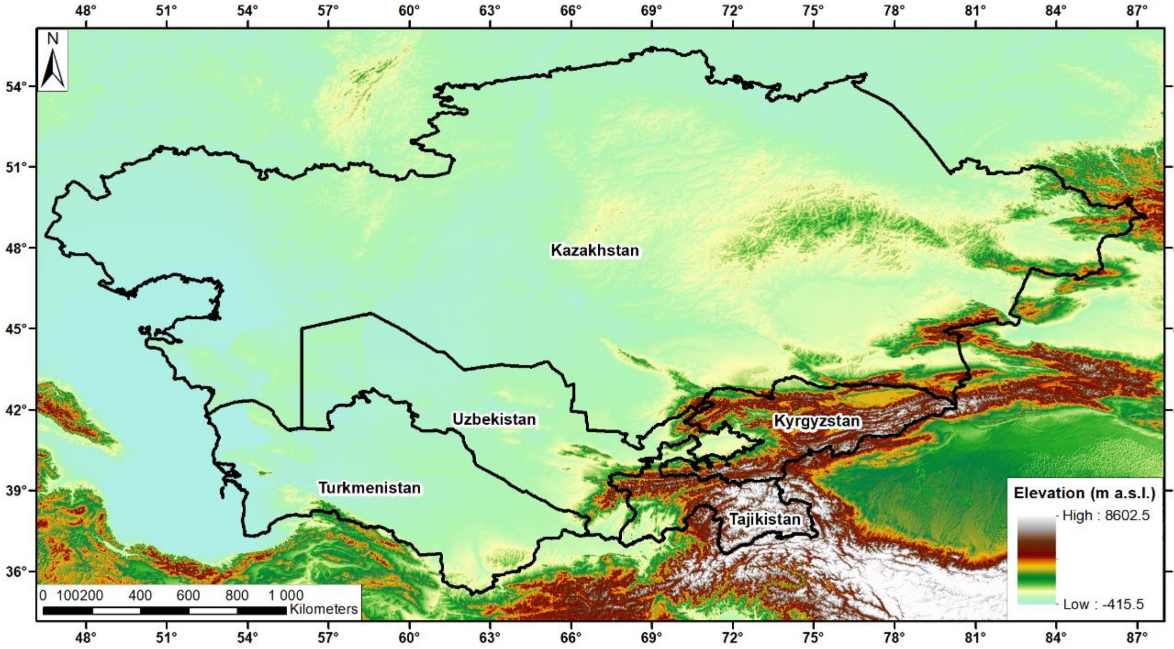

Figure 1. Central Asia elevation map obtained from the MERIT DEM.

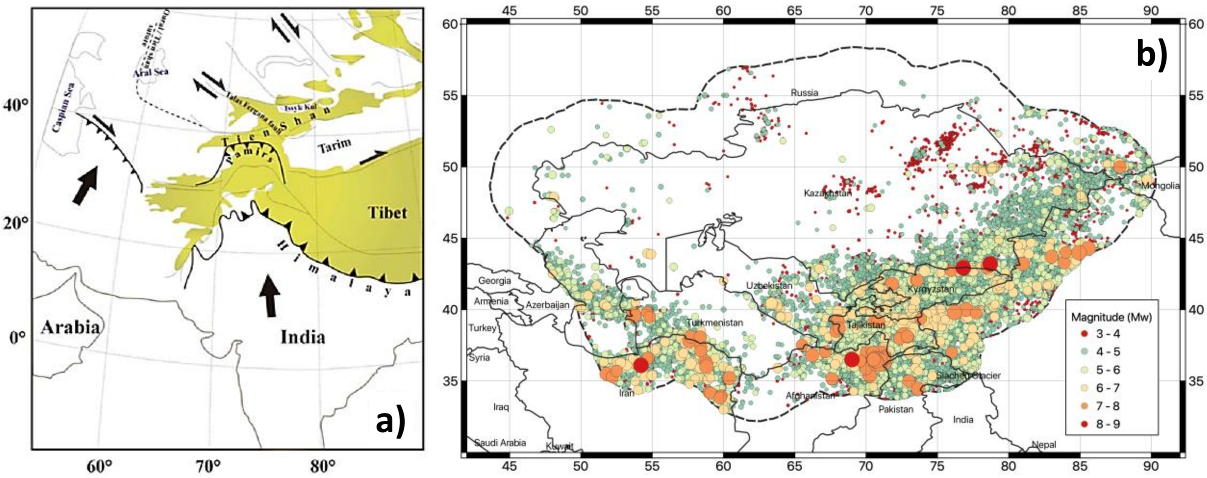

Figure 2. Geological setting of the study area: a) Tectonic map representing the collision between the Eurasian and Indian plates; the regions located at altitudes < 2000 m are coloured in green (after Havenith et al., 2002); b) Geographical distribution of earthquake hypocenters (Mw>3) of the newly developed Mw harmonized catalogue for Central Asia (HECCA) (after Task 2 - Earthquake Hazard Assessment).

Active mountain building started in the Oligocene (Sadybakasov 1972; Chedia 1986) or even later (Abdrakhmatov et al. 1996), forming a complex system of basement folds disrupted by numerous thrusts and reverse faults with significant amount of lateral offset (Delvaux et al. 2001; Bazhenov and Mikolaichuk 2004). Large earthquake events are generated by these structures, often with magnitude larger than 7 (Strom, 2010). Several regional fault zones are aligned along large parts of the mountain belts, others cross the orogen in a NW-SE direction, e.g., the Talaso-Fergana fault, which forms a distinct boundary between the western and central Tien Shan (Trifonov et al. 1992) (Figure 2). Mountain ridges, formed mainly by paleozoic crystalline rocks, are separated by wide lenticular or narrow, linear intermountain depressions, containing Neogene and Quaternary deposits, mainly sandstone, siltstone with gypsum interbeds, and conglomerates (Strom et al., 2010). Mesozoic and Paleogene deposits are typical of the foothill areas. Almost every ridge corresponds to a neotectonic anticline, and most of the main river valleys follow intermontane tectonic depressions, which are linked by narrow deep gorges up to 1 - 2 km deep (Strom et al., 2010). These mountain systems are the sources of most of Central Asia rivers, which, being fed by glaciers, snowmelt water and rain, have deeply incised valleys. Such extreme topography along with complex geological structure, active tectonics and high seismicity determine important landslide predisposing factors, making landslides the third most prevalent natural hazard in Central Asia, following earthquakes and floods (CAC DRMI, 2009) (Figure 3).

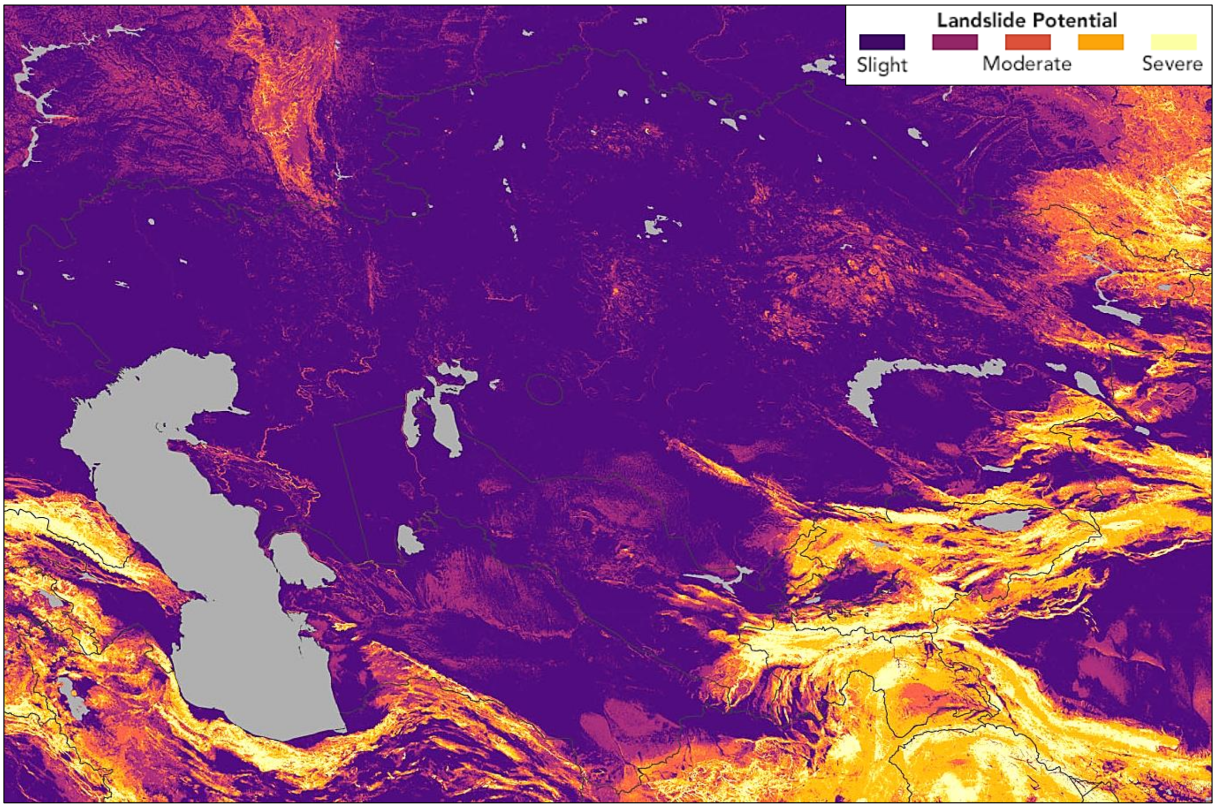

Figure 3. Landslide Hazard Map of Central Asia and the Caucasus (details from Stanley and Kirschbaum, 2017; Emberson et al., 2020).

During the two decades spanning between 1988 and 2007, according to observed estimates, out of 177 reported disasters 13% were landslides, causing 700 deaths (Table 2), while in the same period economic losses have been as high as $150 million, including damage to infrastructures, settlings and agricultural/pasture lands, as well as displacement of the population (GFDRR, 2009).

Table 2. Observed landslide hazard statistics (1988-2007). Source: Risk assessment for Central Asia and Caucasus (UN ISDR, 2009).

Country	No. disasters/year	Total no. of deaths	Deaths/year	Relative vulnerability (deaths/year/million)
Kazakhstan	0.05	48	2.40	0.16
Kyrgyz Republic	0.30	238	11.90	2.27
Tajikistan	0.50	339	16.95	2.51
Turkmenistan	n.a.	n.a.	n.a.	n.a.
Uzbekistan	0.15	75	3.75	0.14

More recent modelled estimates show that in the Central Asia countries an annual average of 3 million persons are affected by earthquakes and floods, with an estimated annual average GDP of 9 billion USD (GFDRR, 2016).

Due to their large size and impact, most of the occurring landslides have profound transboundary implications. Tajikistan and Kyrgyz Republic are the countries most impacted by landslides: in Tajikistan around 50,000 landslide were mapped, 1,200 of which threaten settlements or facilities (Thurman, 2011), while Kyrgyz Republic has been affected by 5,000 landslides, of which 3,500, at various levels of activity, are located in the southern portion of the country (the Fergana Valley) (Pusch, 2004). Only in Kyrgyz Republic, up to 2017, 784 landslides and 1658 among mudflows and flash floods caused 352 victims (Table 3) (Kalmantieva et al., 2009; Havenith et al., 2015a; 2017). Almaty province in Kazakhstan, Tashkent, Samarkand, Surkhandarya, Kashkadarya Provinces of Uzbekistan, and Ahal Province of Turkmenistan are also exposed to landslides (World Bank, 2006).

Table 3. The deadliest single landslides in Kyrgyz Republic, starting from 1990 (Kalmetieva et al., 2009; Ministry of Emergency Situations, Kyrgyz Republic; after Havenith et al., 2015a).

Name	Time (dd/mm/yyyy)	Volume, (m^3)	Victims	Latitude (N)	Longitude (E)	Elevation (m a.s.l.)
Mailuu-Suu, Left slope of Bedre-Sai	21/03/1994	100,000	8	41°15'9.05"	72°26'45.37"	1,009
Komosomol village, Uzgen area/Kyrgyz Republic	26/03/1994	500,000	28	40°43'28.85"	73°31'14.81"	1,319
Tosoy village, Uzgen area/Kyrgyz Republic	08/08/1994	1,000,000	50	40°57'1.73"	73°29'20.89"	1,593
Raikomol village, Aksy region/ Kyrgyz Republic	May 1995	40,000	4	41°36'16.84"	72°14'45.15"	1,060
Kara-Taryk village, Uzgen area/Kyrgyz Republic	20/04/2003	1,500,000	38	40°37'21.85"	72°17'41.35"	1,572
Mailuu-Suu, Right slope of Bedre-Sai	March 2004	50,000	2	41°15'20.38"	72°26'21.38"	1,018
Kainama village, Alay region/ Kyrgyz Republic	24/04/2004	2,000,000	33	40°16'20.77"	73°33'50.72"	1,872
Raikomol village, Aksy region/ Kyrgyz Republic	15/04/2009	200,000	16	41°35'52.67"	72°14'18.43"	1,033

2 Overview on regional landslide studies

Given the increased anthropogenic pressures and the impact of climate change, since the early '90s several projects have tried to improve the knowledge on landslide hazard (Thurman, 2011), by providing landslide losses estimations, location, type, triggering/reactivation dates, inventories and hazard/risk maps (Figure 4), as well as platforms to retrieve open disaster risk data and overviews on landslide risk reduction strategies.

Amongst the regional studies on landslide hazard, providing descriptions, statistics, and inventory maps (see Section 2.2), it is worth mentioning:

- Disaster Risk Management and Climate Change Adaptation in Europe and Central Asia, developed by the World Bank - Global Facility for Disaster Reduction and Recovery (Pollner et al., 2010).

- Disaster Risk Reduction, 20 Examples of Good Practice from Central Asia, developed by the European Union, International Strategy for Disaster Reduction ISDR (European Commission Humanitarian Aid, Civil Protection, 2006).

- Science for Peace Project (983289) 'Prevention of landslide dam disasters in the Tien Shan, LADATSHA'. 2009–2012, NATO Emerging Security Challenges Division[1].

- PROGRESS (Potsdam Research Cluster for Georisk Analysis, Environmental Change and Sustainability). German Federal Ministry of Research and Technology (BMBF)[2].

- Tian Shan-Pamir Monitoring Program (TIPTIMON). German Federal Ministry of Education and Research (BMBF)[3].

- M126 IPL Project funded by the International Consortium on Landslides: M2002111 Detailed study of the internal structure of large rockslide dams in the Tien Shan; M2004126 Compilation of landslide/rockslide inventory of the Tien Shan Mountain System.

[1] https://www.nato.int/cps/en/natohq/88111.htm

[2] https://www.gfz-potsdam.de/en/section/remote-sensing-and-geoinformatics/projects/closed-projects/progress/

[3] https://www.gfz-potsdam.de/en/section/lithosphere-dynamics/projects/past-projects/tiptimon/

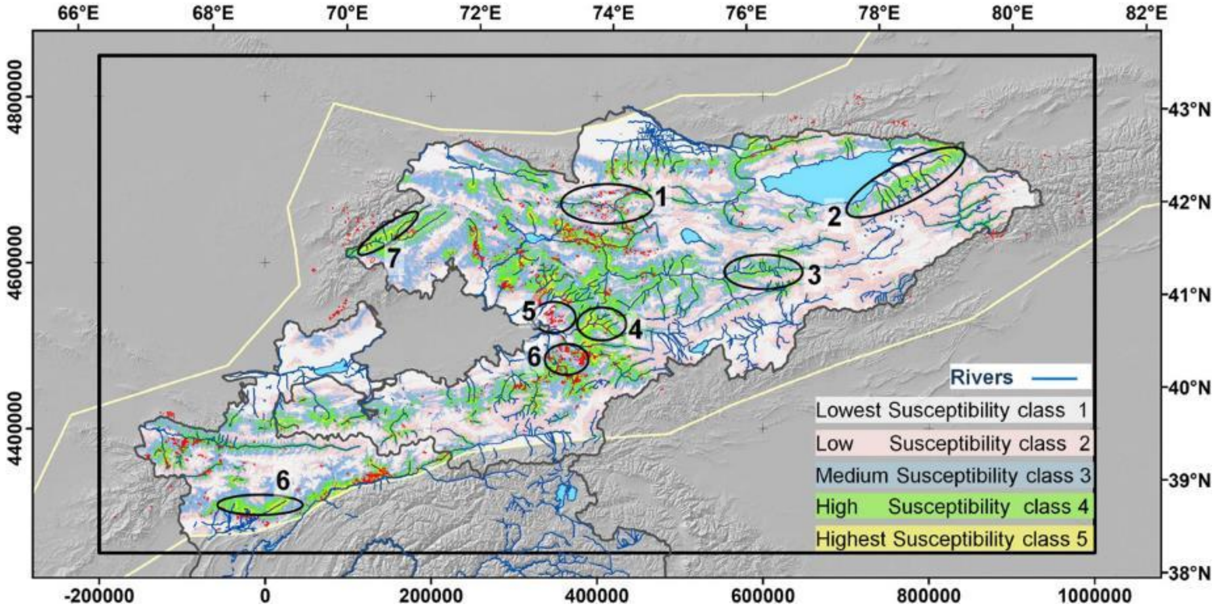

Figure 4. Kyrgyz Republic landslide susceptibility map (from Havenith et al., 2015b).

2.1 Landslide types

According to the international Cruden and Varnes 1996 classification, landslides phenomena in Central Asia include rockslides/avalanches, rotational/translational slides and mud/debris flows (often involving loess), which are triggered by natural events such as earthquakes, floods, rainfall and snowmelt (Behling et al., 2014; Golovko, 2015; Havenith et al., 2015a, 2015b, 2006; Kalmetieva et al., 2009; Saponaro et al., 2014; Strom and Abdrakhmatov, 2017). Glacial lakes outburst flood (GLOF) phenomena, caused by the breach of natural glacial dams, often result in large scale catastrophic mud/debris flows. In Central Asia, landslides often occur in the loess zone of contact with other rocks, on clay interlayers of the Mesozoic and Cenozoic age, reaching a volume from tens of thousands up to 15-40 $\times 10^6 m^3$ (Juliev et al., 2017). Seismically triggered landslides are very common in tectonically active mountain regions, such as Tien Shan and Pamir (Sternberg et al., 2006; Hong et al., 2007; Juliev et al., 2017).

According to the literature background, most large mapped mass movements (especially those with a volume of more than 10^6 m^3) were triggered generally by major (usually prehistoric) earthquakes, possibly in combination with climatic factors (namely snowmelt and heavy rainfall; Havenith et al., 2003; Strom and Korup, 2005; Strom, 2010; Schlögel et al., 2011; Strom and Abdrakhmatov 2017; Strom, 2010; Havenith et al., 2015a; 2020; Behling et al., 2014; 2016; Piroton et al., 2020) (Table 4). The 1989 M 5.5 earthquake in Tajikistan is an incredible example of liquefaction and mudflows triggered by a moderate earthquake (Havenith et al. 2003; 2015b, 2016). Furthermore, in the past few decades, the number and intensity of landslides have grown owing to climate change and the increase of the anthropic pressure, due to several factors such as the uncontrolled land and water use, the rising of the water tables (often induced by the increase of irrigation; Ishihara et al., 1990), deforestation, mining, and excavation activities (Pollner et al., 2010; Thurman, 2011).

Table 4. Major earthquake-triggered landslide database with information on major contributing factors reported after Havenith et al., 2016.

Country	Seism. Event	M	Hipo-central depth	Inten-sity	Fault	Topo. Energy	Clim. Factor	Lith. Factor	N°of observed landslides	Affected area (km²)	Bib. Ref.
Kyrgyz Republic	Kemin 1911	8	25.00	1.12	4	2	0.5	1	4495 (hundreds)	5408	Delvaux et al. 2001; Havenith et al. 2002
Tajikistan	Kait 1949	8	18.00	1.41	3	2	1	2	16906 (several giant landslides and flows)	16722	Evans et al 2009; Havenith and Bourdeau 2010
Tajikistan	Gissar 1989	6	5.00	0.04	0.75	1	2	4	261 (several large slides)	59	Ishihara et al. 1990
Kyrgyz Republic	Suusamyr 1992	7	27.00	0.64	2.25	2	0.2	1	578 (tens)	1646 (2000)	Ghose et al. 1997; Mellers et al 1997; Havenith et al. 2015a, b
Afghanistan Tajikistan Uzbekistan	Hindukush 2002 I	7	226.00	0.03	1.5	4	0.5	2	178 (activation of large distant landslides)	54843 (landslides at >500 km distance)	Yeats and Madden 2003; Niyazov and Nutaev 2010; Niyazov and Nutaev 2013; Niyazov and Nutaev 2014; Torgoev et al 2013

2.1.1 Large landslides and natural dams

Numerous rockslides have occurred in Pamirs and Tien Shan producing hazardous natural phenomena such as long runout rock avalanches and dammed lakes, more than 100 of which still store water (Strom, 2010) (Figure 5). These mainly involve the paleozoic magmatic and metamorphic crystalline bedrock, but also the sandstone and limestone formations. Although, according to Strom (2010), many of the existing dammed lakes should be considered as stable, catastrophic outburst floods that occurred in the 20th century emphasize high the potential hazard of landslide natural blockages. Havenith et al., 2015a report a large catalogue of large to giant landslides (having volumes exceeding $>10^7$ m^3) in the Tien Shan area, showing several information such as location, time of occurrence, volumes, and thickness. Regarding the volumes of these rockslides, these range from 50,000 m^3 to 10 km^3 (Strom and Korup, 2006; Strom, 2010). Many of these phenomena were triggered by earthquakes with M > 6 and have dammed a river valley (some of the dams have been naturally or artificially breached). The largest landslide forming a dam at present time within the area is likely to be the Sary-Chelek rockslide in the western Tien Shan, having an estimated volume of 5–6 km^3. This volume is only exceeded by the already breached rockslide dam of Beshkiol rockslide located in Central Kyrgyzstan (Strom, 2010). This area was hit by the M > 7 1992 Suusamyr earthquake, which triggered the Belaldy rock avalanche - this one formed a dam with an initial volume of 40 million m^3. Giant rockslides as those introduced above occur over highly variable time intervals (often more than several tens of years).

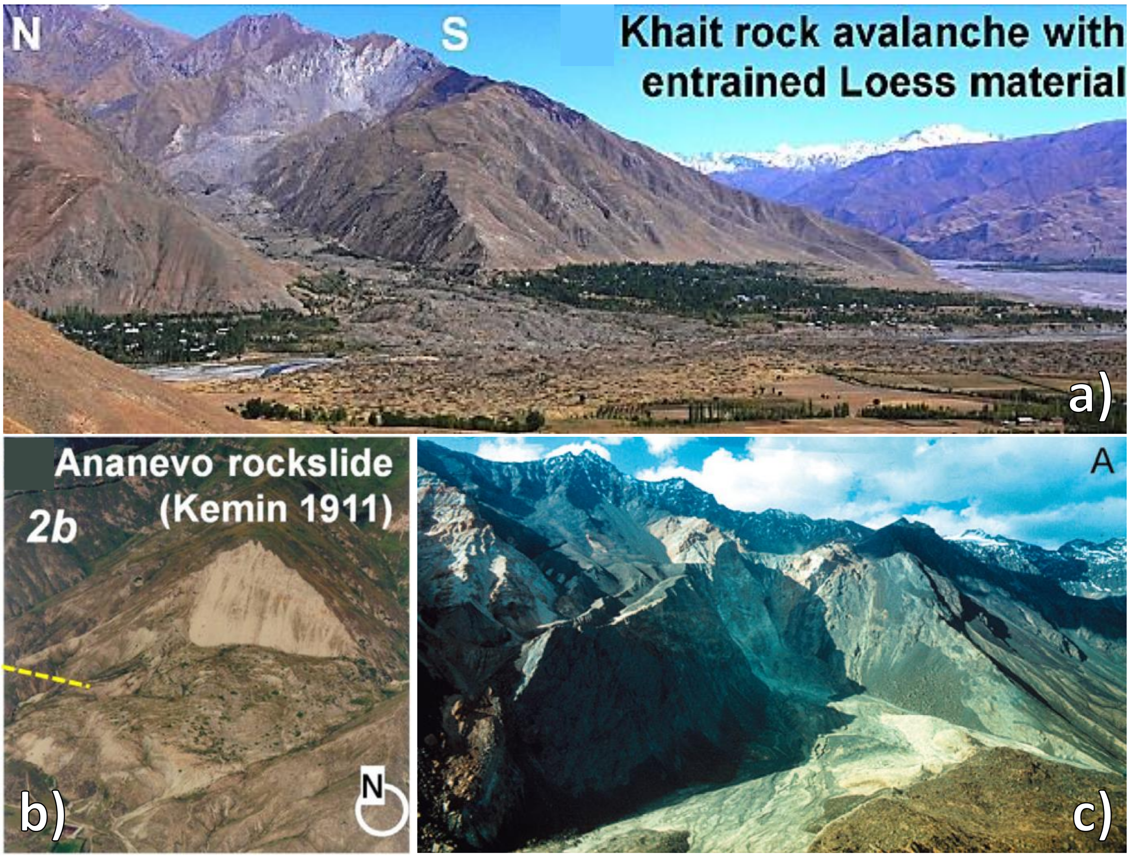

Figure 5. Examples of large rockslide features in Central Asia. Khait rock avalanche (a; after Havenith et al., 2015a); Helicopter view of Ananevo landslides (b; after Havenith et al., 2015a); Helicopter view of the Usoi landslide scarp, triggered by the 1911 earthquake, Tajikistan (Strom, 2010).

2.1.2 Landslide in soft rocks and loose deposits

Much more frequent landslides in the form of rotational slides mostly occur at elevations of between 700 and 2,000 meters in loose unconsolidated Quaternary deposits, and in soft and semi-hard rock layers in Mesozoic-Cenozoic sediments (represented mainly by layers of clays, argillites, siltstones, sandstones, marls, limestone, gypsum and conglomerates, with intercalated clays (Roessner et al., 2004; Kalmetieva et al., 2009) (Figure 6). These phenomena rarely create permanent dams, since usually they are smaller and their bodies are eroded much faster even if the block a river channel (Strom and Korup, 2006). The loess landslides occur quite regularly (on a yearly basis) in the regions presenting an almost continuous and locally very thick (>20 m) cover of this material, generally at mid-mountain altitude (900 - 2,300 m) and mainly along the border of the Fergana Basin (Kyrgyz Republic, Uzbekistan and Tajikistan), and on the southern border of the Tien Shan in Tajikistan (Figure 6). Landslides occurring in Quaternary loess units of up to 50 meters thickness are characterized by very rapid avalanche-like mass movements, which can reach several meters per second (often represent a combination of rotational slide and dry flow resulting in long runout zones; World Bank, 2008).

Table 5. Landslide inventory showing landslide surface area, thickness, and volume (Havenith et al., 2015a).

Landslide	Coordinates	Area (10^3 m^2)	Calculated maximum Thickness (m)	Previous estimated volume (million m^3)	Biblio-graphic reference	Calculated volume (10^6 m^3)	Status
Suusamyr landslide, C.Tien Shan	42.207°N, 73.610°E	126.90	20.1	0.75	Havenit et al. (2003)	0.85	Accept.
Okuli loess flow, Gissar	38.480°N, 68.620°E	2027	45.3	20	Ishihara et al (1990)	30.60	Overest.
Kanima loess flow, Alay	40.275°N, 73.565°E	151.30	13.9	0.40	Danneels et al (2008)	0.7	Overest.
Koyatsh landslides, Maily Say	41.290°N, 72.480°E	277.80	30.6	3	Authors prev. estimate	2.83	Accept.
Tektonik landslides, Maly Say	41.285°N, 72.480°E	326	18.1	2	Authors prev. estimate	1.97	Accept.
Kochkor Ata loess flow, Maly Say	41.260°N, 72.555°E	968.50	20	10	Roessner et al. (2005)	6.46	Underest.
Isolith landslides, Maly Say	41.280°N, 72.470°E	112.90	20.6	0.60	Authors prev. estimate	0.78	Accept.
Yasman loess flow	39.175°N, 70.750°E	33143.10	21.3	245	Evans et al (2009)	235.22	Accept.
Bielogorka Rock avalanche 1. N Tien Shan	42.635°N, 74.280°E	1075.60	48.4	20	Havenit et al. (2003)	17.35	Accept.
Bielogorka Rock avalanche 2. N Tien Shan	42.640°N, 74.290°E	863.80	38.9	10	Havenit et al. (2003)	11.19	Accept.
Ananevo rockslide, NE Tien Shan	42.805°N, 77.630°E	720.80	76.5	15	Havenit et al. (2003)	18.38	Accept.
Kemin rockslide, NE Tien Shan	42.720°N, 76.205°E	750.10	68.8	15	Authors prev. estimate	17.21	Accept.
Kara Suu rock avalanche, C. Tien Shan	41.570°N, 73.220°E	3735.50	106	280	Strom (2010)	132	Underest.
Karakol rockslide	41.650°N, 72.660°E	2786.70	126.5	300	Strom (2010)	110	Underest.
Belady rock avalanche (Partial dam)	42.060°N, 73.280°E	906.10	62.5	40	Korjenkov et al (2004)	18.87	Underest.
Sary-Chelek rockslide, West. Tien Shan	41.850°N, 72.000°E	43567.10	531	6000	Strom (2010)	7711.28	Accept.
Beshkiol rockslide, central Tien Shan	41.400°N, 74.480°E	56059.40	588.6	10000	Strom (2010)	10998.66	Accept.
Khait rock avalanche, S Tien Shan	39.185°N, 70.880°E	5747.60	41.5	75	Evans et al (2009)	79.57	Accept.
Iskander Kul rockslide, SW Tien Shan	39.080°N, 68.420°E	17063.80	196.5	1000	Strom (2010)	1117.95	Accept.
Aini rockslide dam (remaining part)	39.380°N, 68.540°E	592.40	36.5	20	Strom (2010)	7.21	Underest.

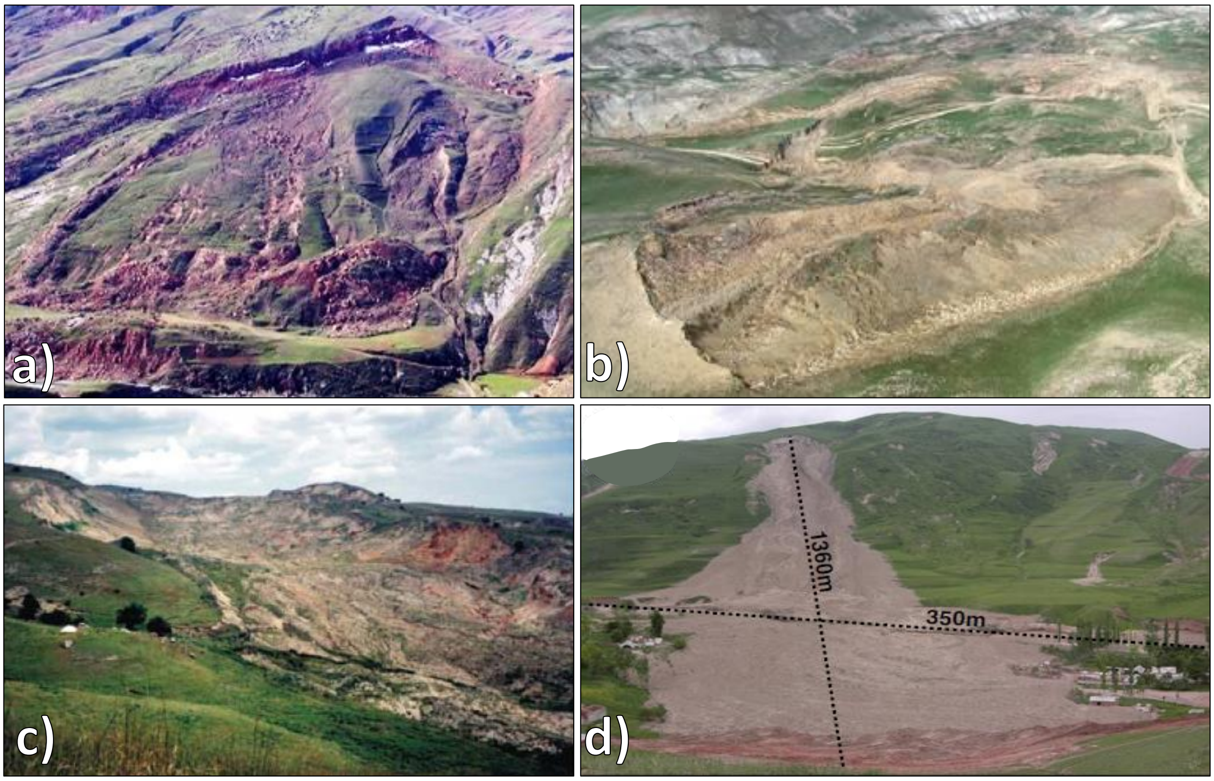

Figure 6. Examples of landslides in Uzbekistan (after Niyazov and Nurtaev, 2013) a) picture the Kamar landslide; b) picture of the liquefaction landslide of Beshbulak; Examples of loess slides and mixed loess—soft landslides in NE Fergana valley c) Kotshkor-Ata landslide failure in spring 1994 (after Roessner et al., 2005); Field photo of the Kainama landslide (after Behling et al., 2016).

Typically, pure loess landslides have a volume of hundreds up to one million cubic meters and appear as clusters (Roessner et al., 2005). From the recent history it appears that pure (or quasi pure) loess slides and flows are particularly dangerous because of their high mobility (and velocity) and long runout which in terms can generate a great destructive power and more severe disasters than other types of mass movements (Havenith et al., 2015a; Behling et al., 2014; 2016) (Table 5). The activity of these landslides can suddenly occur after longer periods of "creep" destabilization, which is indicated by cracks developing sub-parallel to hillslope crests (Roessner et al., 2005). Another form of rotational landslide occurs in Mesozoic and Cenozoic sediments (Jura up to Paleogene). If failure also affects underlying materials (mostly Mesozoic and Cenozoic soft rocks), the volume of these mixed slides can exceed 10×10^6 m^3. These kinds of landslides are particularly deadly and can be triggered by a combination of long-term slope destabilization factors (e.g., rainfall and snowmelt) and short-term triggers (e.g., seismic shocks; Danneels et al., 2008). Even though earthquake-triggered loess slides and flows are far less frequent than rainfall triggered ones, they caused much larger disasters in recent history, such as those triggered, respectively, by the July 1949 Khait and the January 1989 Gissar earthquakes (Table 4). The total number of landslides with volume more than 10^3 m^3 that were formed or reactivated in Uzbekistan during a 60-years long period is about 3,300 – 3,500. 340 – 350 sites have been affected by large landslides exceeding 10^5 m^3 in volume and 120 – 130 events exceeded 1 million m^3 (Niyazov et al., 2020). The largest historical event in Uzbekistan is the Atcha rockslide about 800 million m^3 in volume (Ниязов Р.А. 2009). The flow slides in loess are the most hazardous and unpredictable and pose especial threat.

Such self-excited flow slides are triggered by a combination of rainfall event and low-frequency (0.5 – 3.5 Hz) prolonged (90 – 140 s.) vibrations produced by P-waves of very distant (400 – 700 km) deep (180 – 270 km) Hindukush earthquakes, which cause simultaneous liquefaction of subsurface saturated sediments and tension in the surficial layers (Niyazov, 2020; Niyazov and Nurtaev, 2013). Loess flow landslides and debris flow involving the eluvial slope cover represent a relevant hazardous phenomenon in the mountainous regions of Kazakhstan, in the area of Almaty at the southern border with Kyrgyz Republic and in the Altaj area (Medeu and Blagovechshenskiy, 2016). The number of active debris flow basins in Kazakhstan is over 300 with registered cases of more than 600 debris flows of different genesis (80% of which are represented by heavy rainfall-triggered debris flows, while the glacial debris flows make up about 15% of the total) (Yaning, C., 1992).

2.2 Landslide databases

To implement the adopted susceptibility models the largest, most accurate, and updated landslide inventories were adopted (Figure 7). These were compiled by means of decades of field surveys, remote sensing and geophysical analysis covering the study area in the Tien Shan area, parts of the Pamir Alai system and Altaj mountainous areas in eastern Uzbekistan and southern Kazakhstan. Hereafter we report their description in detail:

- The "Rockslides and Rock Avalanches of Central Asia" (Strom and Abdrakhmatov, 2018): a large inventory including 860 polygons of large-scale (>=1 Mm^3) rockslides and rock avalanches, covering central Asian countries (except for Turkmenistan) plus Chinese Tien Shan, Pamir and Afghan Badakhshan. Compiled in decades of field work and analysis of aerial/satellite imaging, it also comprises information on landslide morphometric parameters (perimeter, area), and 126 polygons on possible landslide bodies, dammed lakes, scarps, scars, headscarps.
- The "Tien Shan landslide inventory" (Havenith et al., 2015a): represents the largest inventory in the study area. Compiled by means of field surveys, remote sensing data interpretation and geophysical surveys, it comprises the rockslides of the previous inventory together with other smaller landslides in soft sediments (Havenith et al. 2006a; Schlögel et al., 2011) for a total of 3,462 landslides polygons, also including information on landslide length and area.
- The "Multi-temporal landslide inventory for a study area in Southern Kyrgyz Republic derived from RapidEye satellite time series data (2009 – 2013)"[4] (Behling et al., 2014; 2016; 2020), is a semi-automated spatiotemporal landslide inventory for the period from 1986 to 2013, covering a 2,500 km^2 in the Fergana valley rim in southern Kyrgyz Republic. This inventory includes 1,582 landslide polygons mapped from multi-sensor optical satellite time series data, together with information on spatiotemporal landslide activity patterns (area and year of trigger).
- "The EMCA landslide catalog Central Asia"[5] (Pittore et al., 2018), including 3,130 points, which covers mostly western and northern Kyrgyz Republic as well as Tajikistan's Region

[4] https://dataservices.gfz-potsdam.de/panmetaworks/showshort.php?id=escidoc:5085889

[5] https://dataservices.gfz-potsdam.de/panmetaworks/showshort.php?id=escidoc:3657915

of Republican Subordination. The catalog is a summary (point locations) of the documented landslides between 1954 and 2009 (Kalmantieva et al., 2009), which are collected by the Central Asian Institute for Applied Geosciences (CAIAG) through geological surveys (field campaigns) on single sites close to urban areas in order to mitigate landslide risk.

- The "Tajikistan landslide database" provided by the Tajik project partners from Institute of Water problems, Hydropower, Engineering and Ecology (IWPHE), which includes 2,710 landslide polygons and 114 landslide-prone areas (with information on length and area).
- The landslide inventory provided by the Uzbek project partners from the Institute of Seismology of the Academy of Science of Uzbekistan (ISASUZ), which covers the Tashkent province, the Akhangaran valley and the Gushay province. It comprises a point inventory (including location, type, volume, length, and date of triggering; Nyazov R.A. 2020) and a polygon inventory digitized for this project from the maps in Juliev et al., 2017 (including a total 345 landslide polygons).
- The landslide inventory, provided by the Kazakh partners of the Institute of Seismology of the Science Committee of the Republic of Kazakhstan (IS), covering mainly the Tien Shan area at the border with Kyrgyz Republic, and small part of the western Altaj, including 254 point-objects with information on type, area/volume, triggering date.
- Part of the "Global Landslide Catalog (GLC)" [6] (Kirshbaum et al., 2015), which covers Kyrgyz republic and Tajikistan, including 15 landslide point with a description on landslide size/type and triggering date/factor. The GLC was compiled since 2007 at NASA Goddard Space Flight Center Nasa and considers all types of mass movements triggered by rainfall, which have been reported in the media, disaster databases, scientific reports, or other sources.

[6] https://data.nasa.gov/Earth-Science/Global-Landslide-Catalog/h9d8-neg4

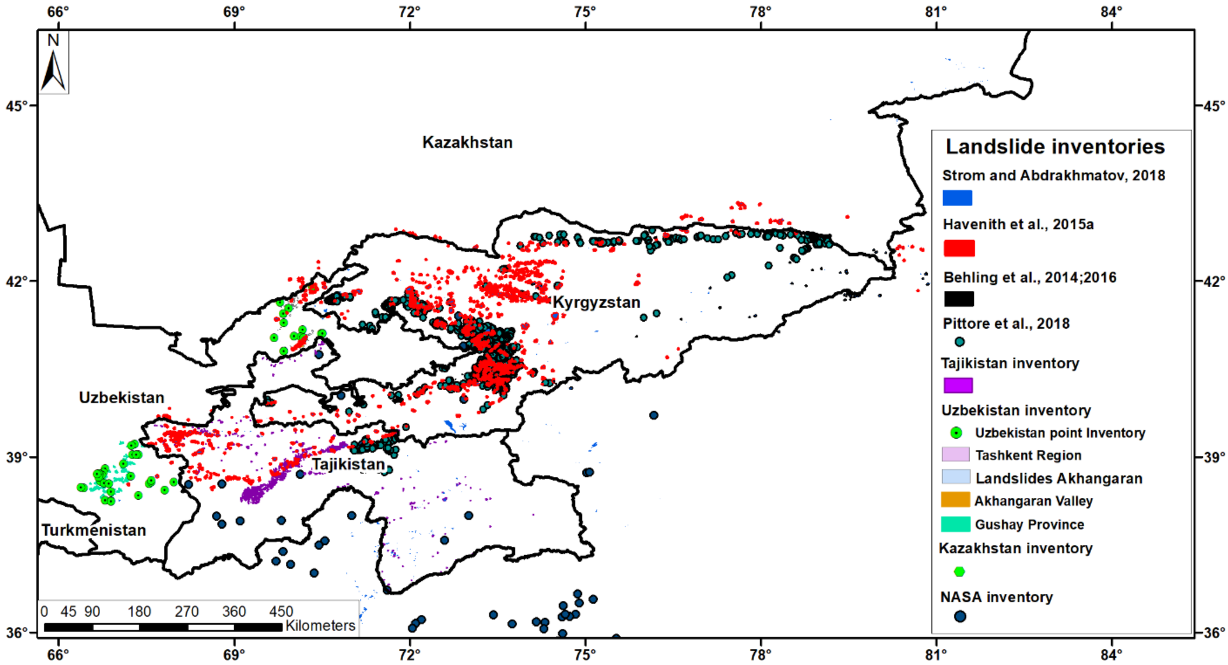

Figure 7. The adopted landslide inventories.

3 Susceptibility assessment

Landslide susceptibility maps (LSMs) depict the relative probability of occurrence of a given type of landslide in a given area, without considering the probability of occurrence in time (Brabb, 1984). In other words, LSMs identify those areas where landslides can occur, based on their geological, morphological, and climatic characteristics. These maps have been extensively adopted as useful tools for land planning (Cascini 2008; Frattini et al., 2010) and hazard assessment (Corominas et al., 2003). More recently, they have been successfully integrated also in quantitative risk assessment (Chen et al., 2016), and early warning systems (Segoni et al., 2018: Tiranti et al., 2019). In the framework of the activities of this Task, LSMs were produced by applying a wide range of mathematical techniques, from the most traditional statistic approaches like frequency ratio (Yilmaz, 2009), discriminant analysis (Carrara, 1983; Trigila et al., 2013) and logistic regression (Lee, 2005; Duman et al., 2006; Manzo et al., 2013), to more recent and more advanced techniques, such as artificial neural network (Tien Bui et al., 2016; Ermini et al., 2005), machine learning (Catani et al., 2013; Xiao et al., 2020) and multi criteria decision analysis (Akgun, 2012).

3.1 Random Forest (RF) model

To generate the landslide susceptibility maps in this work, the Random Forest model was used. The Random Forest model (RF) is a nonparametric and multivariate machine learning technique, which was proposed by Breiman (2001), and first used in landslide susceptibility analysis by Brenning (2005). Since then, it has rapidly gained widespread consolidation through many research and case studies, as it is considered a relatively powerful approach in classification, regression, and unsupervised learning (Lagomarsino et al., 2017). This model has been already developed and tested by the Consortium in a variety of methodologies at different scales and in different geological-geomorphological and geographic settings (Catani et al., 2005, 2013; Trigila et al., 2013; Di Traglia et al., 2018; Segoni et al., 2018; Casagli and Catani, 2020). Among the advantages of using the RF algorithm, there is the possibility of using numerical and categorical variables at the same time, without assumption on the statistical distribution of their values. Furthermore, RF is acknowledged to be capable of handling implicitly the multicollinearity of variables, identifying the uninfluential (or the detrimental) ones (Breiman, 2001; Brenning, 2005). RF also automatically performs a validation by building a Receiver Operating Characteristic Curve (ROC Curve) and calculates the relative Area Under the Curve (AUC). AUC is widely used as a quantitative indicator for the predictive effectiveness of susceptibility models: it can range from 0.5 (completely random predictions) to 1.0. This model, by means of the bootstrapping technique, also calculates the Out-of-Bag Error (OOBE) for each variable. This parameter measures the relative error that would be committed if a given variable is excluded from the RF classifier. OOBE can be used to assess the relative importance of each independent variable, thus representing a powerful tool to interpret the results and to rank the variables according to their importance (Catani et al., 2013). RF contains a series of binary tree predictors, which are generated by using a random selection of the input data (the independent variables which in LSM studies, are a set of physical parameters considered the predisposing factors), in order to split each binary node (yes/no), and to perform a classification of the target dependent variable (in LSM studies, the presence or absence of landslides). Some of the observations are used for internal testing to evaluate the predictive capability of each predictor tree.

This information is used to iterate the procedure hundreds of times by growing other random trees (hence the name "Random Forest"), and to iteratively adjust the prediction effectiveness. Once the best predictor tree is identified, it is applied to the whole study area, to define the LSM. Another important key point of RF is that it has a great predictive performance, and runs fast by summarizing a large number of classification trees (this is particularly useful especially when dealing with large amounts of data).

3.2 Model optimization

The LSM was defined using the whole study area, instead of processing each country individually. This choice allowed to overcome the boundary effects associated with the use of independent countries, but also led to a huge amount of data to be processed.

In order to reduce the processing time and avoid computational problems due to the width of the study area, large flat areas were filtered and not considered in the modeling process, since landslides take place exclusively along slopes. For Turkmenistan no landslide database was made available, so it was decided to train and test the model only with the other 4 countries, to obtain the best predictor model for the available data. The trained model has then been applied to the whole study area, including Turkmenistan, to define the LSM. In addition, a buffer of 10 km was considered around the whole area, to avoid deformation due to boundary effects.

Regarding the dependent variables, the landslides inventory was created by merging the data retrieved from a variety of sources (see Section 2.2). As a result, this landslide data was quite heterogenous, hence an initial control and homogenization phase was necessary. In this framework the landslide data were checked to verify the presence of overlapping polygons or topological errors. Since some landslide inventories were composed solely by points, these were mapped only as a "landslide points", a 100 m buffer was created around them, in order to include them in the model.

3.2.1 Selection of independent variables

As independent variables, twenty "basic parameters" were selected in all 5 countries, based on the available data and according to the ones most widely adopted in literature (Catani et al., 2013; Reichenbach et al., 2018). Many of these are DEM-derived products (e.g., elevation, aspect, slope, slope curvature, flow accumulation, SPI, TWI, TPI – see the list of bullets point below). It must be considered that the resolution of the susceptibility maps depends on the resolution of the input data. Therefore, it was decided to use pixels corresponding to the MERIT DEM[7] resolution. In addition, the DEM itself was used as a reference map, so that the other parameters were processed to have a perfect overlapping. Therefore, the resulting landslide susceptibility maps will also be perfectly overlapping to it. The variables such as lithology and land use were rasterized with this resolution by choosing the most frequent value in a reference window. The twenty "basic parameters" used are listed below, including a brief description (between brackets the shorted name assigned to each parameter is reported):

[7] http://hydro.iis.u-tokyo.ac.jp/~yamadai/MERIT_DEM

- Digital Elevation Model (Elevation): elevation in which the pixel is located expressed in meters above sea level. Elevation varies from - 210 m to 7,775 m
- Aspect (Aspect): a categorical variable representing the orientation of the slope surface compared to the geographical north. It is derived from the processing of the DEM. Aspect values range from -1 (flat areas) to 360 (north-facing areas)
- Slope (Slope): the slope gradient obtained by calculating the first derivative of the DEM. Slope ranges from 0° to 80.6°
- Total Curvature (Curv_Tot): the slope curvature obtained by calculating the second derivative of the DEM. It indicates the shape of the slope, therefore if it is concave (<0), planar (=0), or convex (>0). For each pixel the second derivative of the DEM is calculated both in the direction of the maximum slope gradient, and in the normal direction to the maximum slope gradient, in a window of 3 by 3 pixels (then averaged). Total Curvature varies from -37.7 to 32.9 (it is a dimensionless parameter)
- Profile Curvature (Prof_Curve): the curvature in the direction of the maximum slope gradient. Profile Curvature ranges from -18.5 to 16.3 (it is a dimensionless parameter)
- Planar Curvature (Plan_Curv): the curvature in the direction normal to the maximum slope gradient. Planar Curvature ranges from -25.9 to 20.7 (it is a dimensionless parameter)
- Flow Accumulation (Flow_Acc): the size of the drainage area above each pixel (expressed in number of pixels). It is obtained by calculating the flow direction by processing the DEM. Flow Accumulation ranges from 0 to 7.5×10^6 pixels
- Topographic Wetness Index (TWI): it is an index commonly used to characterize the spatial distribution of soil moisture. It is defined as $ln(A/tanB)$, where A represents the Flow Accumulation and B the Slope. It ranges from 8.2 to 41.4 (it is a dimensionless parameter)
- Stream Power Index (SPI): it expresses the measurement of the erosive potential of water runoff. It is defined as $A \times tan(C)$, where A represents the Flow Accumulation and C the Slope. SPI ranges from 0 to 1.2×10^{11} (it is a dimensionless parameter)
- Topographic Position Index (TPI): it expresses the difference between the elevation of the cell under consideration and the average elevation within a 3 by 3 window around it. Positive TPI values represent locations that are higher with respect to the average of their surroundings, as defined by the neighborhood (e.g., ridges). Negative TPI values represent locations that are lower than their surroundings (e.g., valleys). TPI values near zero are either flat areas (where the slope is near zero), or areas of constant slope (where the slope of the point is significantly greater than zero). TPI ranges from -422.7 m to 417.6 m
- Lithology (Lithology): it is a raster map derived from the geological map of the former Soviet Union made by the USGS (Persits et al. 1997). It is a categorical variable
- Land Use (Land_Use): it is a land use\cover map from the DSMW database (Copernicus land use[8]). This is a categorical variable
- Distance from Faults (Faults_Dist): it is minimum distance, in meters, between each landslide and the nearest fault. The fault database is derived from the AFEAD (The Database of the Active Faults of Eurasia; Styron and Pagani, 2020[9]) and was provided by the OGS Consortium partners involved in Task 2 - Earthquake Hazard Assessment.

[8] https://land.copernicus.eu/

[9] https://github.com/GEMScienceTools/gem-global-active-faults

- Distance from Roads (Roads_Dist): it is minimum distance, in meters, between each landslide and the nearest road. The roads database is derived from the OSM (OpenStreetMap) [10] database.
- Distance from Rivers (Rivers_Dist): it is minimum distance, in meters, between each landslide and the nearest river. The river network database was provided by the RED Consortium partners involved in Task 3 - Flood Hazard Modeling.
- Distance from Hypocentres (Hypo_Dist): it is minimum distance, in meters, between each landslide and the nearest earthquake hypocentre with a magnitude greater than 6.5 (following the methodology adopted by Haventih et al., 2015a). The Hypocentre database was provided by the OGS Consortium partners involved in Task 2 - Earthquake Hazard Assessment.
- Peak Ground Acceleration (PGA): Seismic hazard map in term of peak ground acceleration. It is expressed in multiples of gravity acceleration (g). It was selected 4 kinds of PGA maps according to different return periods and different geological materials (soils and rocks) to which it refers:
  - PGA with a return period of 475 years and related on outcropping soil layers (PGA_soil _475y)
  - PGA with a return period of 1000 years and related on outcropping soil layers (PGA_soil _1000y)
  - PGA with a return period of 475 years and related on outcropping bedrock (PGA_rock _475y)
  - PGA with a return period of 1000 years and related on outcropping bedrock (PGA_rock _1000y)

  The peak ground acceleration maps were provided by the OGS Consortium partners involved in Task 2 - Earthquake Hazard Assessment.

- Random Raster (Random): it is a dimensionless raster with random values from 0 to 1, used to test the predictive capabilities of the model and to verify the absence of overfitting issues.

In addition to these twenty "basic parameters", in this study it was decided to use some innovative parameters, related to the propensity of the territory to be affected by precipitation. These parameters were obtained from the ERA5 database. These data, spanning from 1981 to 2020 and having an hourly resolution (which were summed to daily resolution for this work), provided a robust data set for the analyses. The innovative parameters are five, and are listed below:

- Mean Annual Precipitation (MAP): average annual precipitation. It ranges from 0 to 3578.7 mm/y (Figure 8)
- Sigma 1.5 – 120 days (rain_1.5s_120gg): cumulative rainfall value at 120 days at 1.5 standard deviations. It ranges from 70 mm to 1778.8 mm (Figure 9.A)
- Sigma 1.5 - 30 days (rain_1.5s_30g): cumulative rainfall value at 30 days at 1.5 standard deviations. It ranges from 0 mm to 563.1 mm (Figure 9.B)
- Sigma 3 - 1 days (rain_3s_1g): cumulative rainfall value at 1 day at 3 standard deviations. It ranges from 0 mm to 62.2 mm (Figure 9.C)
- Sigma 3 - 7 days (rain_3s_7gg): cumulative rainfall value at 7 days at 3 standard deviations. It ranges from 0 mm to 271.9 mm (Figure 9.D)

[10] https://planet.openstreetmap.org/

The sigma parameters represent the probability of having a given rainfall amount over a defined time interval. In this work, three intervals were selected (1, 7, 30 and 120 days) to consider both short and long rain events, which can lead to the triggering of surficial or deep-seated landslides, respectively. For 1 and 7 days the maps of the rainfall values corresponding to 3 standard deviations over the mean rainfall were selected, to verify if short and very intense rainfall could influence the slope stability in the study area. Regarding the 30-days and 120-days intervals, rainfall values corresponding to 1.5 standard deviation were calculated, in order to assess the influence of longer and less intense rainfalls over slope stability.

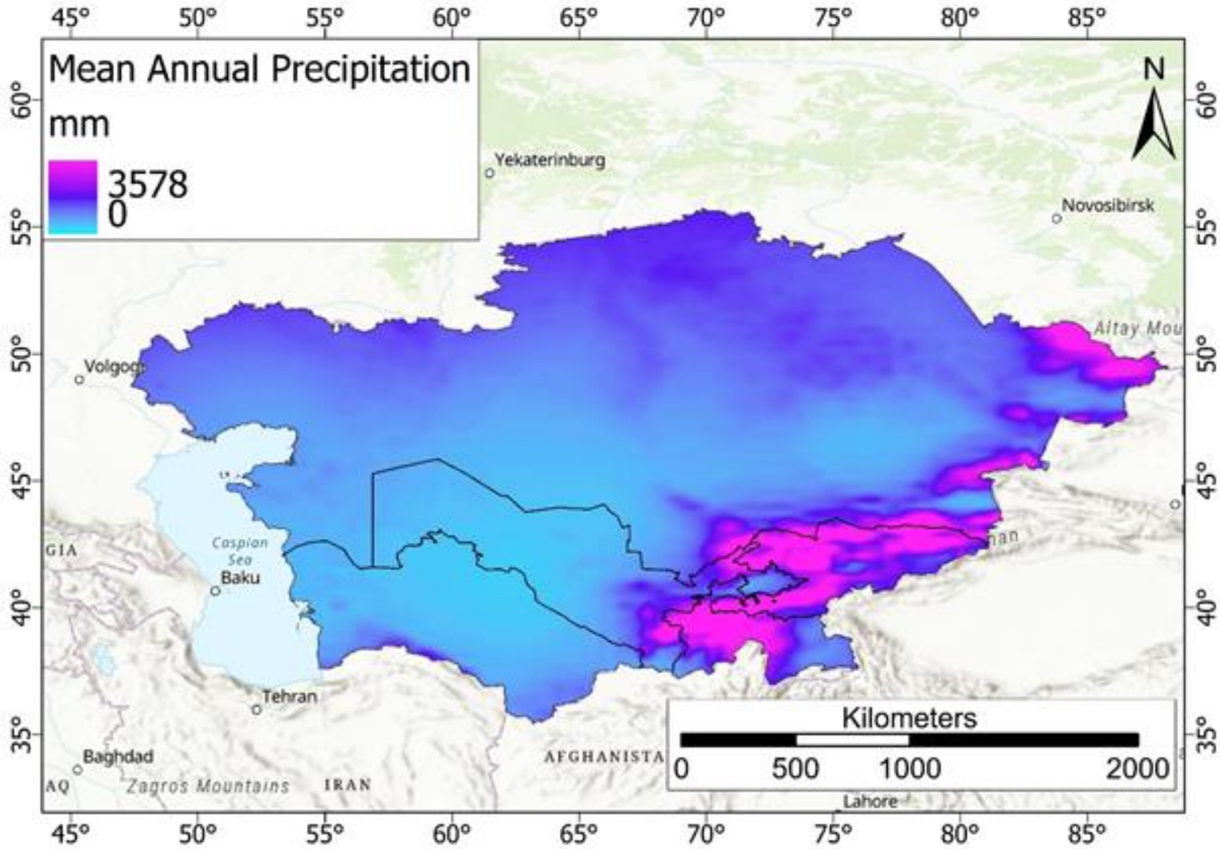

Figure 8. Mean Annual Precipitation map for the whole Central Asia.

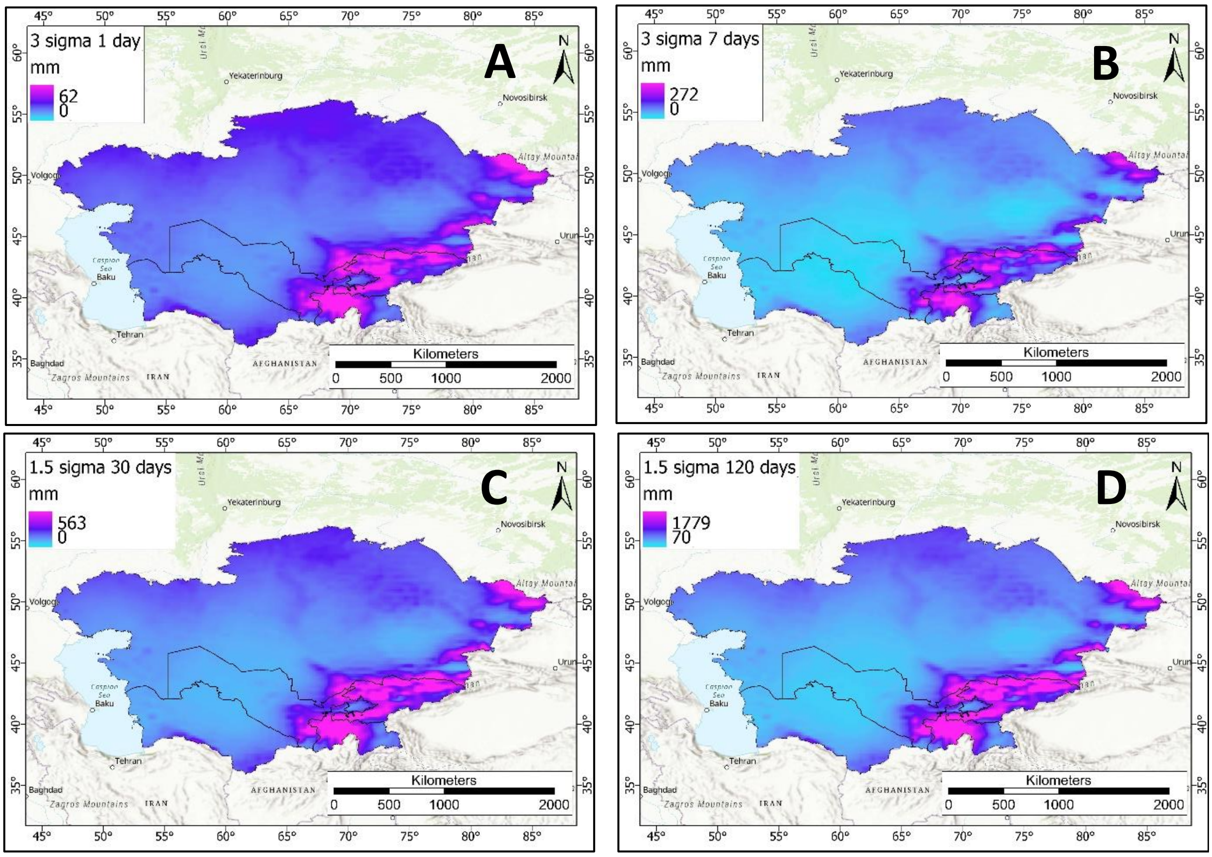

Figure 9. Rainfall maps. A: rainfall amounts corresponding to 3 standard deviations for 1-day rainfall; B: rainfall amounts corresponding to 3 standard deviations for 7-days rainfall; C: rainfall amounts corresponding to 1.5 standard deviations for 30-days rainfall; D: rainfall amounts corresponding to 1.5 standard deviations for 120-days rainfall.

3.3 Model training

Once all the data were prepared and organized, the algorithm to create the landslide susceptibility maps was developed. A crucial step in LSM analysis is the approach used to sample the variables to train and validate the model. As in any other statistical procedures, the size of the dataset influences the results, therefore the higher the number of samples to perform the statistical calibration/validation of the model, the more reliable are the obtained results. To avoid a generalized hazard overestimation, Catani et al. (2013) demonstrated that a random sampling improves the predictive capability of the map, and that the susceptibility model should also be trained/validated with respect to information about non-landslide locations. Regarding the proportion between the calibration and validation dataset samples, it is common practice to split them according to a 70/30 ratio. As a consequence, using ESRI *ArcGIS Pro* software, the variables were sampled pixel by pixel, after which, with the *Matlab* software, from the total of the sampled points, all the points within a landslide and a same amount of randomly chosen non-landslide points were extracted. This database was divided into two parts, 70% of the data (calibration dataset) was used for the training phase, and the remaining 30% (validation dataset) for the testing phase. Each one of these datasets was created to be equally composed by pixel within a known landslide and pixel outside a landslide. Particular attention was given to the landslides database containing point geometries. As highlighted above, a buffer of 100 m has been created around these "point-object landslides", to consider their whole body in the calculation.

However, when the points refer to large landslides, a common kind of landslides in the study area, it is possible that part of the body of these landslides is still outside the perimeter achieved with the buffer. To avoid classifying these areas as non-landslide points, it was decided to create an additional buffer of 1 km around points, used as a mask where non-landslide points were not be selected. This process reduced the probability of pixels misclassification (e.g., landslide points considered as non-landslide points) during the training of the model. All the points inside the 1-km buffer were then considered during the model application, as well as point from Turkmenistan.

All these data were then used to train and test the algorithm created to predict the landslide susceptibility of the whole area. The best predictor tree identified in the training phases was then applied to all the available data (also for Turkmenistan and for the 1-km buffer area around the point-object landslides) for the development of the susceptibility map on the whole Central Asia area. The results obtained from the application of the aforementioned methodology are the susceptibility map, the ROC (Receiver Operating Characteristic) curve with its AUC (Area Under the Curve) value, and the histogram of the importance of variables. ROC and AUC are used to verify the quality of the landslide susceptibility model, both by graphical and analytical approach (Figure 10).

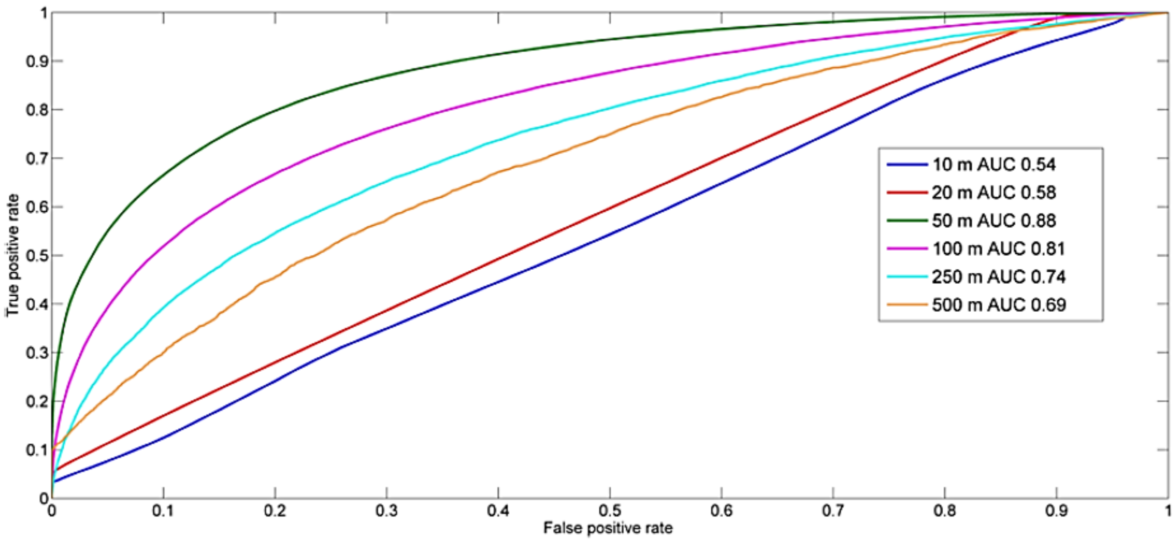

Figure 10. Example of ROC curves and AUC values. Higher AUC values indicate models with better performances (from Catani et al. 2013).

The quality of the susceptibility model has been also evaluated by the mean of a confusion matrix: a table where true classes of the pixels are compared with the predicted classes, to verify how many pixels are correctly (TN or TP) or wrongly (FP or FN) classified (Figure 11).

By this matrix four classes can be identified:

- True Negative (TN): pixels outside a landslide that are correctly classified
- True Positive (TP): pixels within a landslide that are correctly classified
- False Positive (FP): pixels outside a landslide that are identified as landslide pixel
- False Negative (FN): pixels within a landslide that are classified as outside a landslide.

		Predicted Classes	
		0	1
True classes	0	TN	FP
	1	FN	TP

Figure 11. Example of confusion matrix.

Since this matrix needs some ground-truth parameters (True classes), it can be applied only where is known the presence or absence of landslide is known. For this reason, in this work, this matrix was calculated considering only the test dataset. The algorithm that was created for this work, was set to be able to perform several activities:

- Reading and properly formatting the input data and the dividing them between independent and dependent variables
- Automatically and randomly selecting locations associated with landslides or outside the landslide
- Creating the training and test datasets
- Identifying the best predictor and evaluating its performances by the calculation of the error between the values calculated by the model, and the training dataset
- Evaluating the overall performances of the model by the mean of ROC and AUC
- Identifying the most importance parameters affecting landslide susceptibility
- Applying the model to the whole study area and extraction of the final map.

The algorithm was set to work in classification mode, e.g., for each pixel a value (1 or 0) is assigned to identify the presence or absence of a landslides (dependent variable), along with the values of the independent variables. Using these data, the RF model identifies the best association of independent variables linked to presence or absence of landslides (landslide susceptibility prediction model). The prediction model is then applied to all the pixels of the investigated area, and the probability of landslide occurrence is then evaluated. These probability values are those used to create the landslide susceptibility maps. It must be noticed that the landslide inventories adopted to train the RF rarely reported the type of landslide, so the LSMs must be considered not related to a specific type of landslide.

3.4 Results

In the map presented in the following Figure 12 and Figure 13, the susceptibility values, ranging from 0 to 1, were classified into five classes (Table 6), according to the Natural Breaks Method of Jenks, widely adopted in literature. "Natural Breaks" is a data clustering method designed to determine the best arrangement of values into different classes. This is done by seeking to minimize each class's average deviation from the class mean, while maximizing each class's deviation from the means of the other classes. In other words, the method seeks to reduce the variance within classes and maximize the variance between classes.

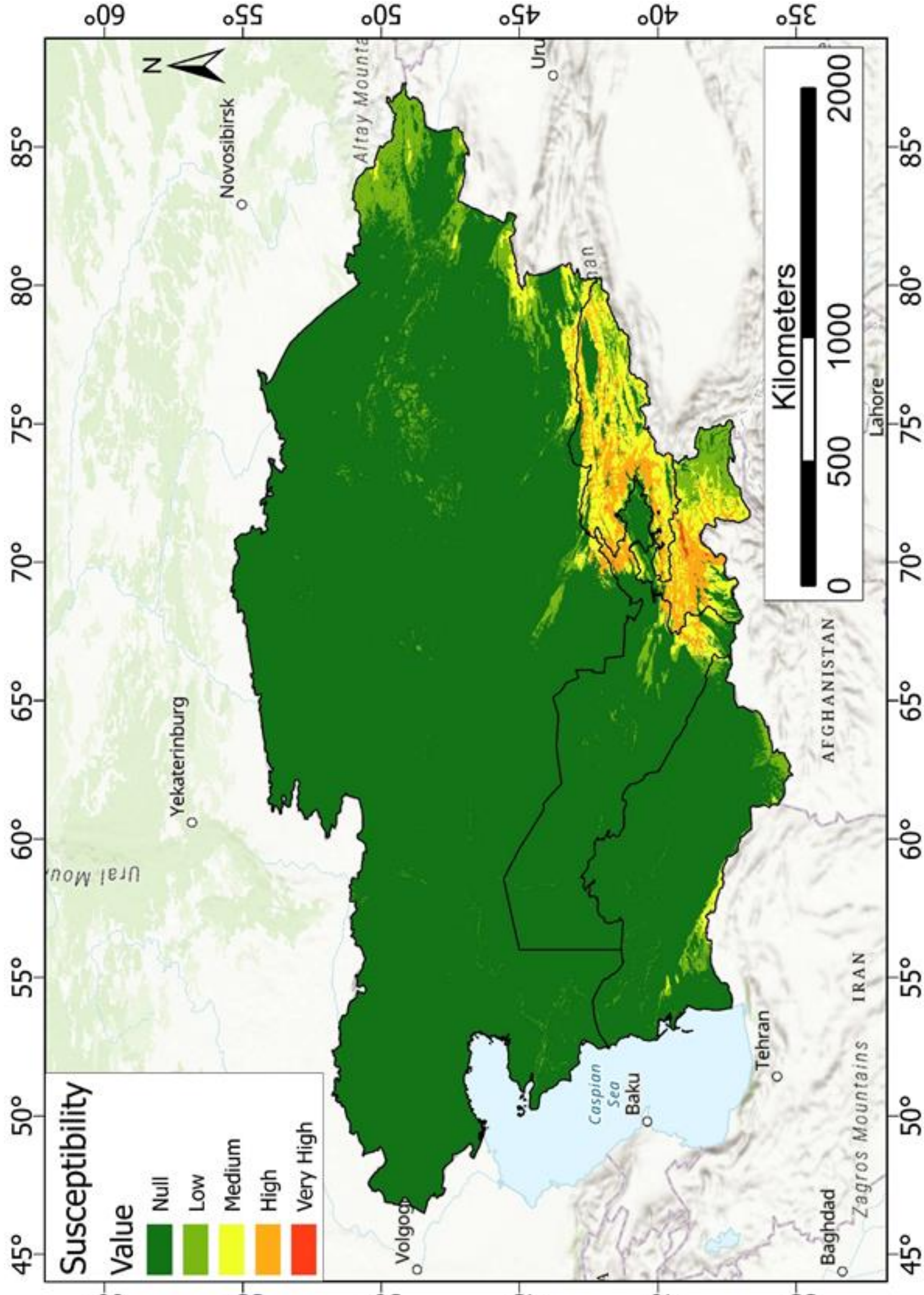

Figure 12. Landslide susceptibility map of the whole Central Asia

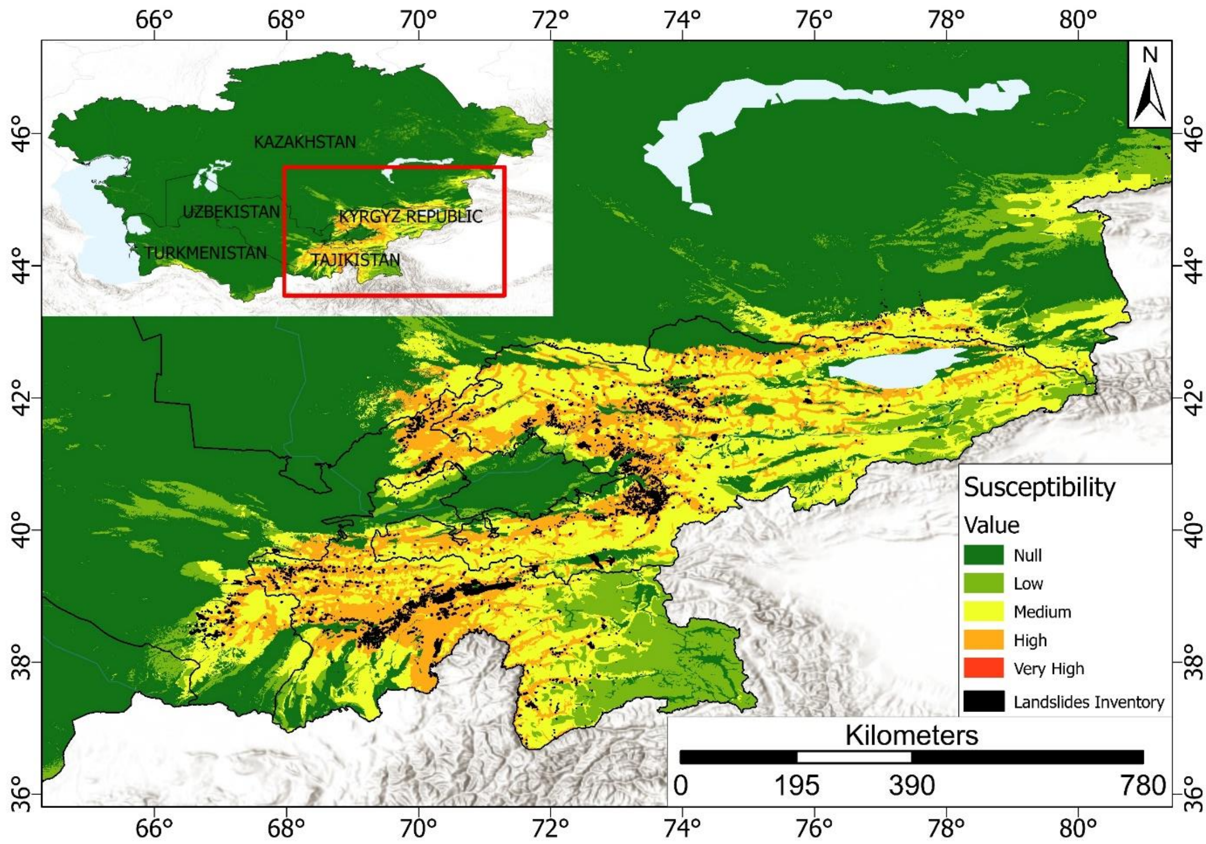

Figure 13. Detail of the landslide susceptibility map with the overlapping landslide polygons (in black).

Table 6. Landslide susceptibility class intervals, corresponding area, and percentage with respect to CA.

Susceptibility class	Landslide spatial probability interval	Corresponding area (km²)	Corresponding percentage of CA (%)
Null	0 - 0.05	2,890,811.5	88,5
Low	0.05 - 0.31	156,615	4.8
Medium	0.31 - 0.48	144,868.3	4.4
High	0.48 - 0.78	72,450.7	2.2
Very High	0.78 - 1	2,151	0.1

Here the corresponding extension and percentage of the study area are also reported, showing that the most frequent susceptibility class for the whole study area is the null class (=85%; landslides don't occur in flat areas), followed by low-medium classes (see also Figure 14). Only the 2.3% of the central Asian territory is represented by areas with high-very high landslide susceptibility (Table 6).

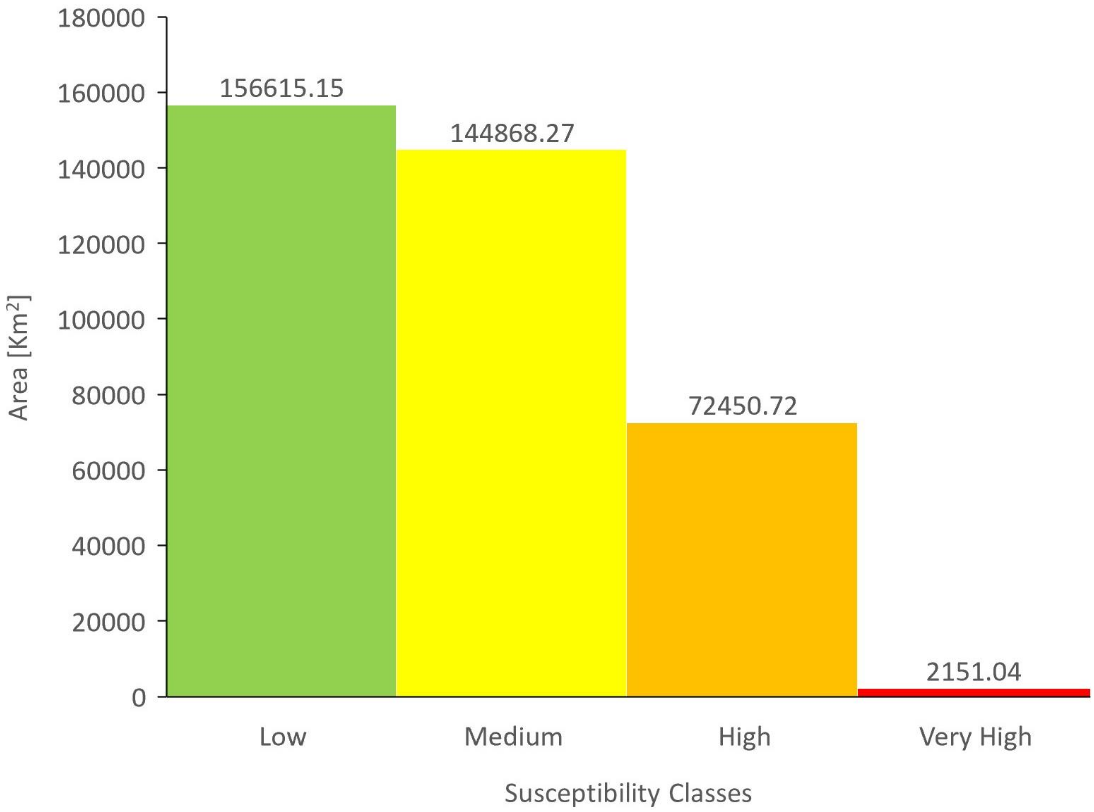

Figure 14. Frequency histogram of susceptibility classes for Central Asia; on each bar the corresponding area in km^2 is reported ("Null class" was not included to emphasize other classes).

As previously stated, for Turkmenistan there was not a landslide inventory available to train the RF model, therefore the corresponding LSM was obtained applying the model trained for the other four countries. The lack of landslide data did not allow any validation of the result or estimation of the quality of the susceptibility map of Turkmenistan. Furthermore, applying the model developed for the other countries, the same importance of the conditioning factors (e.g., the independent variables) was assumed. For these reasons, the landslide susceptibility map for Turkmenistan is more uncertain than those evaluated for the other four countries.

As we can see in the ranking of the susceptibility parameters, reported in Figure 15, land use, lithology, elevation, the distance from roads and hypocentres play a crucial role in landslide susceptibility, since they are the five most influencing factors (for the four countries where the model was trained). Rainfall parameters are also important in the obtained landslide susceptibility, in particularly the 1-day rainfall value that shows the highest importance among the rainfall parameters. Also, the PGA maps are a relevant factor, while TWI and slope curvature are the less important parameters. The AUC value of the models is 0.935 (where 0 is bad predictor, 1 represents a perfect predictor), indicating their very good quality. Such high AUC values can indicate the presence of overfitting issues, but this hypothesis can be discarded, since the random variable resulted to without any importance in landslide susceptibility (negative OOBE value).

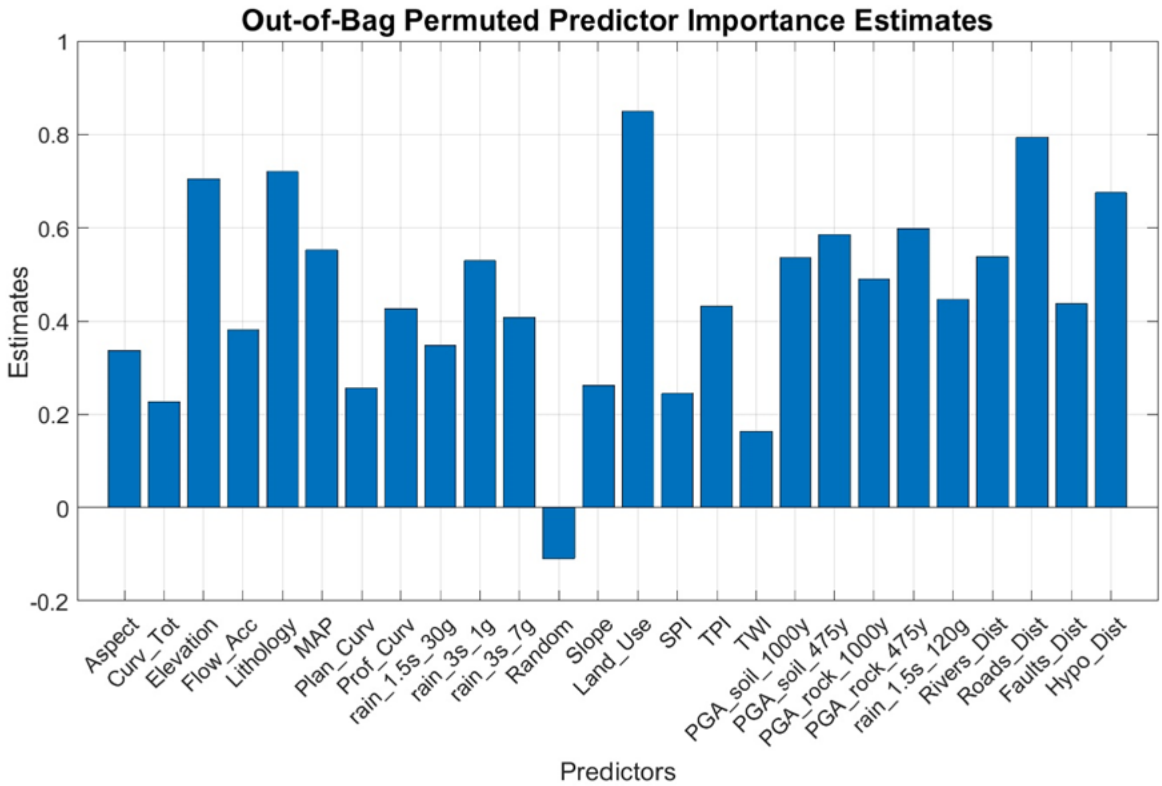

Figure 15. Variable importance in landslide susceptibility for the four countries where the model was trained.

In the following figures, the susceptibility maps of five selected areas are displayed.

- Figure 16 shows the area north of the city of Denov, in the south-east of Uzbekistan, which is characterized by a high susceptibility, despite the almost total absence of mapped landslides.
- Figure 17 shows a detail of the city of Uroteppa, in the North-West of Tajikistan, where there are not any known landslides, but a high susceptibility has been obtained in the surrounding mountain relief.
- In Figure 18 there is an enlargement on the city of Bishkek, north-west of the Kyrgyz Republic, where close to roads and inhabited centers a high landslides susceptibility is observed.
- The shores of Lake Issyk-Kul, in the Kyrgyz Republic, are generally flat areas, with a low or null landslide susceptibility, but in the central zone, shown in Figure 19.
- Finally, Figure 20 shows a detail of the western area of the Kyrgyz Republic, where a high landslide susceptibility is observed along the slopes adjacent to the river network.
- From these details it is possible to ascertain the high usefulness of the landslide susceptibility map realized by applying the Random Forest model, which, mainly based on the hydro-geomorphological properties, can establish the degree of susceptibility even in areas where there is no awareness of the predisposition to instability due to the absence of reported landslides.

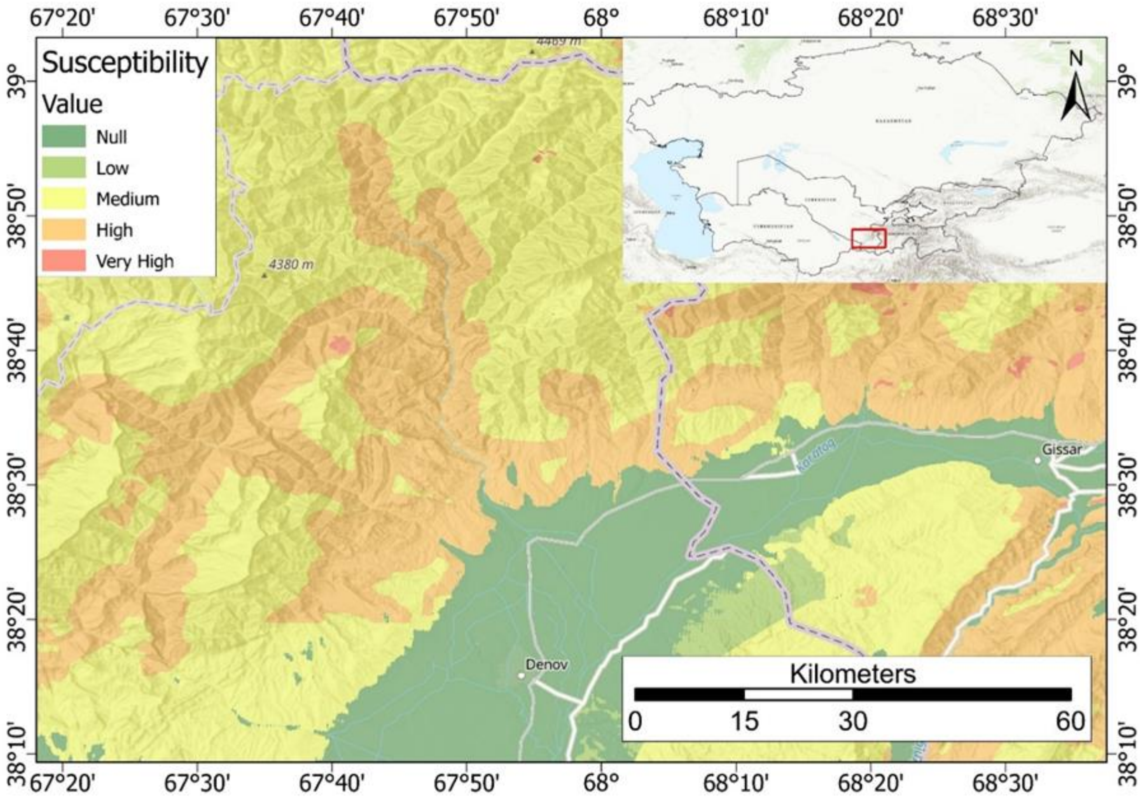

Figure 16. Detail of the landslide susceptibility map for the area north of the city of Denov, in the south-east of Uzbekistan.

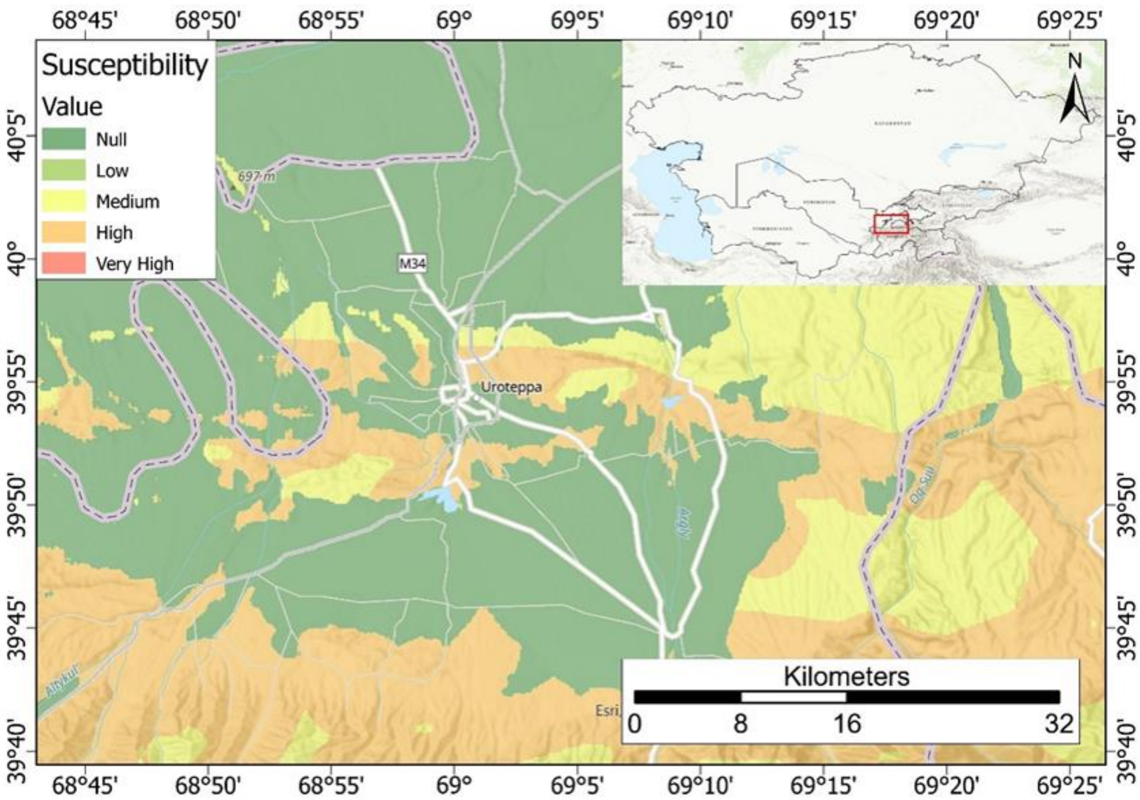

Figure 17. Detail of the the landslide susceptibility map for the city of Uroteppa (north-west of Tajikistan).

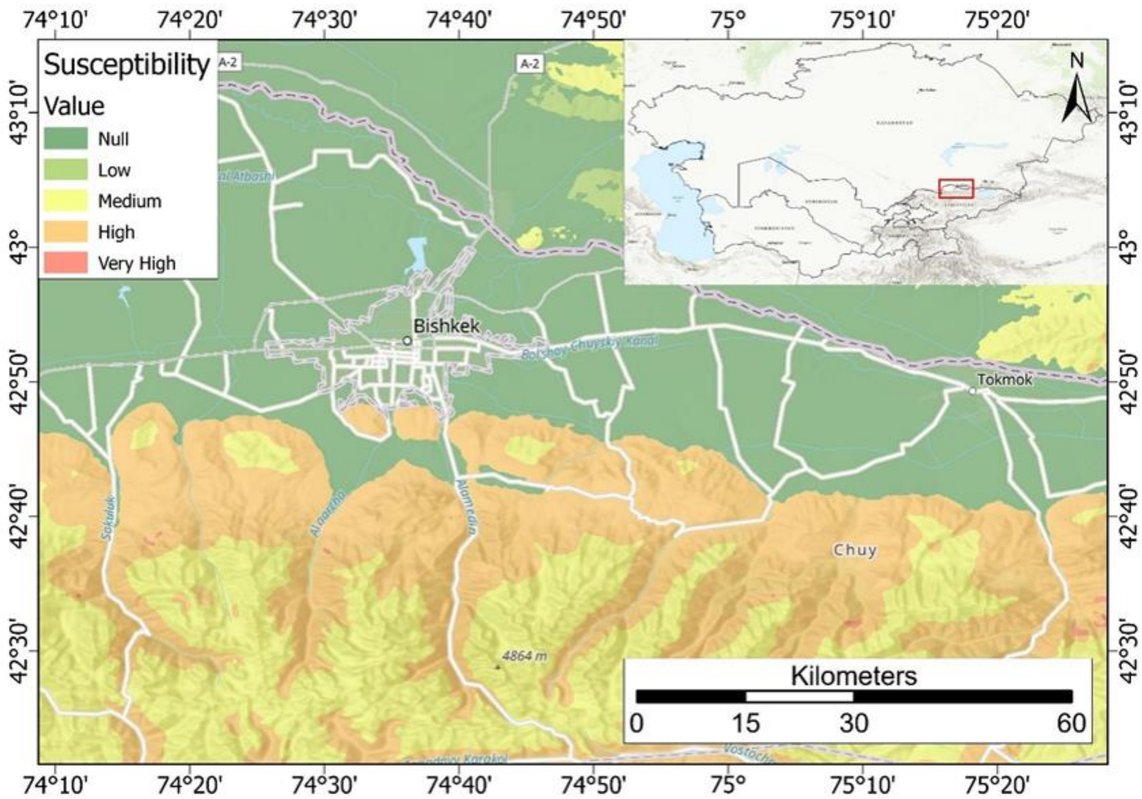

Figure 18. Detail of the the landslide susceptibility map for the city of Bishkek (north-west of the Kyrgyz Republic).

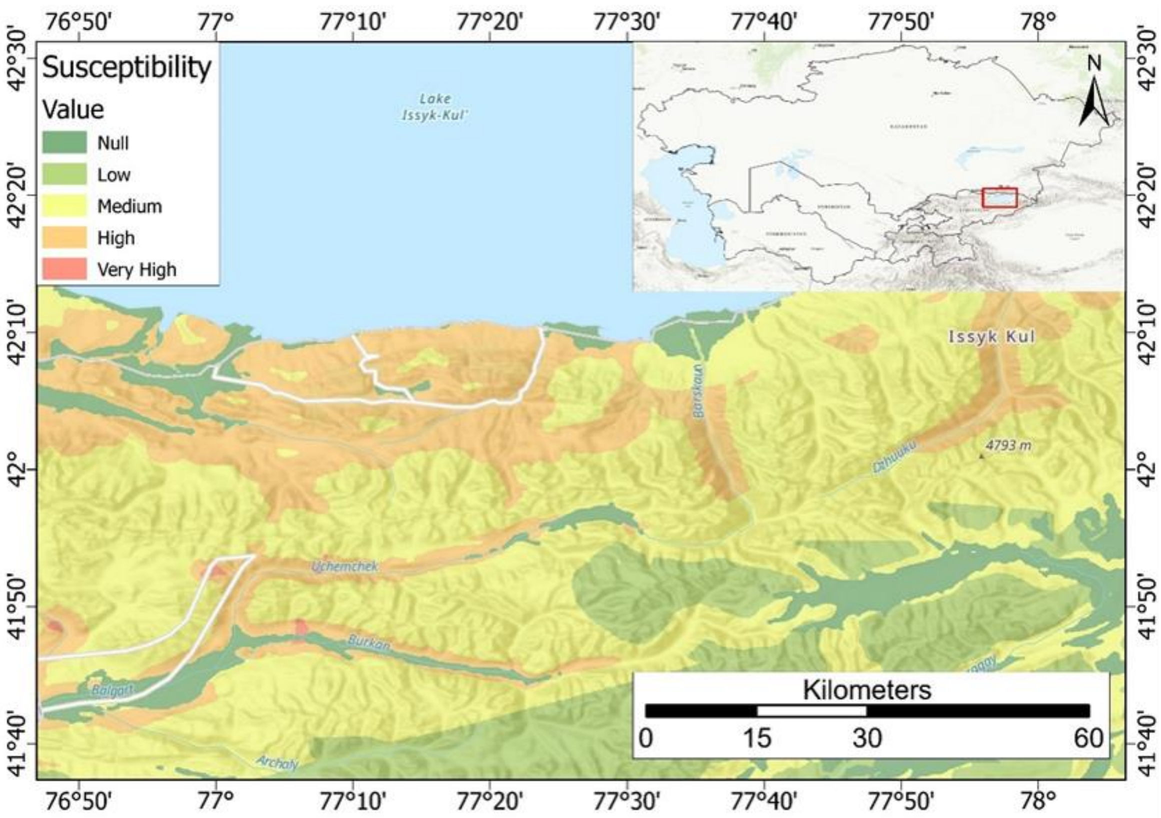

Figure 19. Detail of the the landslide susceptibility map for the Lake Issyk-Kul, in the Kyrgyz Republic.

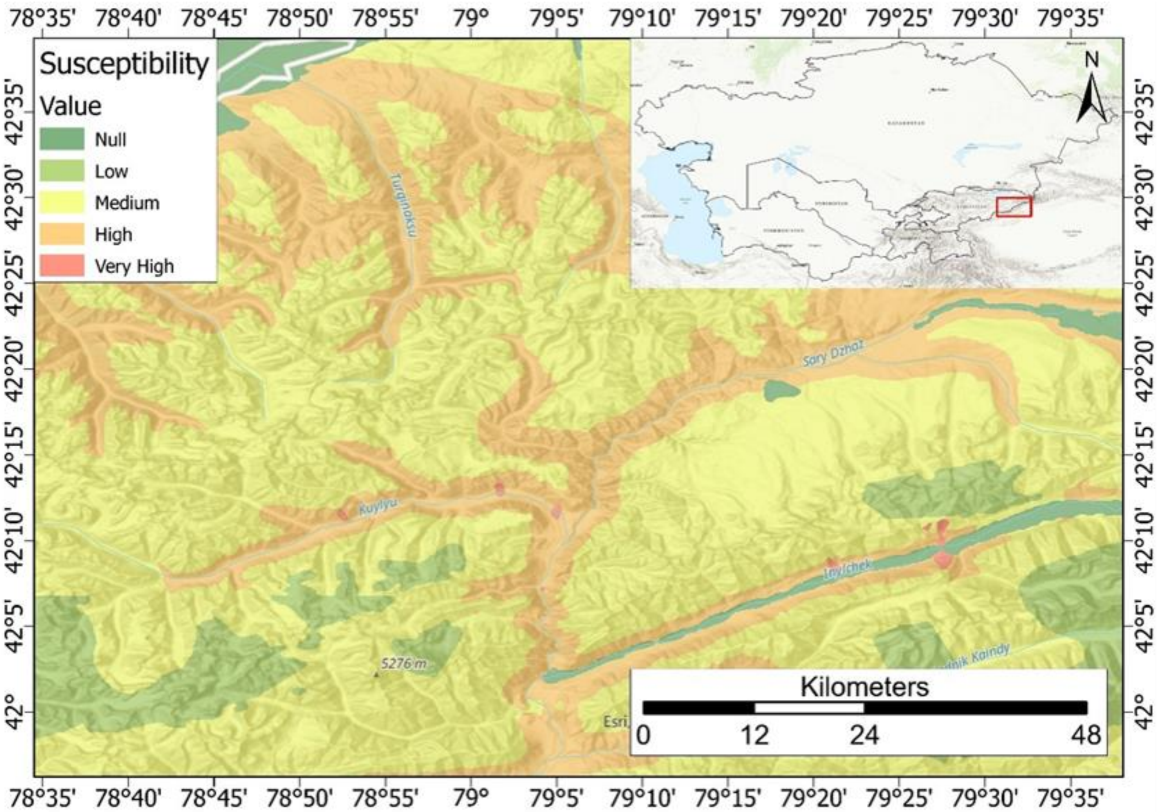

Figure 20. Detail of the the landslide susceptibility map for the western area of the Kyrgyz Republic.

3.4.1 Model validation

To verify the quality of the susceptibility models, beside the AUC value previously reported, a confusion matrix for the four countries where the model was trained was created (Figure 21). In each matrix the predicted landslide classes are compared with the ground truth to verify the presence of significant misclassification error. In all the matrix the value 1 represents the presence of landslide, the value 0 represents the absence of landslides; the numbers in each cell represent the number of pixels classified in that combination of 0 and 1, according to this scheme (the first number represent the predicted class, the second number the ground truth):

- 0-0 (True negative): pixels outside any landslides are correctly identified as no-landslide pixels by the model
- 1-1 (True positive): pixels inside a landslide are correctly identified as landslide pixels by the model
- 0-1 (False negative): pixels inside a landslide are wrongly identified as no-landslide pixels by the model
- 1-0 (False positive): pixels outside any landslides are wrongly identified as landslide pixels by the model.

In Figure 21 the 0-0 and 1-1 combinations represent well classified pixels (blue cells), while 0-1 and 1-0 represent misclassification error (light red cells).

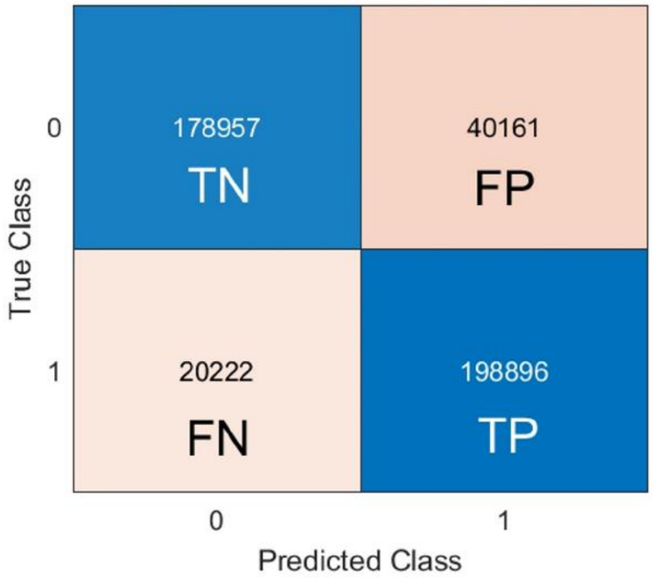

Figure 21. Confusion matrix for the four countries where the model was trained.

4 Landslide susceptibility and elements at risk

4.1 Methodology

The susceptibility map of the study area was intersected with the elements at risk, consisting of roads-railways, population, and cultural heritage sites. The database about the first three elements were obtained by the activities of Task 4 – Exposure Development, while Cultural Heritage data (including cultural and natural sites) were collected from the UNESCO World Heritage List website[11] and digitized in a *GIS environment*. The aim of this activity is to define the landslide susceptibility distribution in the area covered by elements at risk through a simple overlapping of the abovementioned databases and susceptibility map. In order to perform the analysis several approaches were defined based on the different types of elements at risk (Figure 22).

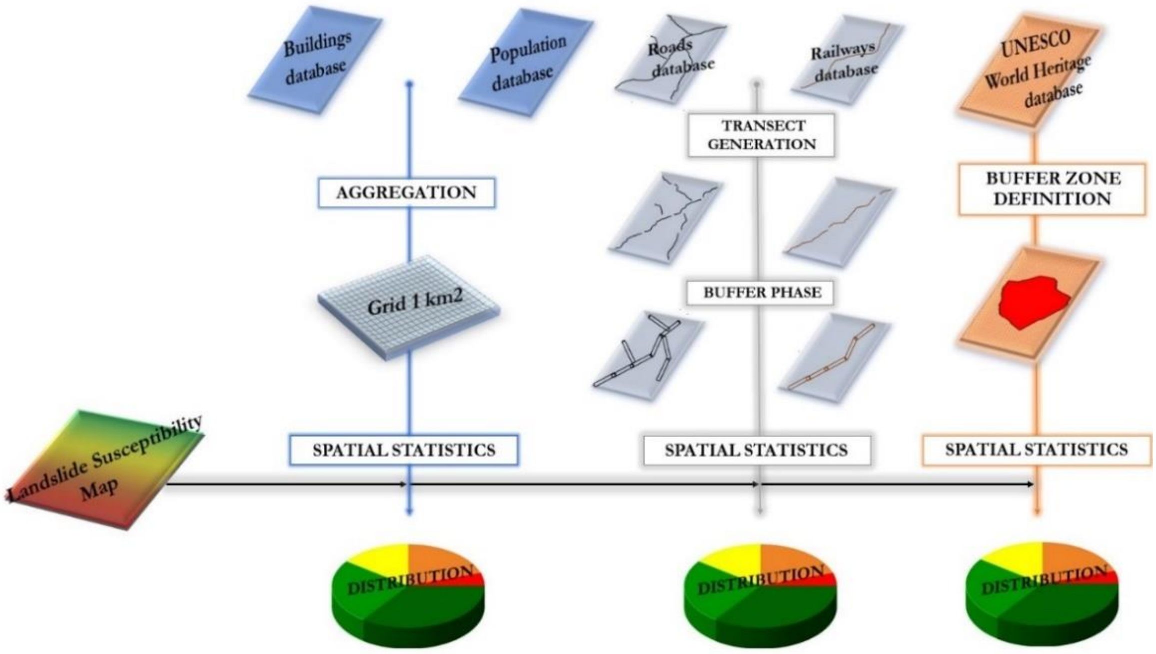

Figure 22. Flowchart of the adopted methodologies for the intersection of landslide susceptibility with the elements at risk.

The population and buildings data were based on a grid with a spatial resolution of 1km^2, defining for each cell the number of inhabitants, the number of different types of buildings (residential, commercial, industrial, education and healthcare), and the mean susceptibility class by means of spatial statistics between input databases (population-buildings data and susceptibility map). The results carried out from the spatial statistics allowed to assess the people and buildings distribution within each susceptibility class. On the contrary, the linear elements (roads and railways) were divided in segments with 1-km in length, and buffered, setting a distance parameter equal to 100 m. After this preliminary process, the spatial statistics with the landslide susceptibility have been carried out. The analysis performed on cultural heritage was set on simple spatial statistics about the susceptibility value within the buffer zone of each central Asian UNESCO site, which were

[11] https://whc.unesco.org/en/list/

previously defined in GIS environment. In detail, for each site the maximum, minimum and mean values of landslide susceptibility were obtained, subsequently the sites were classified into a landslide susceptibility class (based on the proposed classification described in the previous chapter). Obviously, these activities were performed for sites such as natural and cultural (e.g., historic centres), while for the Silk Road the approach has been the same adopted for roads and railways.

4.2 Results

Concerning the outcomes regarding buildings and population, they are represented by both Table 7, in which, for each susceptibility class, the number of people and the number of different building types are reported, and in the pie charts (Figure 23, Figure 24). In these latter the distribution of elements at risk in the susceptibility class "Null" weren't reported, in order to emphasize the percentages of elements in the other classes, since the "Null" one contains most elements at risk.

Table 7. Population and buildings distribution in each landslide susceptibility class.

Susceptibility class (Grid 1 km^2)	Element at risk	Number
Null	Population	68,422,152
	Residential buildings	8,769,270
	Commercial buildings	2,196,037
	Industrial buildings	705,352
	Education buildings	42,472
	Healthcare buildings	15,476
Low (0.05-0.31)	Population	3,046,892
	Residential buildings	319,776
	Commercial buildings	103,745
	Industrial buildings	14,776
	Education buildings	1802
	Healthcare buildings	224
Medium (0.31-0.48)	Population	1,612,487
	Residential buildings	245,754
	Commercial buildings	68,187
	Industrial buildings	6396
	Education buildings	960
	Healthcare buildings	84
High (0.48-0.78)	Population	2,812,081
	Residential buildings	386.628
	Commercial buildings	68.232
	Industrial buildings	7024
	Education buildings	2102
	Healthcare buildings	226
Very High (0.78-1)	Population	97,934
	Residential buildings	12,753
	Commercial buildings	3,410
	Industrial buildings	110
	Education buildings	96
	Healthcare buildings	2

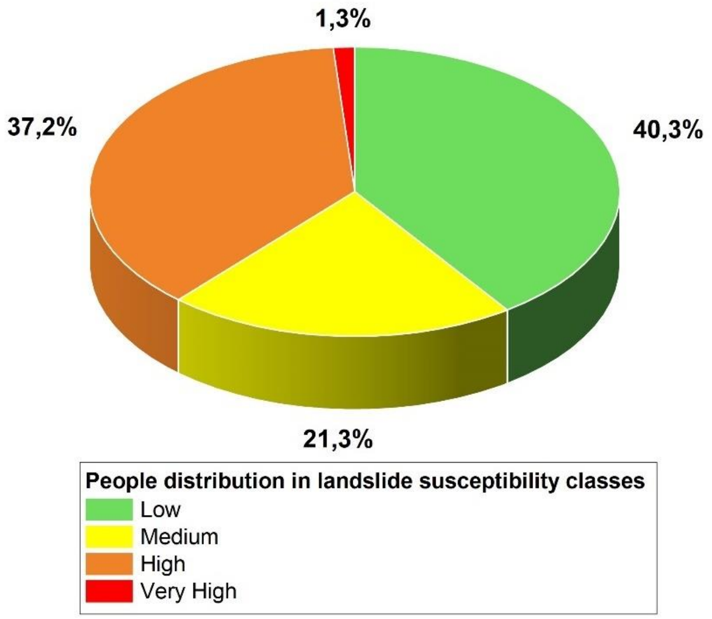

Figure 23. Pie chart of population distribution in landslide susceptibility classes.

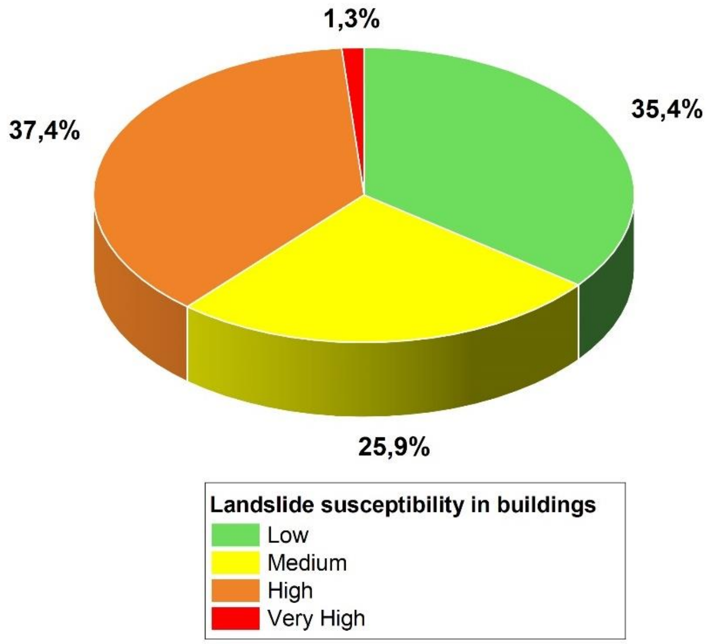

Figure 24. Pie chart of landslide susceptibility distribution in 1-km^2 cells with buildings.

The obtained results about roads and railways are reported in the respective maps in Figure 25, and Figure 27), where 1-km long lines (hereafter "transects") were divided in the corresponding landslide susceptibility class. Their as well as their distributions are represented in Table 8-Table 9, and in the pie charts in Figure 26 and Figure 28. In detail, statistical analysis for roads and railways was also performed considering the major classes: primary, secondary, tertiary, trunk, and motorway for roads; high-speed and conventional for railways.

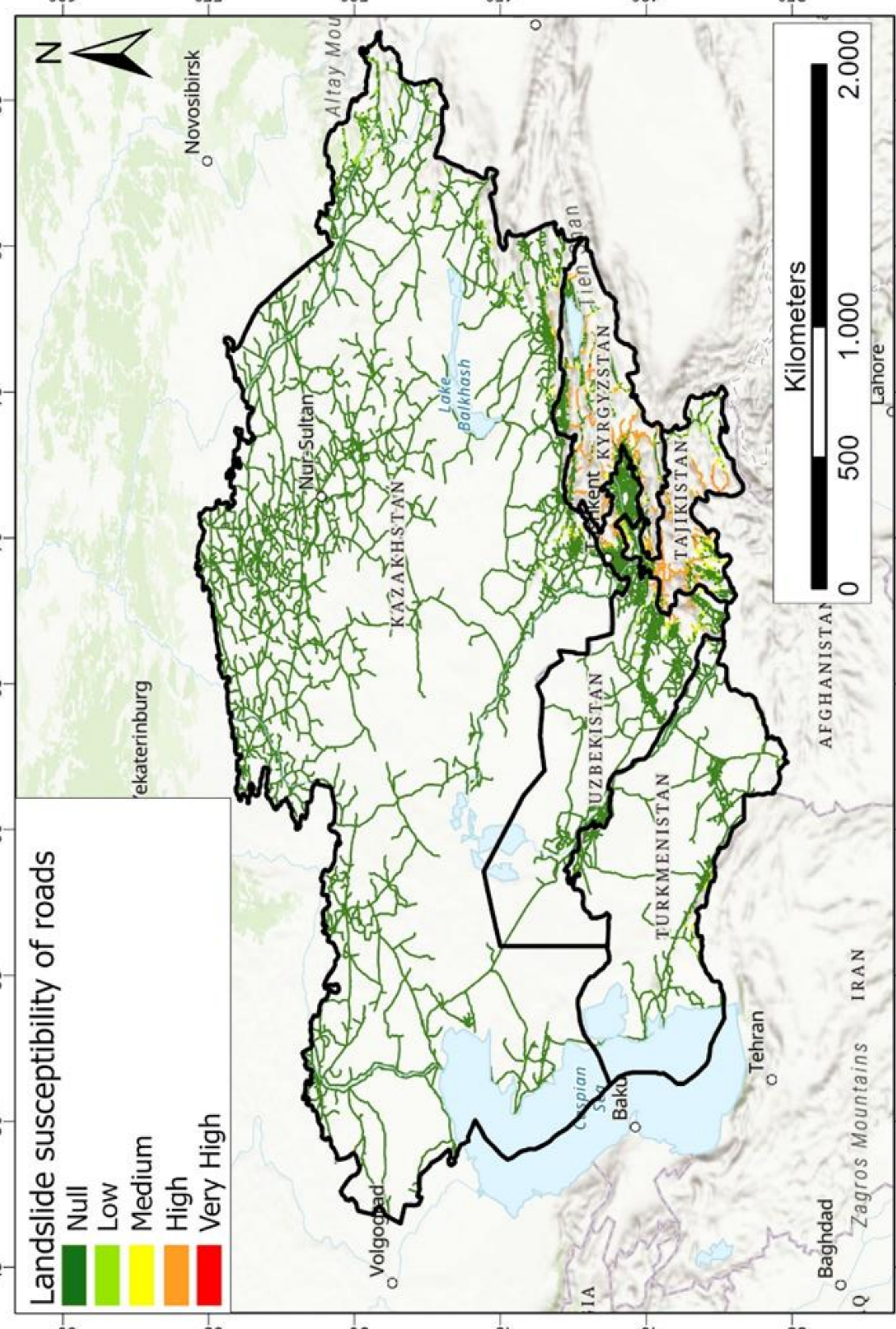

Figure 25. Landslide susceptibility map of roads in Central Asia.

Table 8. Distribution (corresponding km) of road classes in landslide susceptibility classes.

Susceptibility class	Road class	Corresponding km
Null	Primary	15,000
	Secondary	28,773
	Tertiary	71,515
	Trunk	30,058
	Motorway	1,732
Low (0.05-0.31)	Primary	646
	Secondary	911
	Tertiary	2,637
	Trunk	1,887
	Motorway	/
Medium (0.31-0.48)	Primary	368
	Secondary	589
	Tertiary	1,643
	Trunk	686
	Motorway	/
High (0.48-0.78)	Primary	873
	Secondary	1,173
	Tertiary	3,898
	Trunk	1,887
	Motorway	/
Very High (0.78-1)	Primary	26
	Secondary	30
	Tertiary	55
	Trunk	77
	Motorway	/

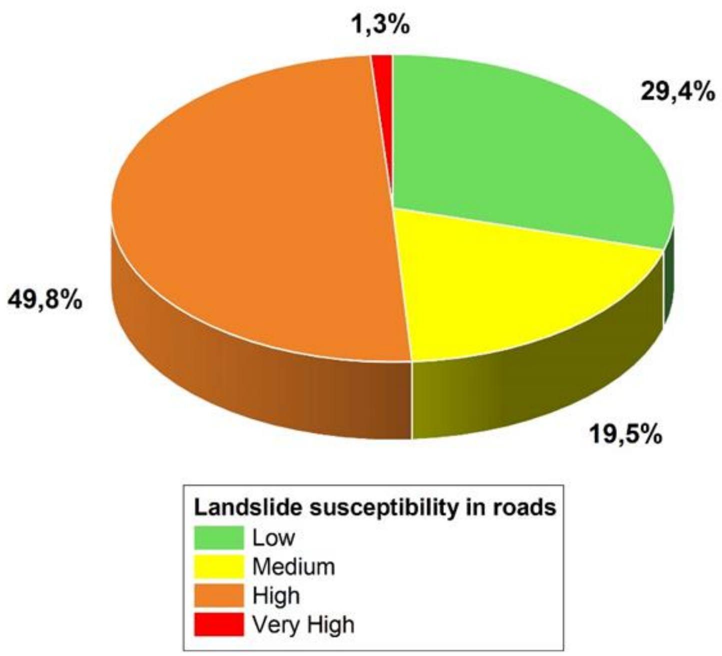

Figure 26. Pie chart of landslide susceptibility distribution in road segments.

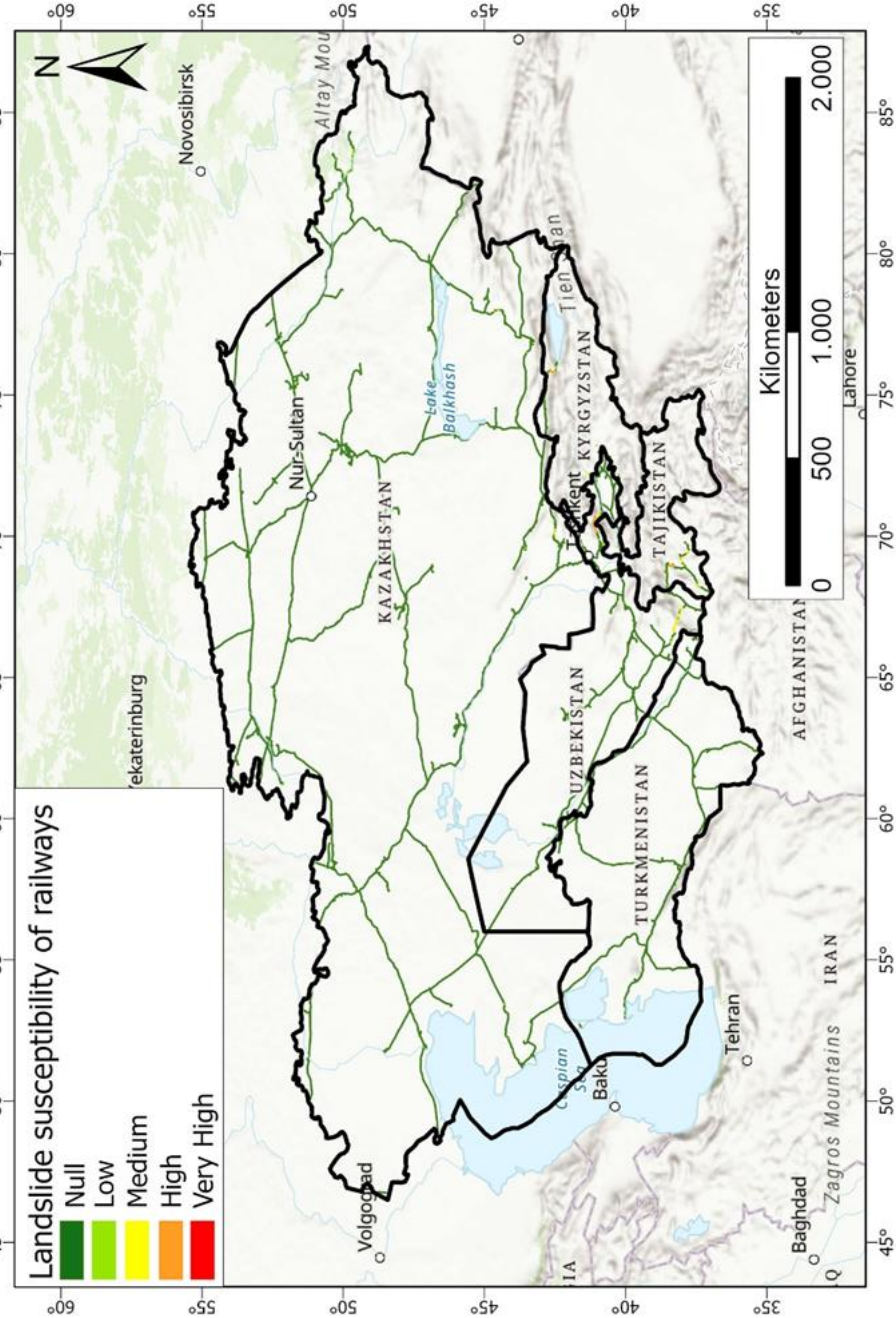

Figure 27. Landslide susceptibility map of railways in Central Asia.

Table 9. Distribution of railways classes in landslide susceptibility classes and corresponding length.

Susceptibility class	Railway class	Corresponding km
Null	High-Speed	45,866
	Conventional	128
Low (0.05-0.31)	High-Speed	589
	Conventional	4
Medium (0.31-0.48)	High-Speed	317
	Conventional	16
High (0.48-0.78)	High-Speed	187
	Conventional	12
Very High (0.78-1)	High-Speed	25
	Conventional	/

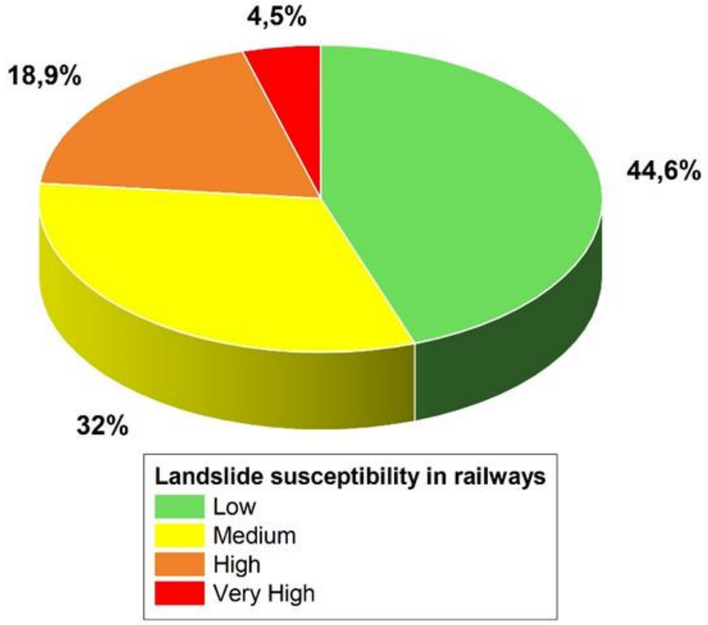

Figure 28. Pie chart of landslide susceptibility distribution in railway segments ("Null" class was not included to emphasize other classes).

The location of the 15 UNESCO World Heritage sites of Central Asia is reported in Figure 29. The outcomes carried out by statistics between landslide susceptibility map and Cultural Heritage sites showed a general trend: most sites reported a landslide susceptibility class equal to "Null" (Table 10), since most of them are located in flat areas, where obviously the landslide susceptibility is null. On the contrary, the Tajik National Park and the Western Tien-Shan present areas with a "Very High" landslide susceptibility within them, while their mean class is "Medium" and "High" respectively (Figure 30). The obtained map of landslide susceptibility of Silk Road is reported in Figure 31, while the corresponding statistics are summarized in Table 11.

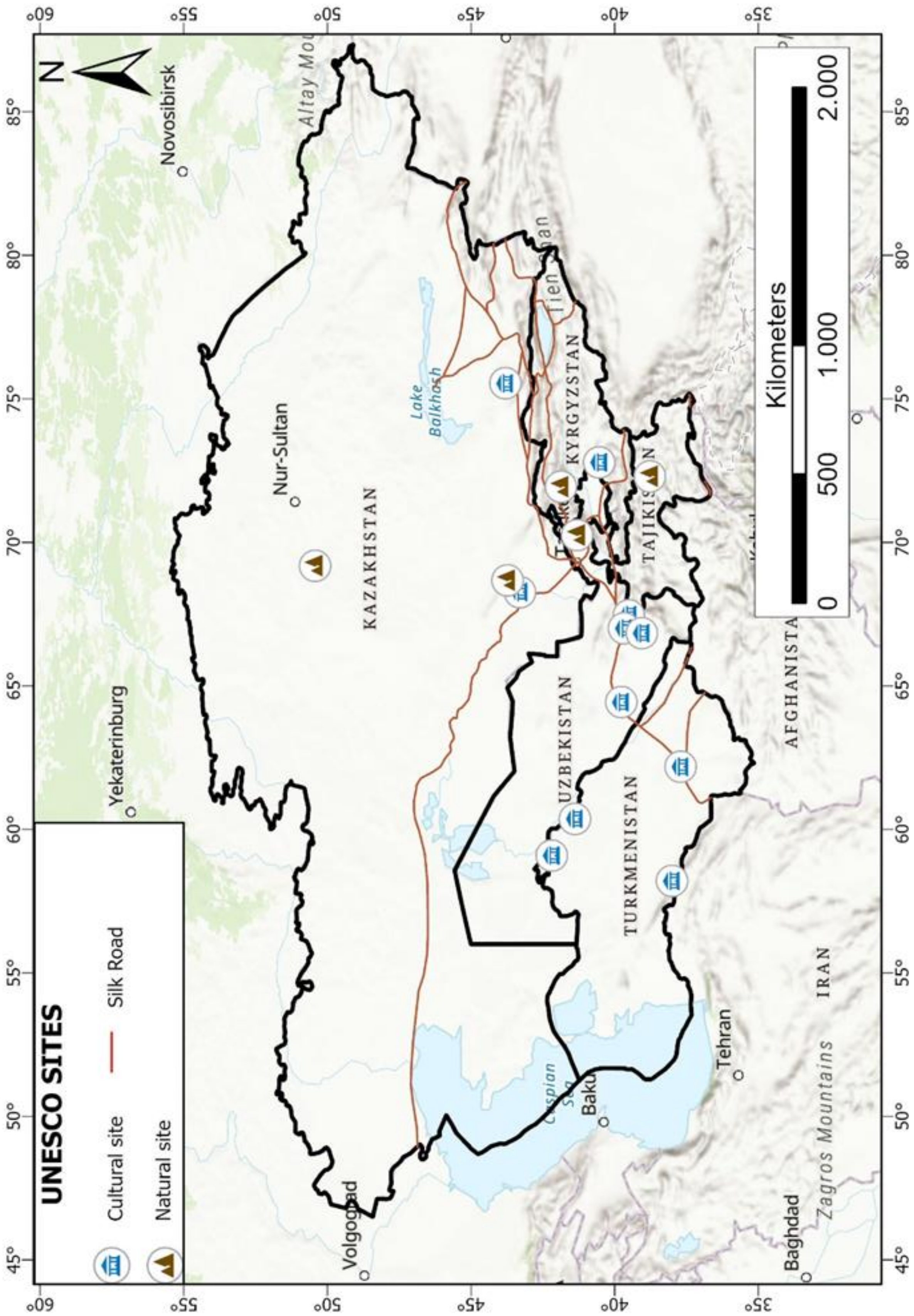

Figure 29. Location of UNESCO World Heritage sites in Central Asia.

Table 10. List of Cultural Heritage sites and corresponding landslide susceptibility classes.

Cultural Heritage Sites	Type	Country	Major class of landslide susceptibility	Minor class of landslide susceptibility	Mean class of landslide susceptibility
Saryarka	Natural Site	Kazakhstan	Null	Null	Null
Mausoleum of Khoja Ahmed Yasawi	Cultural site	Kazakhstan	Null	Null	Null
Proto-urban Site of Sarazm	Cultural site	Tajikistan	Null	Null	Null
Petroglyphs of the Archaeological Landscape of Tanbaly	Cultural site	Kazakhstan	Low	Null	Low
Kunya-Urgench	Cultural site	Turkmenistan	Null	Null	Null
Sulaiman-Too Sacred Mountain	Cultural site	Kyrgyz Republic	Null	Null	Null
Parthian Fortresses of Nisa	Cultural site	Turkmenistan	Medium	Null	Null
Tajik National Park (Mountains of the Pamirs)	Natural Site	Tajikistan	Very High	Null	Medium
Western Tien-Shan	Natural Site	Kazakhstan - Kyrgyz Republic - Uzbekistan	Very High	Low	High
Itchan Kala	Cultural site	Uzbekistan	Null	Null	Null
Historic Centre of Bukhara	Cultural site	Uzbekistan	Null	Null	Null
Samarkand – Crossroad of Cultures	Cultural site	Uzbekistan	Null	Null	Null
Historic Centre of Shakhrisyabz	Cultural site	Uzbekistan	Null	Null	Null
State Historical and Cultural Park “Ancient Merv”	Cultural site	Turkmenistan	Null	Null	Null
Silk Road	Cultural site	All	Very High	Null	Low

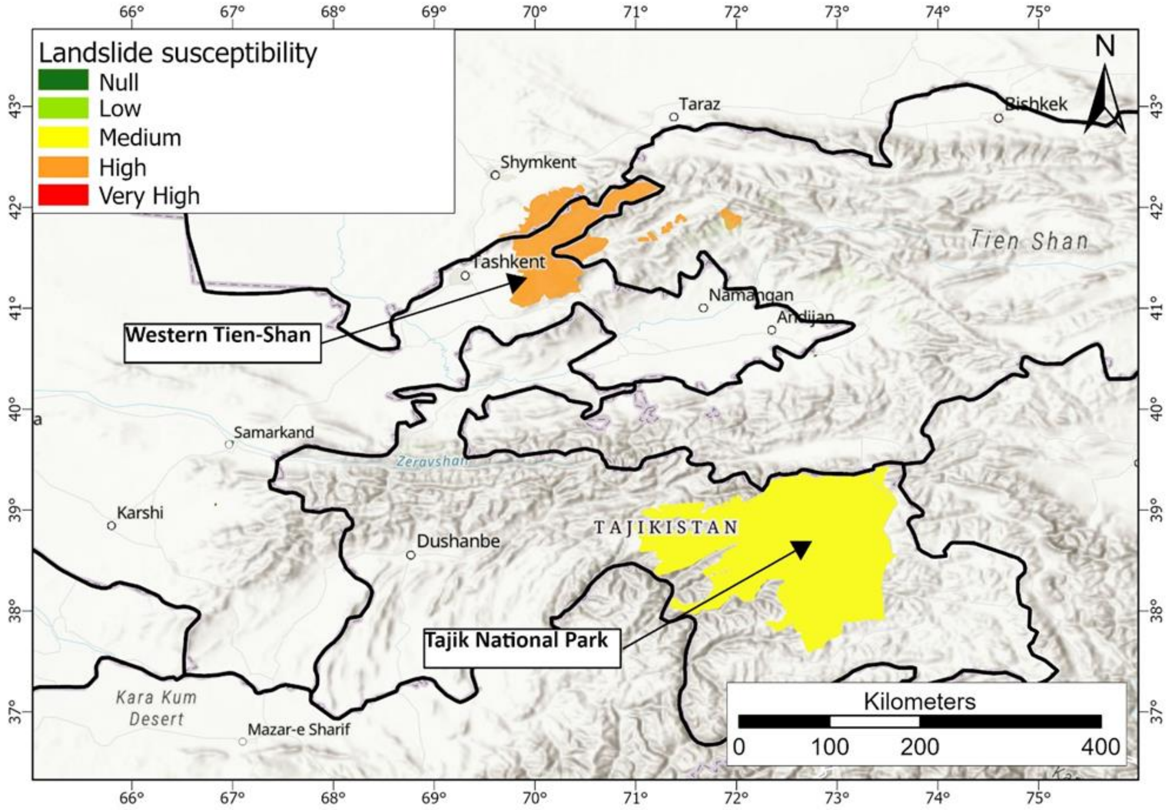

Figure 30. Landslide susceptibility map of Western Tien-Shan and Tajik National Park.

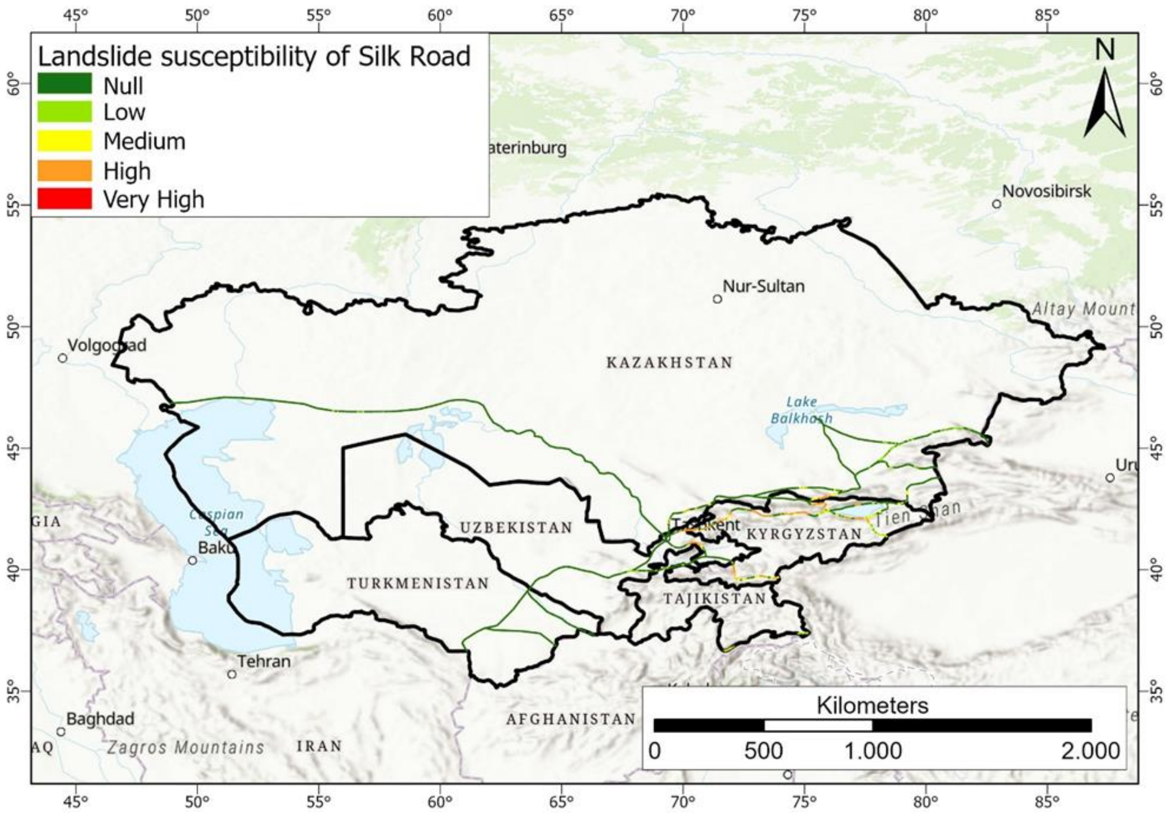

Figure 31. Landslide susceptibility map of Silk Road.

Table 11. Distribution (corresponding km) of Silk Road in landslide susceptibility classes.

Susceptibility class	Corresponding length (km)
Null	9,368
Low (0.05-0.31)	771
Medium (0.31-0.48)	667
High (0.48-0.78)	838
Very High (0.78-1)	4

5 Landslide dam Susceptibility

5.1 Methodology

Landslide dams are natural processes that occur when a river channel is completely obstructed by a landslide. In mountain regions landslide dams are quite common events and sometimes they cause serious hazards such as upstream backwater formation, catastrophic downstream flooding, channel instability, changes in the riverbed dynamics and triggering of secondary landslides with a cascading effect. As most of the human activities are located in valley floors, consequences of a downstream flooding have significant economic and social impacts with loss of business and human life. Population can suffer casualties and restoration costs are often substantial, as they are direct, (e.g., safety measures and infrastructure rebuilding) and indirect (e.g., damage caused to industrial and agricultural productivity or loss in real estate value); the latter are more difficult to estimate. Most of landslide dams last a short period of time and about 40% of the dams collapse within a single day after formation and about 80% within one month, so that the available time to assess the dam stability usually is not enough for a reliable in-depth analysis, and only techniques allowing for rapid data collection and analysis are possible. Nevertheless, some consequences from landslide damming can be reduced with mitigation and prevention measures where the expected damming probability is high, and the possible related consequences catastrophic. Therefore, planning and prevention instruments, such as risk and susceptibility mapping, are fundamental to reduce the consequences of natural hazard and increase the cost efficiency of environmental management.

Landslides dams are often generated by the reactivation of ancient movements triggered in the past during different climatic and environmental conditions. In such cases, they are now dormant and hard to recognize because the vegetation hides the landslide morphology, and the sliding surface strength parameters are close to the residual ones. Therefore, these prehistoric phenomena can be reactivated by natural causes (e.g., river undercutting, earthquakes, heavy rainfall, or snowmelt), as well as man-made activity. For these reasons, all dormant landslides able to reach a river section along their path can potentially obstruct the stream and should be subject to investigation. New landslides, instead, may potentially develop wherever suitable conditions are met within hillslopes. The spatial probability of occurrence is usually estimated by landslide susceptibility analysis, that is highly dependent on landslide volume, which in turns is difficult to predict with accuracy.

According to some research (Swanson et al.; 1986; Tacconi Stefanelli et al., 2016), landslide dam behavior can be forecasted through the computation of geomorphological indexes, composed by parameters characterizing the involved natural systems: the landslide (or the dam) and the river (or the lake, if present). Geomorphological indexes are a powerful classification and prediction tool but, being mostly empirical, depend on extensive studies and measurement efforts. In most cases such indexes need parameters that are not always available and easy to obtain, like landslide velocity (Swanson et al., 1986). The recently proposed Morphological Obstruction Index (MOI) (Tacconi Stefanelli et al., 2016) is a bivariate index that requires only simple morphometrical parameters which are easily obtained from common Digital Elevation Models. This tool shows a proven capability in assessing the probability of formation of landslide dams in Italy and Cordillera Blanca, Peru (Tacconi Stefanelli et al., 2016; 2018) with respect to other popular indexes (Swanson et al., 1986).

The MOI expression combines two of the most important parameters, the landslide volume V_l (m^3) and the valley width W_v (m):

$$MOI = \log (V_l/W_v). \quad (1)$$

According to MOI, analyzed landslide dams can be classified within three evolutionary domains: formed, not formed and of uncertain evolution. The limits of these regions are drawn by two straight lines, the “Non-Formation Straight line” and the “Formation Straight line” (Figure 32).

The equation of the former is expressed as follows:

$$V_l' = 1.7 \times W_v^{\,2.5} \quad (2)$$

where V_l' is called “Non-Formation volume” and is the minimum landslide volume (m^3) able to potentially dam a river with a width W_v. Lower volumes do not completely obstruct the river. The expression of the latter is the upper limit for not formed dams and the inferior boundary of the Formation domain and is expressed as follows:

$$V_l'' = 180.3 \times W_v^{\,2} \quad (3)$$

where V_l'', called the “Formation volume”, is the minimum landslide volume (m^3) to have the river valley dammed, with a confidence interval of 99%.

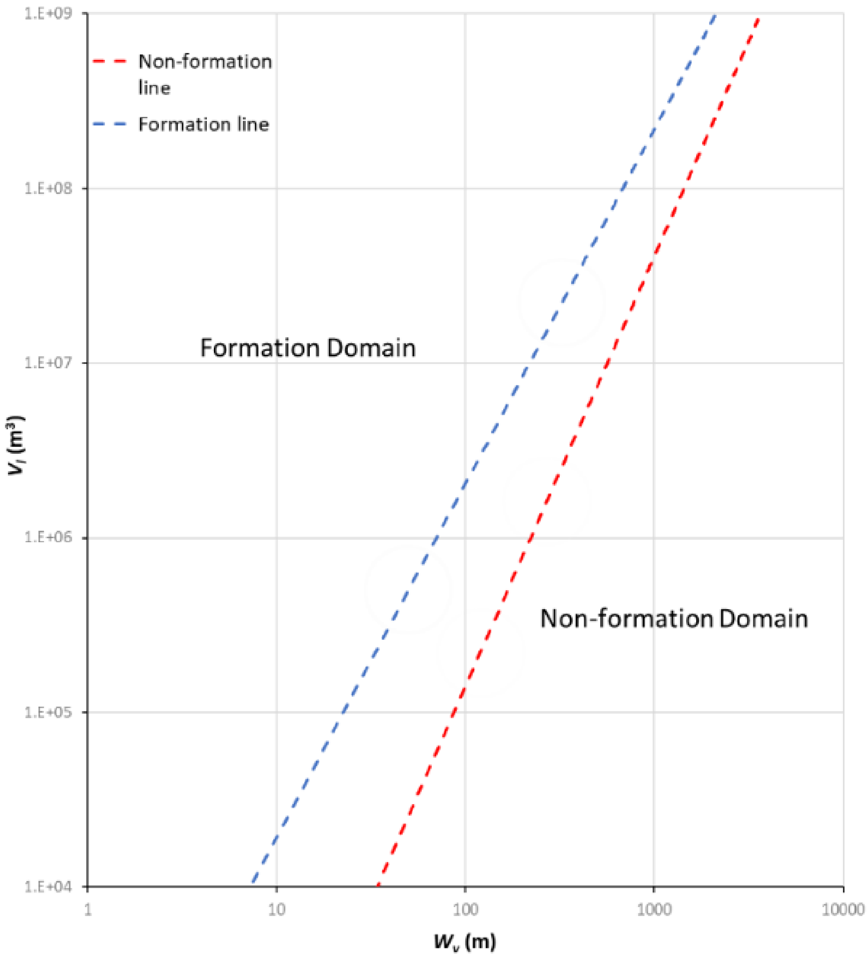

Figure 32. Schematic plot of the Non-Formation line and Formation line.

A simple semi-automatic methodology was applied to the study region to verify the damming susceptibility from existing and neo-formed landslides with geomorphological indexes. The valley width can be considered as a static variable in the MOI equation, since this parameter does not change significantly over decades within each river stretch. From this assumption, according to Equation (2) and Equation (3), if we evaluate the average river width W_v within each river stretch, two threshold landslide volumes V_l' and V_l" (Non-Formation volume and Formation volume) able to block a river can be calculated at each section. Landslide dams, as all kinds of landslides, are often reactivations of ancient movements started in the past. Through an updated landslide database, it is possible to estimate the landslide volumes with some assumptions and simplifications. Mapped landslides with volume bigger than V_l' and V_l" for their river section are identified as potentially prone to block in the future the river in that point. Therefore, a "Map of the Damming Susceptibility" for reactivation of existing landslides can be produced.

The prediction of probability for new landslides, with volume bigger than V_l' and V_l", is a more challenging task as the volume is a difficult value to be computed. To have an estimation of the damming susceptibility for neo-formed landslides the two volume threshold values of Formation and Non-Formation can be assessed for all the river network, computing the river width of every river stretches, through the corresponding two equations. The following semi-automated procedure can be developed entirely in a GIS (Geographic Information System) environment.

The data used for the procedure are a Digital Elevation Model (with the higher resolution freely available from the NASA's SRTM project with 30 m resolution), the river network database provided by the RED Consortium partners involved in Task 3 - Flood Hazard Modeling, and several landslide inventories (see Section 2.2). The latter input has data only in the southeast area mainly due to the morphologic characteristics of the study area, with the higher peaks concentrated in that zone. The data quality and resolution such as the landslides inventory completeness, the river network reliability and the DEM resolution heavily affect the quality of the result. The methodology adopted to obtain the maps of Damming Susceptibility is summarized in the following main steps. According to the literature (Swanson et al.; 1986; Tacconi Stefanelli et al., 2016), river blockage takes place almost exclusively in hilly or mountainous areas and preferentially along steep slopes. Therefore, considering the extension of the study area, in order to reduce the processing time and improve the visualization effect, a series of unnecessary data were removed from the calculations. For this reason, sections that run in flat areas (with less than 4° slopes) were not considered in the elaborations, since their damming probability is certainly negligible. Furthermore, to make maps easier to display and manage, the river network was divided in 5-km long river stretches.

In the last decades the analysis of digital terrain models has evolved, and different algorithms have been developed to automatically extract terrain features using commercial GIS software or stand-alone programs. The valley width, such as any other landform, is not an easy parameter to identify and measure, but Wood (2009) created "LandSerf" software (integrated as a module in SAGA GIS or QGIS software), which is designed to automatically classify landforms from digital models. The module derives land-surface parameters from DEMs (e.g., slope, aspect, and curvature), using a multi-scale approach, that are used within image processing for pattern recognition and texture analysis. During the processing, the method allows the landscape classification, dividing it into homogeneous morphometric units (peaks, ridges, passes, channels, pits, and planes) (Figure 33-a.). Using the module proposed by Wood (2009), it is possible to identify the polygons representing the channels morphological unit, which can be used as an objective tool to define the valley floor limits over a broad spatial scale (Figure 33-b.). The ability to discriminate different geomorphologic landforms is more effective in mountainous areas with strong elevation differences, with respect to flat areas where the differences between different landforms are less clear. The reliability of the result is directly linked to the DEM resolution, which ideally should be about 1 m. Coarser resolutions determine landslide volumes with a proportional uncertainty.

A further step is to associate a valley width value, W_v, for each river stretch. To measure the distance between the two lateral valley floor boundaries, the river network is sampled creating 1-km long lines ("transects"), perpendicular to the river stretches, outdistanced by 500 meters (Figure 34-a). Then, the created valley floor polygons can be used to "cut" the perpendicular transects by using a simple cut command in any GIS software (Figure 34-b.). The valley widths, W_v, of each river stretch is then assigned equal to the average value of the n perpendicular transects without the extreme (maximum and minimum) values, as in the simplified formula:

$$W_v = (\sum_{i=1}^{n} W_i - W_{min} - W_{max})\frac{1}{n-2}$$

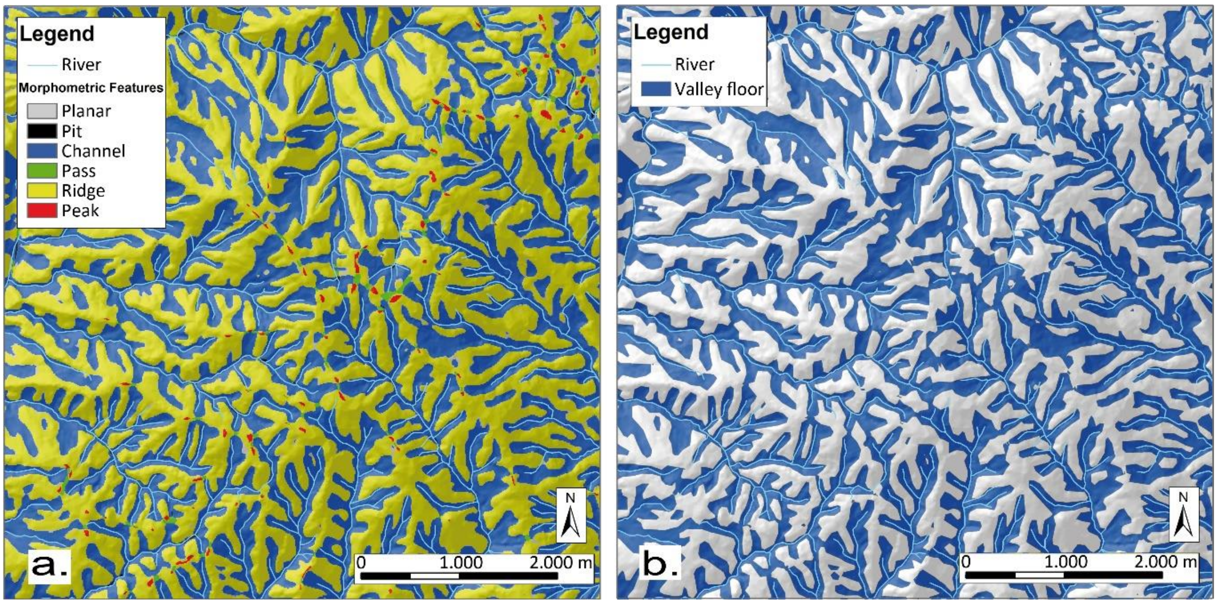

Figure 33. a) Landscape division in morphological units; b) Extraction of valley floor polygons.

Knowing the W_v value for each river stretches the two boundary landslide values of "Non-Formation volume" and "Formation volume", V_l' and V_l", can be easily computed by applying the equations of "Non-Formation" (Equation (2)) and "Formation" straight lines (Equation (3)) to both classify the damming susceptibility of the landslides inventory (for their reactivation) and of the river network (for new landslides). Thanks to an updated landslide polygons archive, it is possible to assess which landslide, if reactivated, is big enough to dam its own valley floor by using the two boundary volumes V_l' (below which a landslide definitely does not produces complete river blockages) and V_l" (above which the river valley is certainly dammed). It is reasonable to assume that a reactivated landslide will move downstream by gravity, following a path like a surface water flow. Draining directions within each slope are easily computed along the river network with a GIS software (Figure 35).

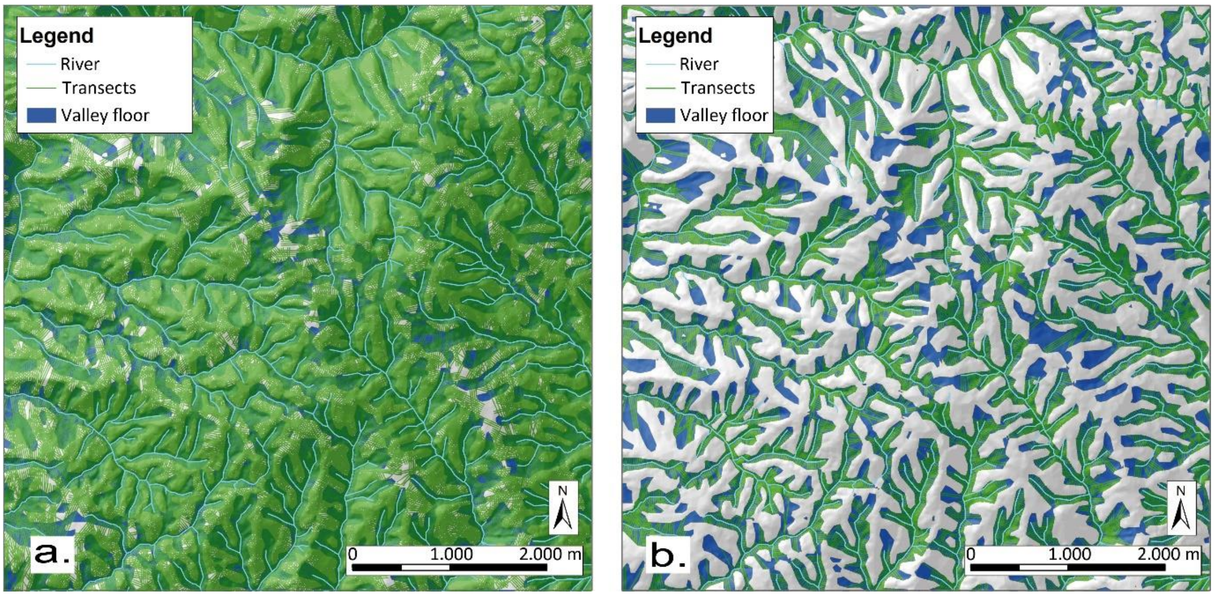

Figure 34. a) 500 m long transects perpendicular to the river stretches; b) Clip of transects on valley floor polylines.

Each landslide can then be associated to the river stretch that it should reach if reactivated, according to the belonging draining surfaces. Since the areas of the landslide polygons were the only available information to compute the landslides volume, an empirical relation between areas and volumes has been used. The general form of the existing statistical relations is:

$$V_l = \varepsilon \times A_l^{\alpha}$$

where V_l and A_l are respectively the volume and the area of a landslide, ε and α are respectively the constant and the exponent of the power law describing the landslides volumes frequency distribution.

Various empirical relations of ε and α have been employed for landslide volume calculations by researchers located in different countries. After an evaluation of these relations in the study area, the parameter proposed by Guzzetti et al. (2009) have been chosen because of the number of the studied cases (667) and the magnitude range of the landslides area investigated (from 10^1 to 10^9 m^2). The landslide volume computed using this procedure is based on some approximations, since they use geometric simplifications, but it does still reflect the magnitude of the process. The result of the computation in Figure 36 shows an almost bimodal distribution, in which most landslides (83%) have small volumes, lower than 10 million m^3 (with 63% lower than 1 million m^3), but 4% have value higher than 100 million m^3.

Each landslide is then classified by assigning two dimensionless values with the simple scheme shown in Table 12: a value of 2 is assigned if the computed landslide volume, V_l, is bigger than the boundary value V_l' (or V_l''), whereas a 0 is assigned if it is smaller. If the boundary value V_l' (or V_l'') is bigger than V_l but smaller than the V_l values increased by 20% ($V_l \times 1.2$) then is assigned a comparison value of 1. Following a cautionary principle, the V_l values increased by 20% ($V_l \times 1.2$) is used as an arbitrary value to prevent any possible underestimation during parameter computation and because a possible increase of landslide body size after the reactivation due to entrainment (Hungr and Evans, 2004).

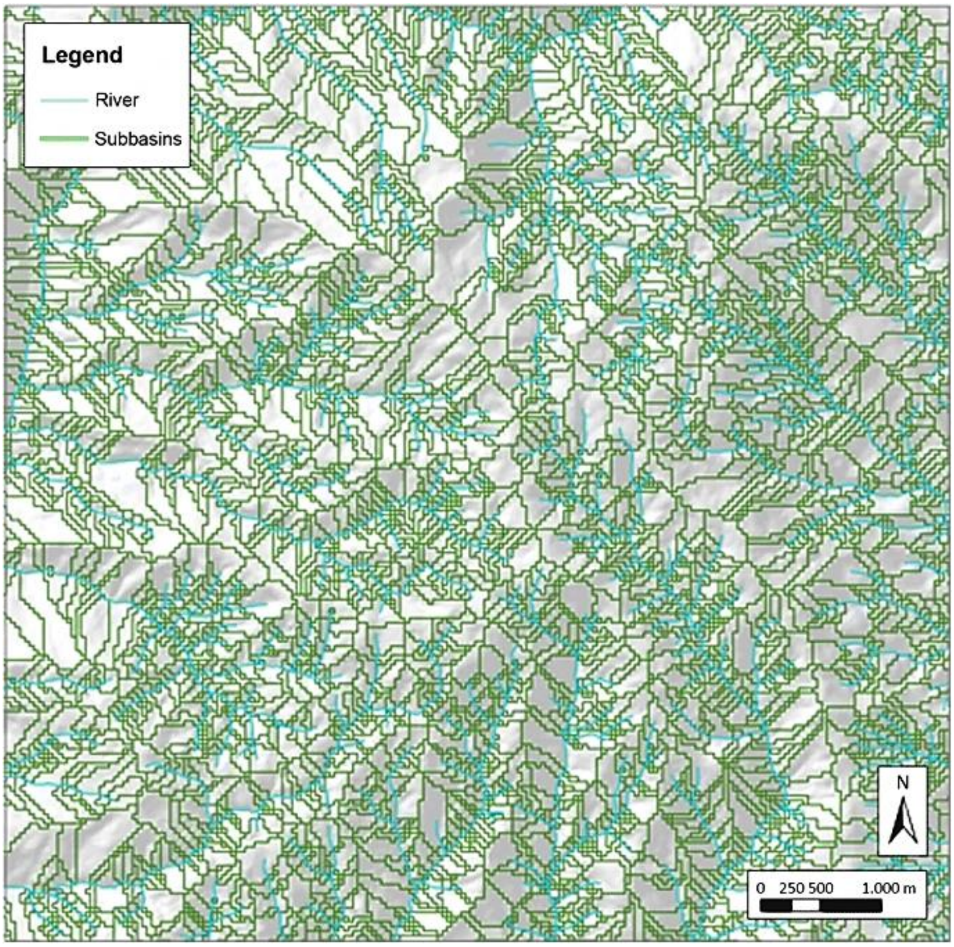

Figure 35. Watershed sub-basins for draining surfaces reconstruction.

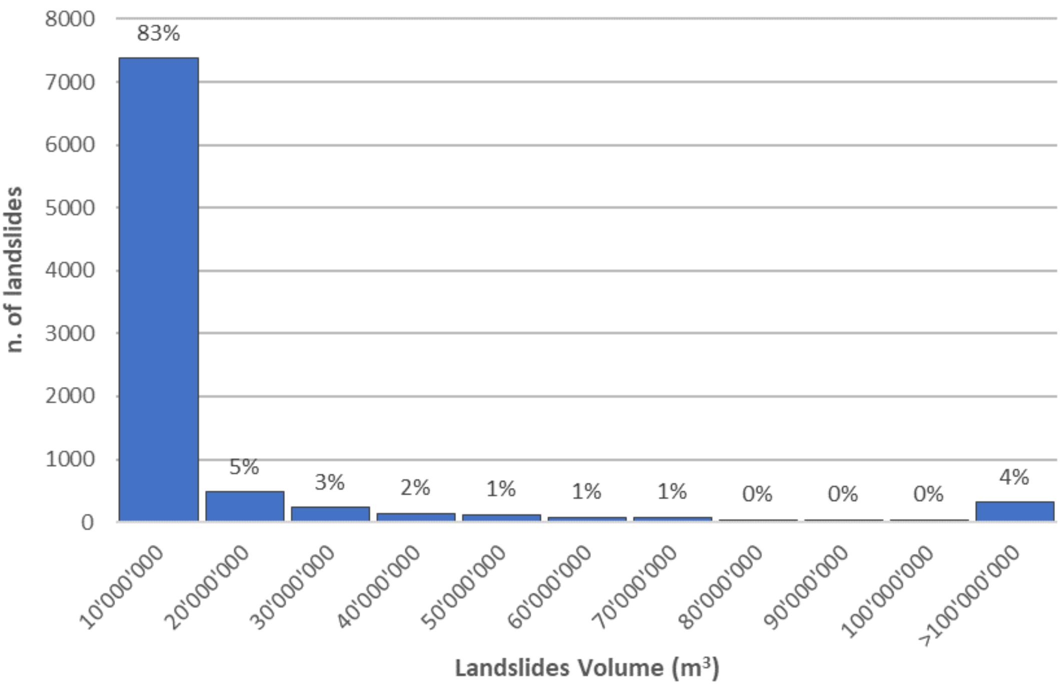

Figure 36. Landslide volumes frequency distribution in the central Asia regions.

A classification of the Damming Susceptibility for every mapped landslide is assigned through the combination of the two comparison values in the intensity matrix of Figure 37. The matrix divides the severity of the damming susceptibility in five classes of a qualitative scale, i.e., Very Low, Low, Moderate, High, and Very High, colored with dark green, light green, yellow, orange and red, respectively. The gray squares, corresponding with high V_l'' values (1 or 2) and lower V_l' value (0 or 1), are not possible combination, because V_l'' is always bigger than V_l' according to their formulation.

Table 12. Comparison table between landslide calculated volumes, V_l, with the boundary volume of Non-Formation and Formation, V_l' and V_l''.

	$V_l > V_l'$ (V_l'')	$V_l < V_l'$ (V_l'') $< V_l \times 1.2$	$V_l < V_l'$ (V_l'')
Value	2	1	0

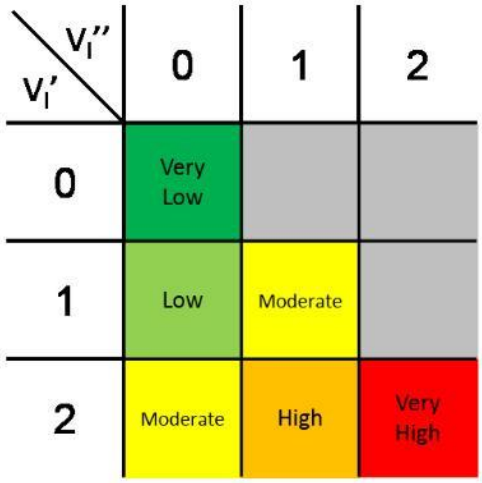

Figure 37. Predisposition matrix used for the assignment of the damming predisposition intensity to the mapped landslides.

5.2 Results

The assessment of Damming Susceptibility on the available landslide inventory is shown in the map of Figure 38, while a detail for the Kyrgyz Republic territory is reported in Figure 40. In the class distribution shown in Figure 39 the most frequent class is the Very Low, with 81% of the whole database, followed by the Moderate with 9% and the remaining percentage divided among Very High (7%), Low (2%) and High (1%) classes. This distribution is quite coherent with the landslide volumes frequency distribution since it is reasonable to associate landslides with very low volume (83%, shown in Figure 36) with those classified with very low susceptibility (81%, Figure 39). The landslides classified with the higher values of susceptibility (Moderate, High, and Very High with a total of 17%) instead do not only include landslides with higher volumes (more than 100 million m^3 representing 4% of the total), meaning that also even smaller landslides can potentially block narrow river stretches. The high number of landslide (644 cases) classified with Very High damming predisposition should be very concerning and in particular cases placed close to urban areas they should receive more attention and accurate analysis.

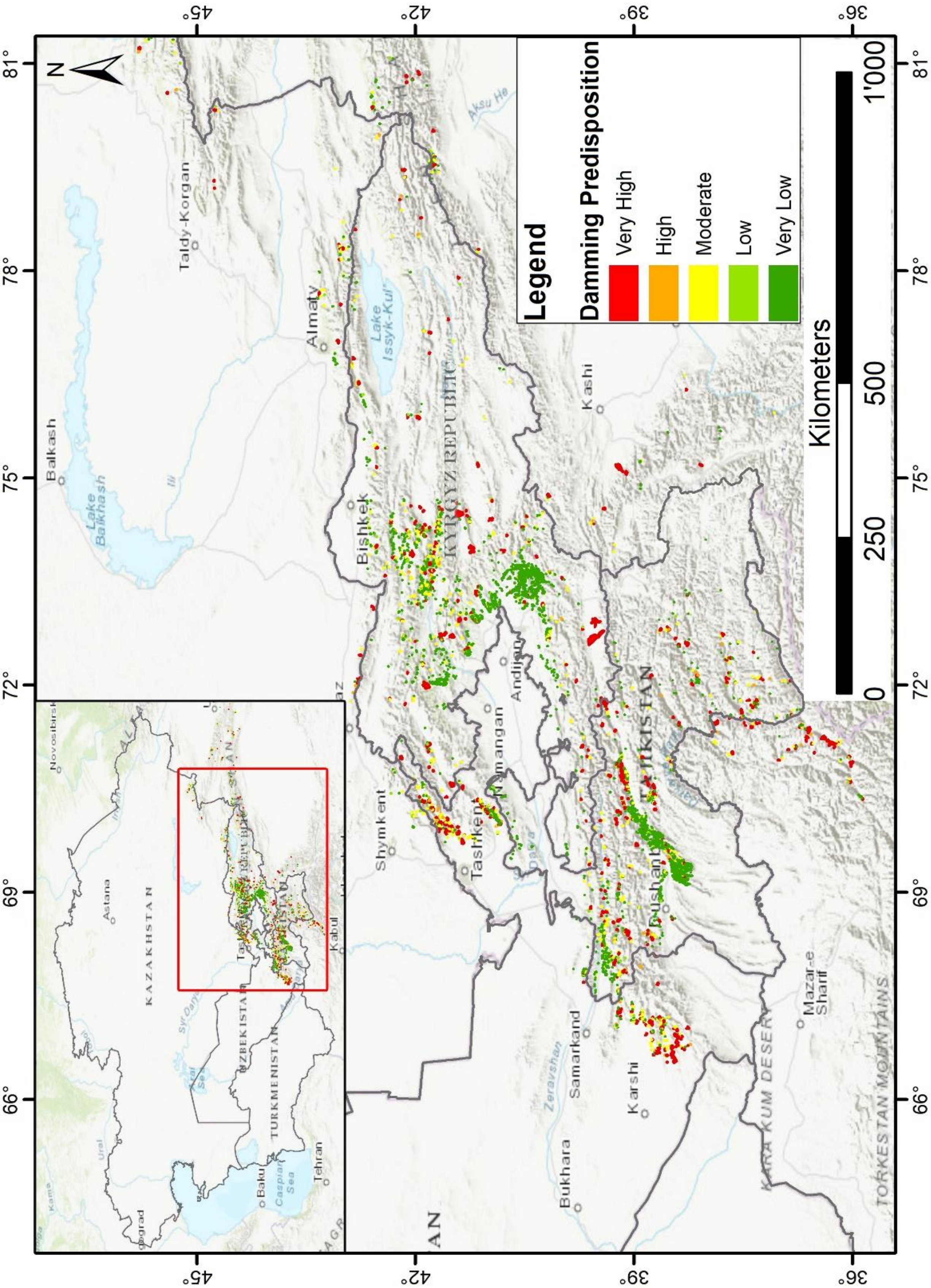

Figure 38. Map of Damming Predisposition by reactivation of landslides from the available inventories in Central Asia.

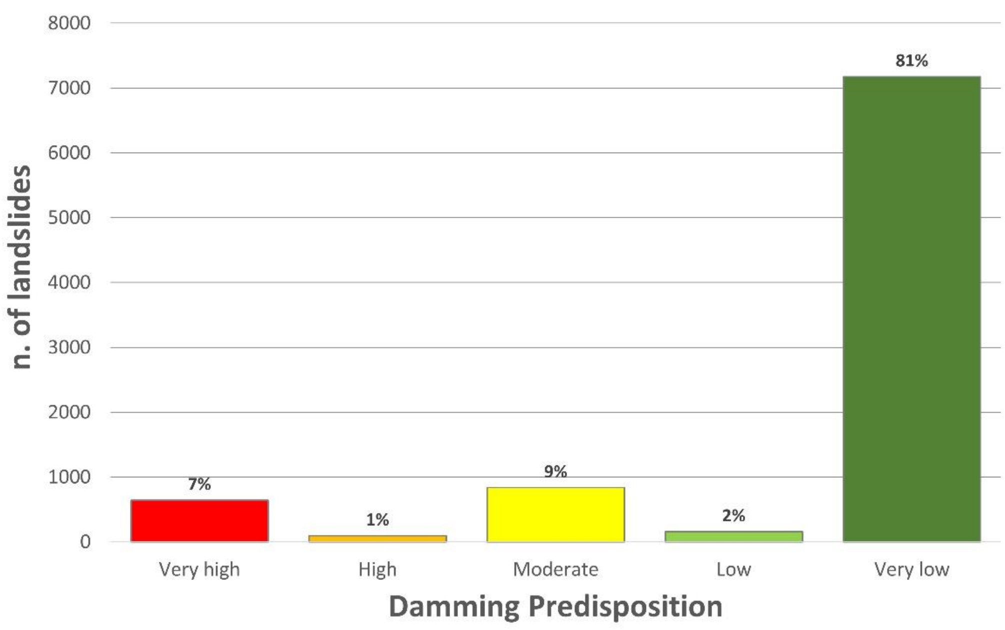

Figure 39. Classes distribution of the damming predisposition for landslides reactivation.

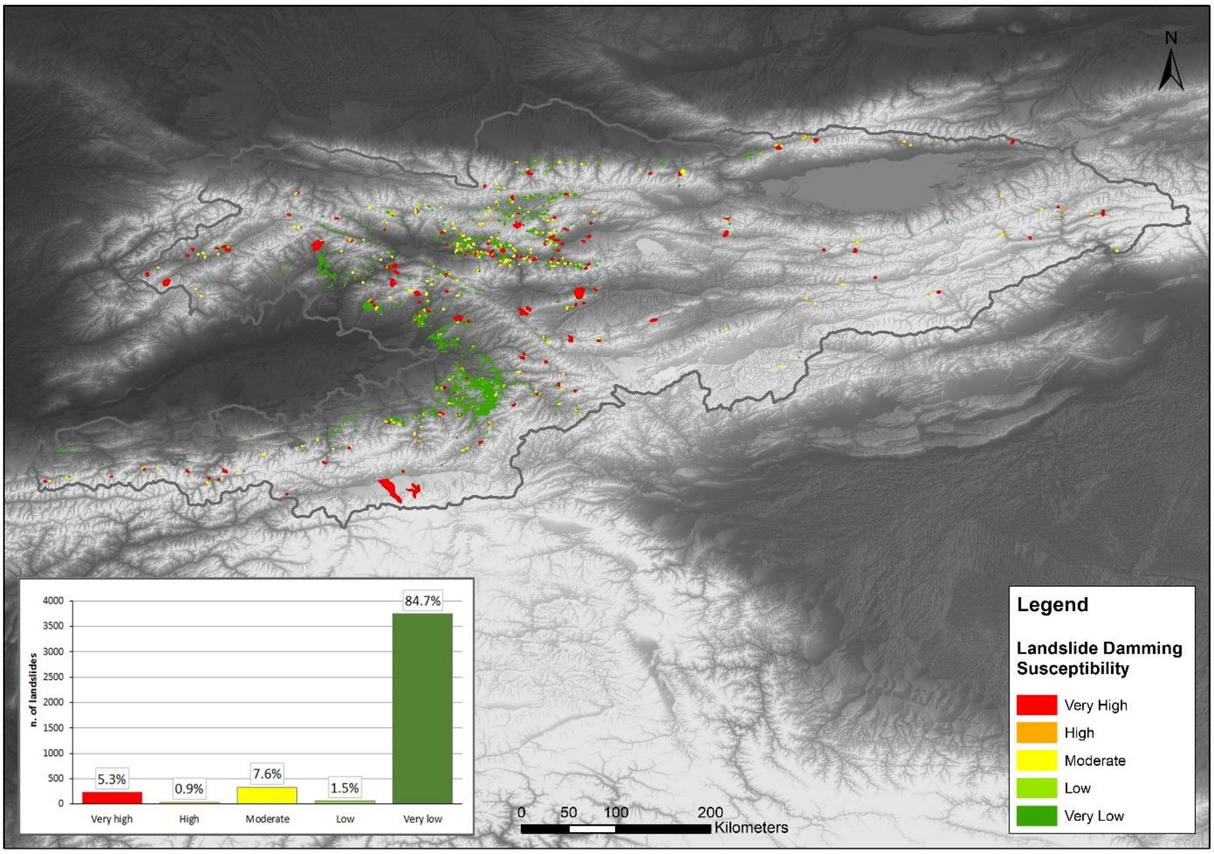

Figure 40. Map of Damming Predisposition by landslides reactivation in Kyrgyz Republic territory.

Concerning the damming susceptibility caused by new landslides along all the river network in the study area, two different maps have been produced using the Non formation and Formation volumes values.

Although counterintuitive, these maps provide complementary information. The former provides the volumes of landslides that surely create an obstruction, while the latter the volumes below which it does certainly not form. According to the preliminary steps of the described methodology, the river stretches running in flat areas (slope degree less than 4° representing the 88.4% of the entire river network) are not considered in the analysis because the procedure is not applicable. The magnitude of the damming susceptibility has been classified in five categories according to landslide volumes classes. The five volumes intervals describing damming susceptibility were decided according to general value distribution of landslides volumes and the expert judgement. Since small landslides are more frequent than large ones, as reported in Figure 36, the lower is the landslide volume required to realize an obstruction, the higher is the magnitude (Figure 41 and Figure 44). In the map of damming susceptibility related to the "Non formation", reported in Figure 41, the central classes, Moderate and Low are the most frequent with 4.4% and 5.8% respectively, as reported in Figure 42. This means that in most of the river stretches in the study area the minimum landslide volume able to potentially dam the riverbed is between the limit values of the two classes, from 2,5 to 25 million m^3. An example of close-up on the Tajikistan territory is reported in Figure 43. The following most frequent class is the Very Low with 0.8% and only a very small portion of the river stretches are classified as High and Very High with just 0.4% and 0.2% with a required landslide volume less than 2.5 million m^3. Regarding the map of damming susceptibility related to Formation values, Figure 44 shows slightly different results. The most frequent classes are the two lower ones, Low and Very Low with 4.4% and 6% respectively, as described in Figure 45, meaning that the minimum landslide volume to have the river valley dammed, with a confidence of 99%, has values bigger than 25 million m^3. A close-up on the Kyrgyz Republic is reported in Figure 46. Only just the 0.3% and 0.4% fall in the classes Very High and High damming susceptibility with a landslide volume required of less than 5 million m^3. The results for each country are shown from Figure 47 to Figure 51. The landslides of Tajikistan, Kyrgyz Republic, Uzbekistan and Kazakhstan regions have been classified according to damming predisposition (Figure 47-a., Figure 48-a., Figure 49-a. and Figure 50-a. In the Turkmenistan territory, it was not possible to assess any damming predisposition by landslides reactivation since the absence of any available landslide inventory. The results of Uzbekistan and Kazakhstan regions (Figure 49-a. and Figure 50-a.) are a bit different from Kyrgyz Republic and Tajikistan regions due to the different availability of landslide inventories and a different reliefs orographic structure and valleys morphology of the formers national territories. For a better comprehension of the damming susceptibility classification of the river network at the national level, the river stretches flowing in lowlands have not been considered in the analysis. Concerning the Damming Susceptibility of Non-Formation (Figure 47-b., Figure 48-b., Figure 49-b., Figure 50-b. and Figure 51-a.), the most frequent are Low and Moderate classes, followed by Very Low class. Fortunately, only very few river stretches have been classified as Very High and High. For the Damming Susceptibility of Formation (Figure 47-c., Figure 48-c., Figure 49-c., Figure 50-c. and Figure 51-b.) most of the rivers fall into Very Low and Low classes, followed by Moderate class. Only very few river stretches have been classified as Very High and High. The results of the Tajikistan territory are quite similar to the Kyrgyz Republic and Uzbekistan with which it shares a similar orographic distribution and morphology of the territory. Turkmenistan and Kazakhstan show a slightly different distribution with higher percentage on Moderate class in the Damming Susceptibility of Non-Formation and Low class in the damming susceptibility of Formation.

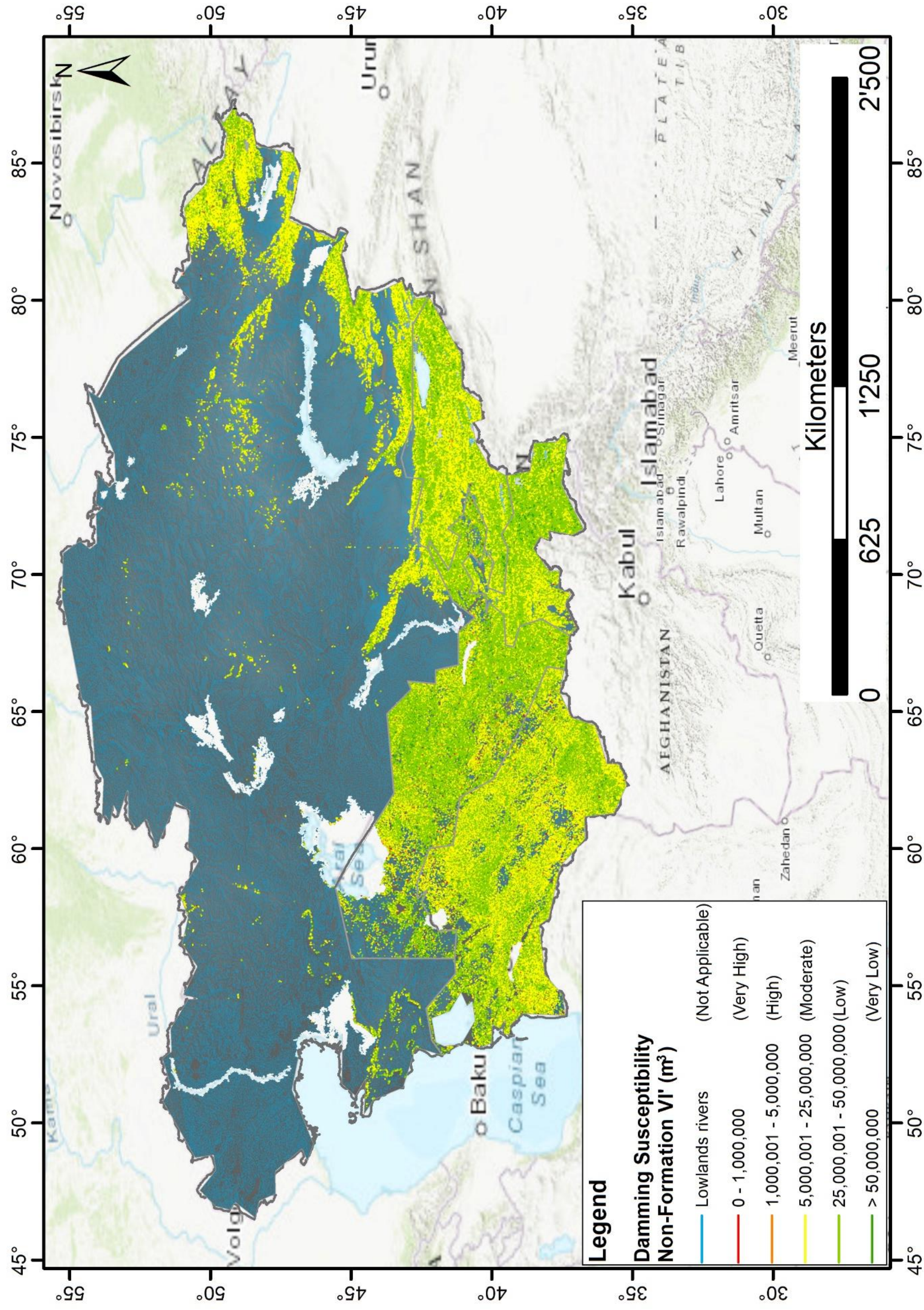

Figure 41. Damming susceptibility map of Non-Formation of river stretches by new landslides in the region.

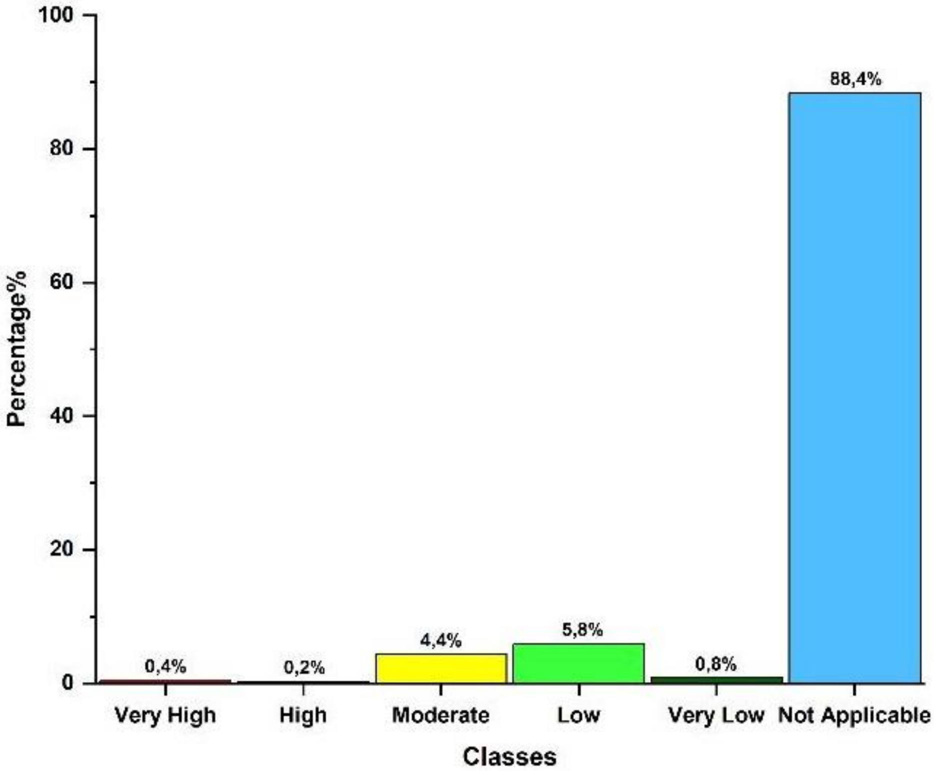

Figure 42. Distribution of the damming susceptibility in the study area by new landslides related to Non formation boundary values.

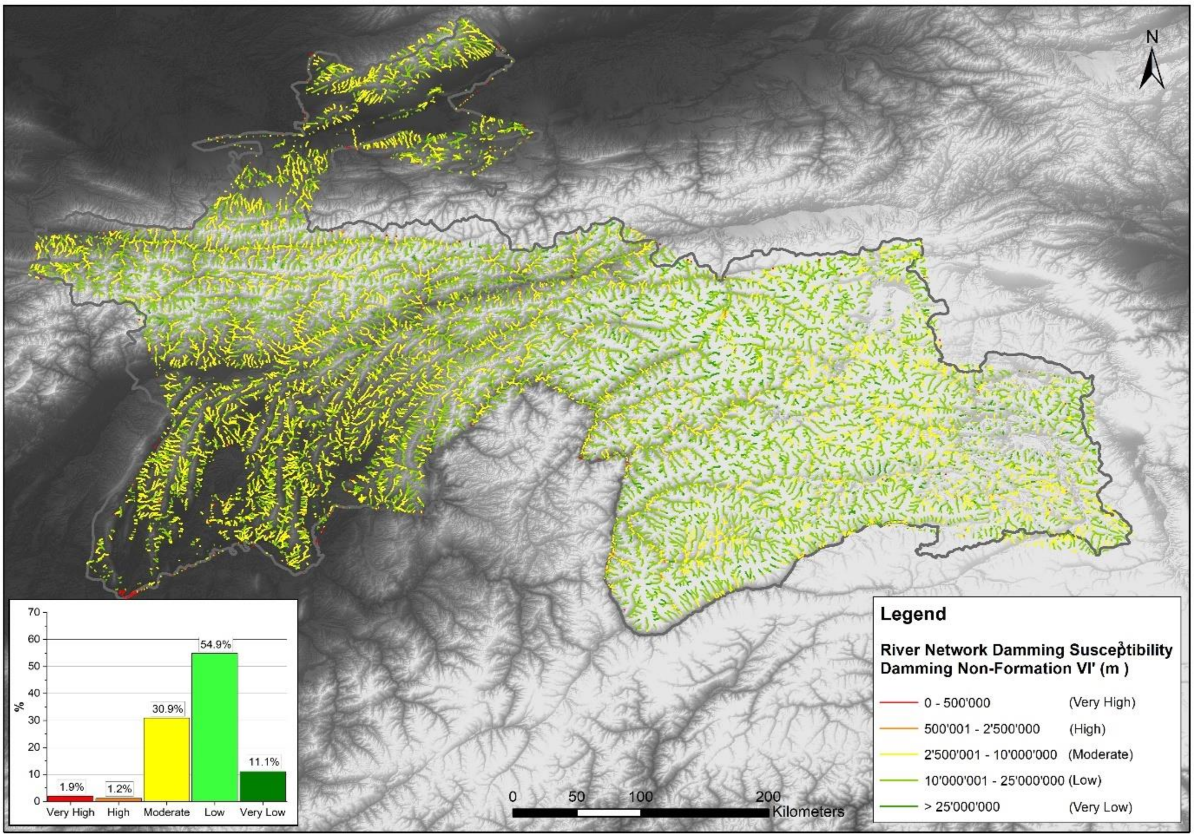

Figure 43. Damming Susceptibility Map of Non-Formation of river stretches by new landslides in Tajikistan.

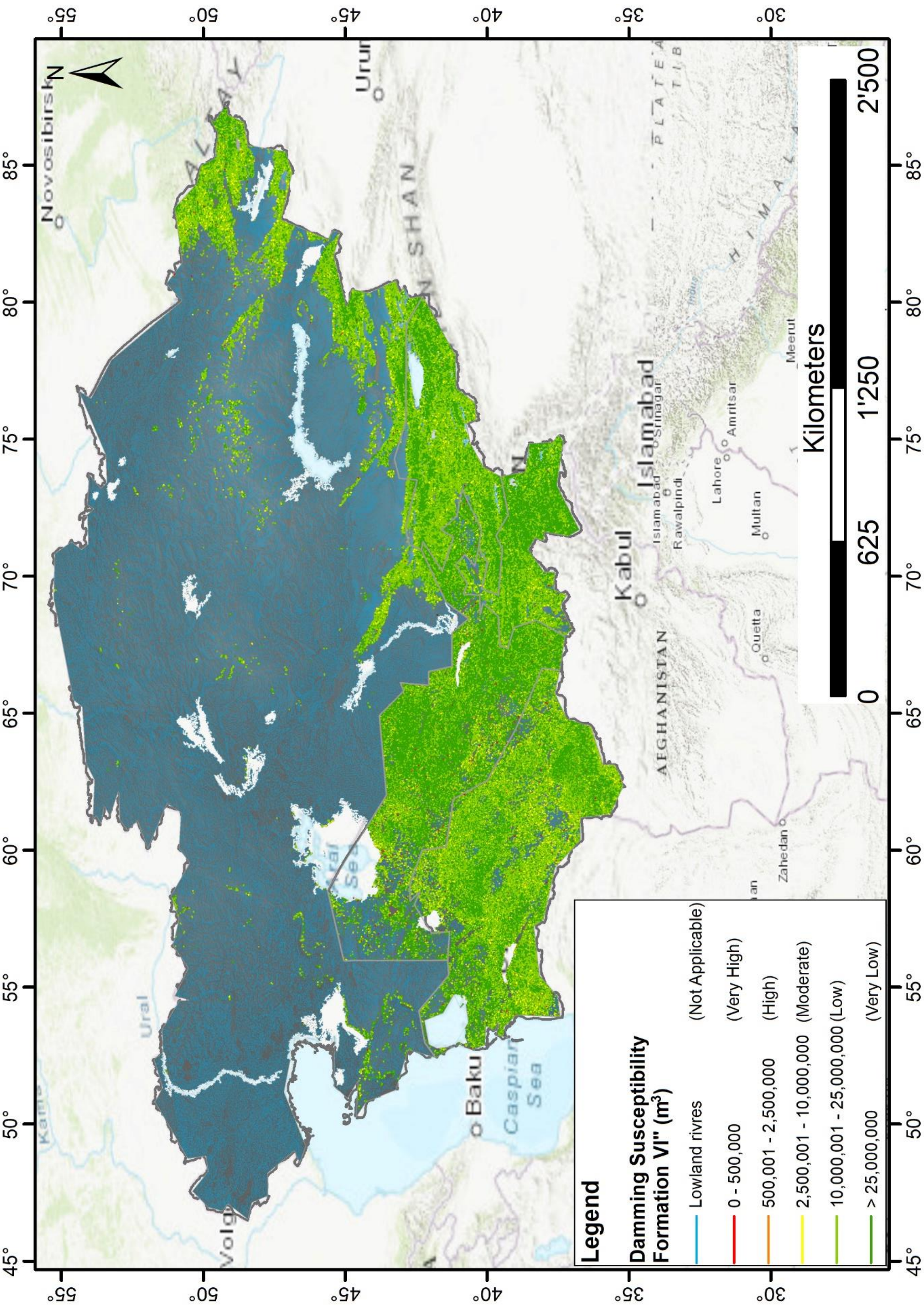

Figure 44. Damming Susceptibility Map of Formation of river stretches by new landslides in the region.

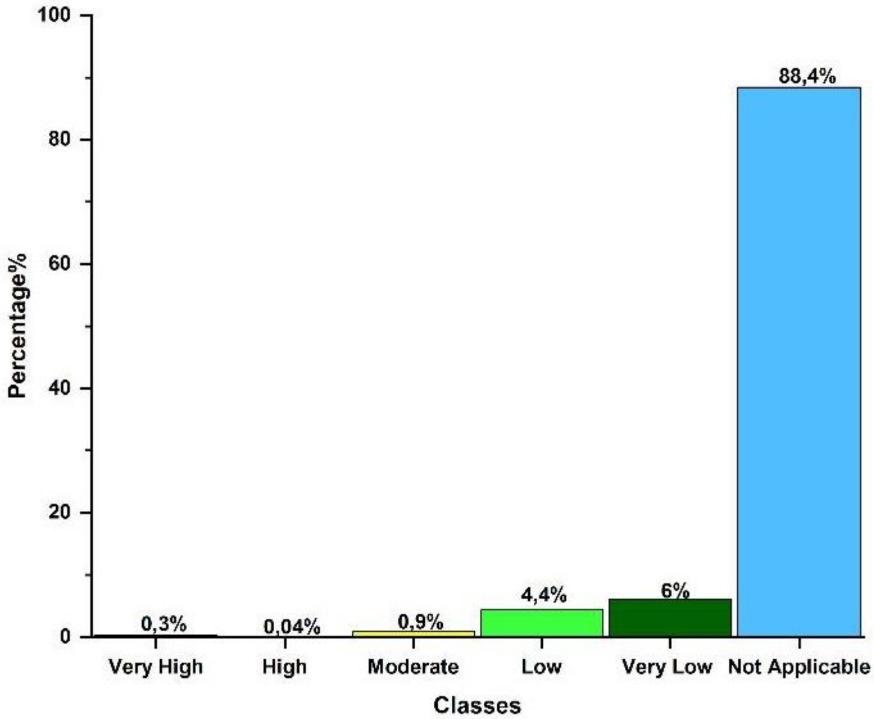

Figure 45. Distribution of the Damming Susceptibility in the study area by new landslides related to Formation boundary values.

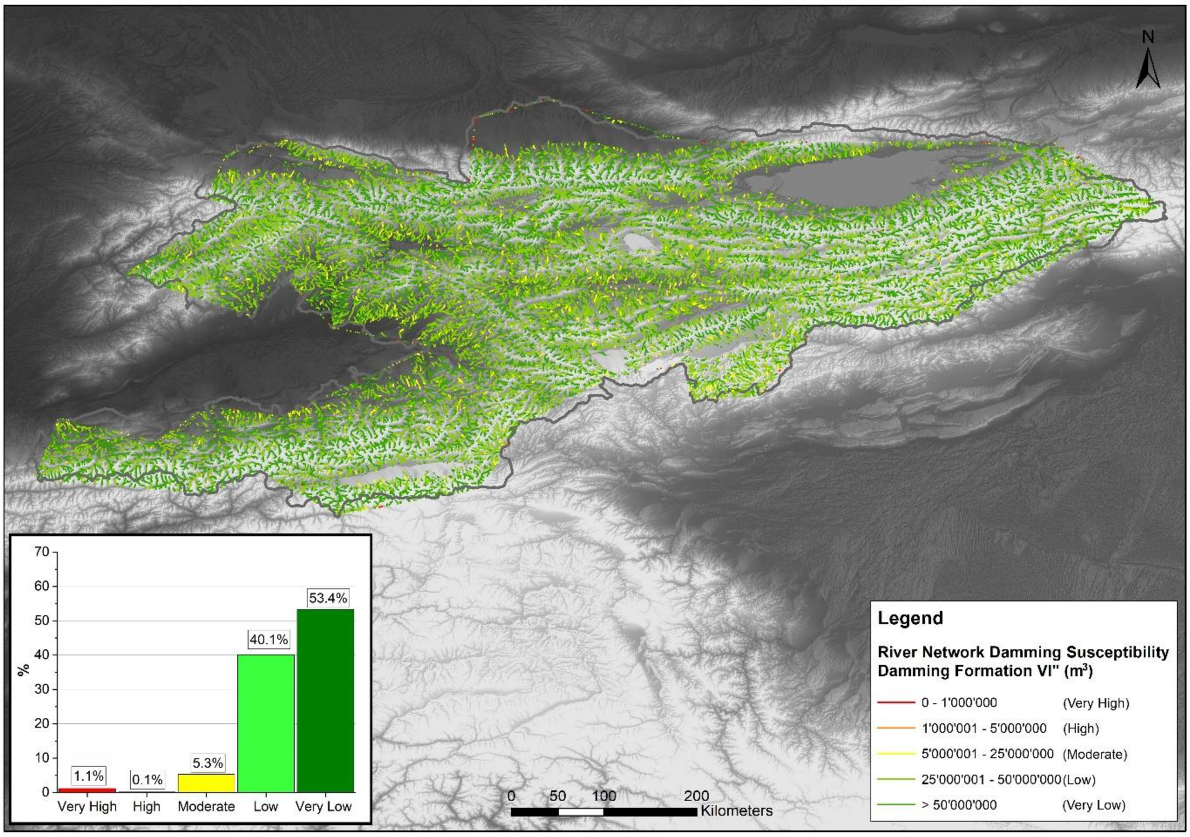

Figure 46. Damming Susceptibility Map of formation of river stretches by new landslides in the Kyrgyz Republic territory.

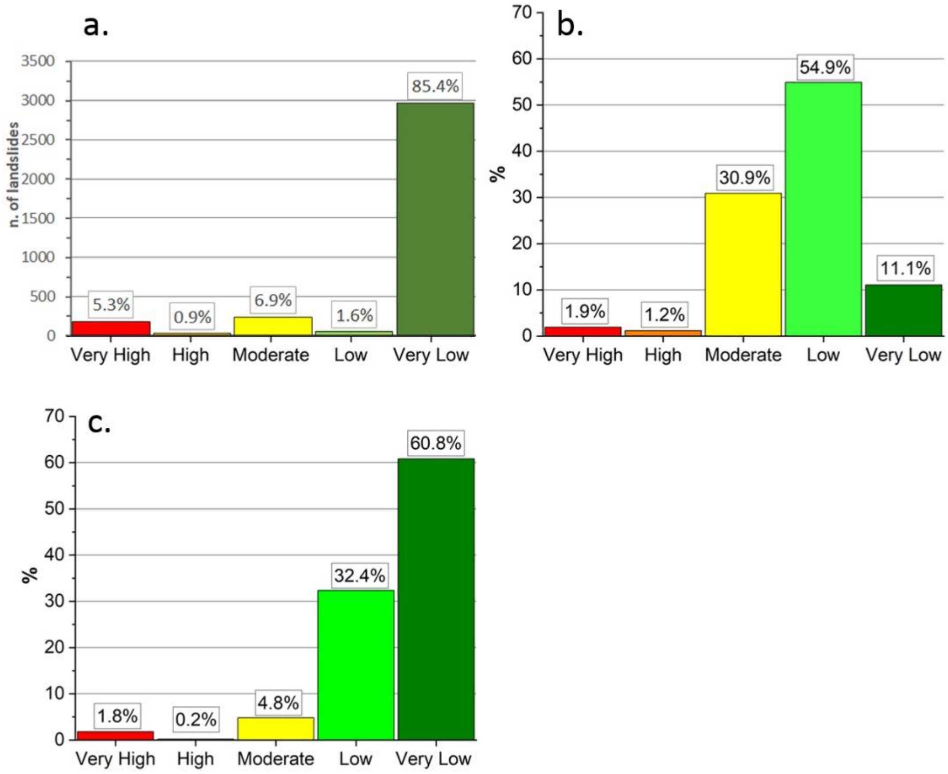

Figure 47. Classes distribution in Tajikistan of the Damming Predisposition for landslides reactivation (a.), Damming Susceptibility of Non-Formation (b.) and of Formation (c.) for new landslides.

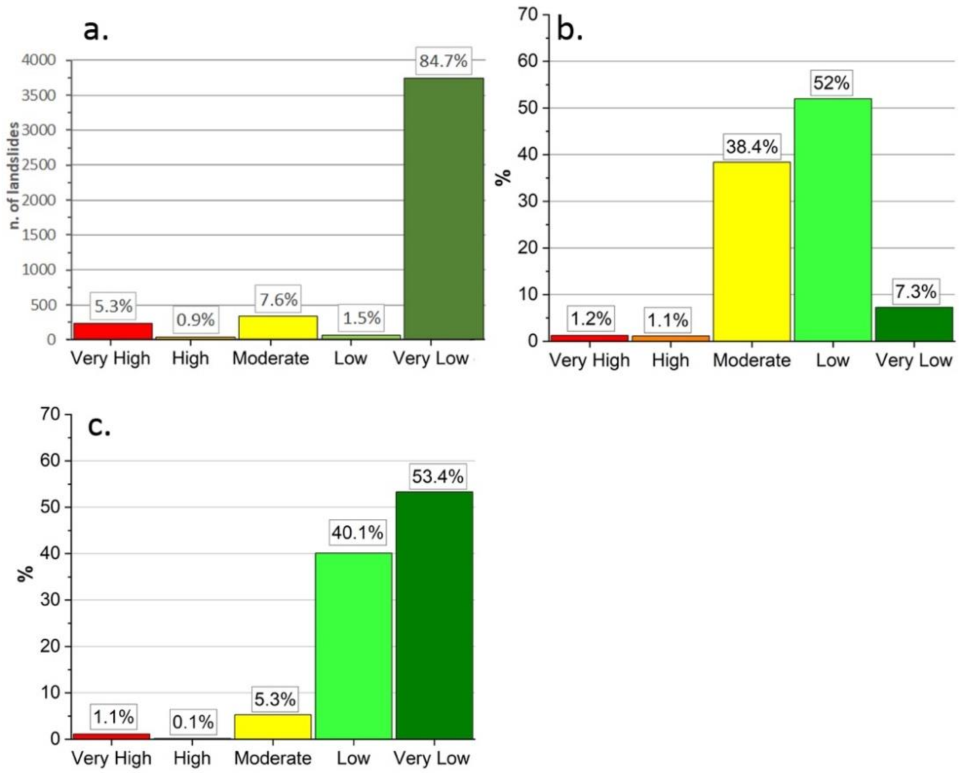

Figure 48. Classes distribution in the Kyrgyz Republic of the Damming Predisposition for landslides reactivation (a.), Damming Susceptibility of Non-Formation (b.) and of Formation (c.) for new landslides.

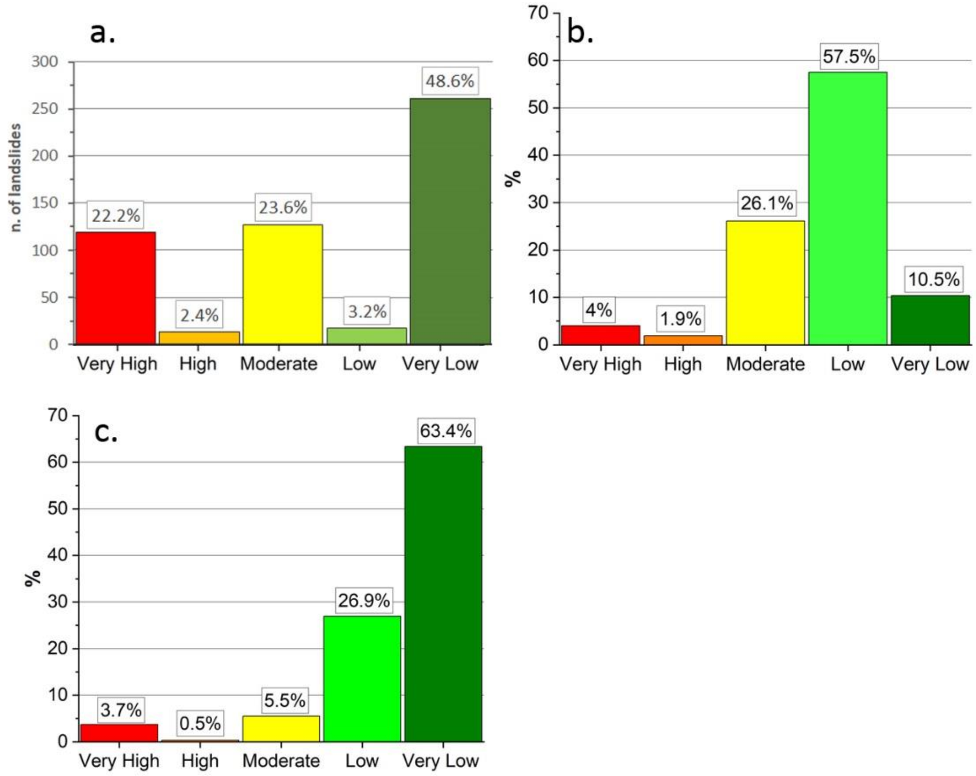

Figure 49. Classes distribution in Uzbekistan of the Damming Predisposition for landslides reactivation (a.), Damming Susceptibility of Non-Formation (b.) and of Formation (c.) for new landslides.

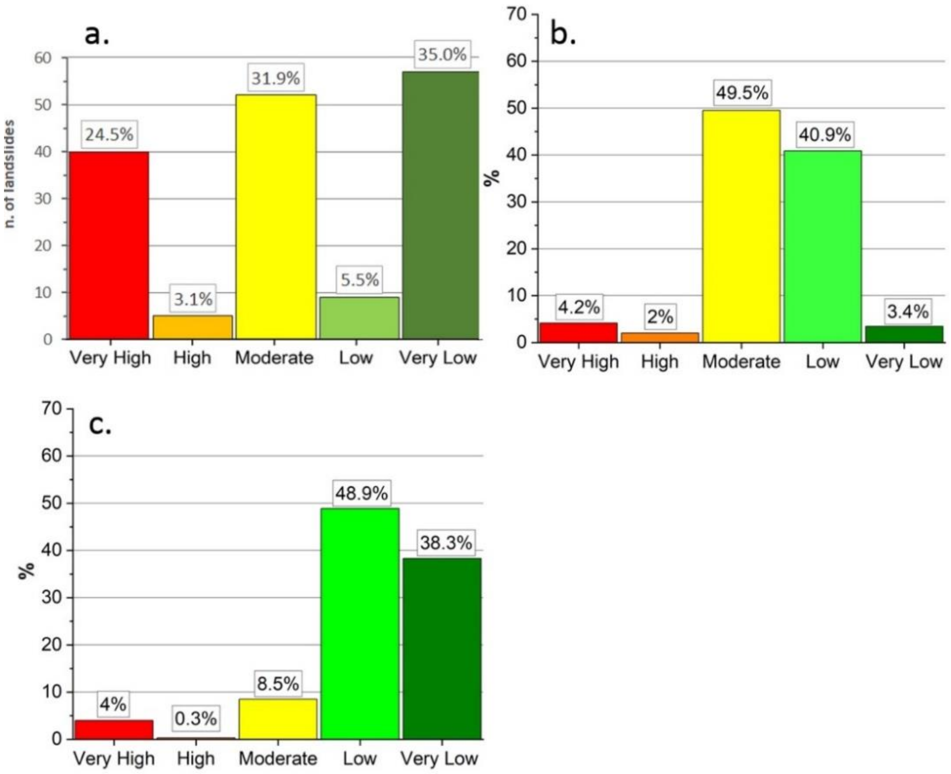

Figure 50. Classes distribution in Kazakhstan of the Damming Predisposition for landslides reactivation (a.), Damming Susceptibility of Non-Formation (b.) and of Formation (c.) for new landslides.

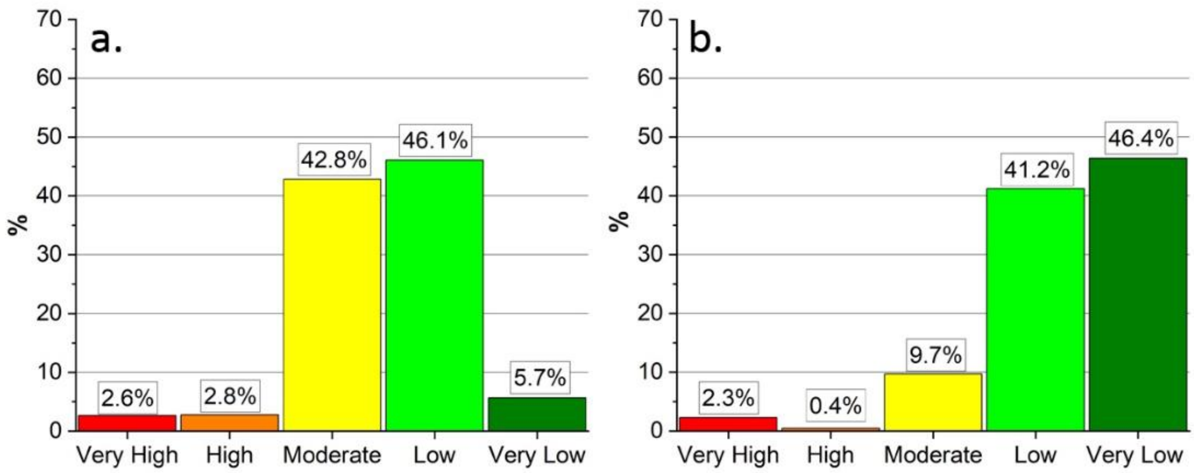

Figure 51. Classes distribution in Turkmenistan of the Damming Susceptibility of Non-Formation (a.) and of Formation (b.) for new landslides.

6 Landslide scenario assessment

In this section we report different landslide scenarios by addressing several potential landslide problematics in selected case studies, by using open-source tools, platforms, and software (SAGAGIS, Matlab, Copernicus Sentinel Hub EO Browser, ESA's Geohazard Exploitation Platform). In order to improve the effectiveness of the proposed scenarios analysis, we acquired the AirBus WorldDEM™. This kind of data is acquired by Tandem-x radar satellite and is a DSM (core basic version) at a 12m-resolution.

The landslide scenarios were developed as follows:

- Lake Sarez (Tajikistan): remote sensing techniques were applied to identify potential landslide areas along the slopes surrounding the Sarez landslide reservoir, and in particular the area surrounding the landslide dam. Potential and advantages of satellite InSAR will be demonstrated, especially for the creation of a reference baseline of ground deformation, which represents an added value for practitioners managing hazard in such a vast, remote and inaccessible scenario
- Mailuu Suu valley (Kyrgyz Republic): a simulation of the selected landslides, possibly evolving in flows was simulated, in order to assess their impact on the valley roads and buildings, and especially the uranium tailings connected the past mining activity
- Osh-Bishkek EM-02 Highway (Kyrgyz Republic): an assessment of the landslide impact on this key linear infrastructure, which has suffered in the past damage and interruptions due to slope instabilities, was performed in a selected transects of its mountainous section
- Upper Pskem river valley in Ugam Chatkal National Park (Uzbekistan): the landslide river damming potential was assessed in a mountainous valley, located upstream with respect to a series of artificially dammed reservoirs and a densely populated area, therefore constituting an area at high risk of landslide cascading effects
- The Fergana Valley mountainous rim (Uzbekistan, Tajikistan, Kyrgyz Republic): the potential transboundary landslide problems were assessed by analysing landslide susceptibility and river damming potential in the mountain rim surrounding the valley

The AirBus WorldDEM™ was used only in the first three case studies; in the last two it was not available, either for local restrictions (the Pskem river valley is a sensitive area due to its reservoirs) or due the large extension and consequent high costs (the Fergana valley), therefore, the SRTM DEM was used instead.

6.1 Lake Sarez

6.1.1 Introduction

Some of the existing landslide-dammed lakes in Central Asia can be considered stable and relatively safe; some other river blockages, on the contrary, represent a very high hazard, as catastrophic outburst floods can occur (Strom, 2010). Main concern is related to the occurrence of future large-magnitude earthquakes which could trigger material liquefaction and consequent collapse of the dam body, which, finally could unleash a catastrophic flood, which destructive power would be exacerbated within steep and narrow valleys.

Lake banks can be also scene of slope instabilities: large-scale failure may occur, causing huge waves that can overcome the dam or leading to dam's complete or partial breach. Long-term stability assessment of these dams and lake banks is of paramount importance as they represent a significant threat for the communities living there. Earth Observation (EO) data and remote sensing techniques can represent a valuable tool for assessing and measuring ground deformation at a wide scale, especially where remoteness and inaccessibility of the sites make field surveys extremely difficult. In this scenario, SAR (Synthetic Aperture Radar) techniques have a major role to play, as they have successfully demonstrated to be highly valuable in mapping land motion (Crosetto et al. 2016 and reference therein), allowing to measure surface deformations of wide areas with millimeter to centimeter accuracy and at a frequency varying between few to several days with most recent satellite platforms.

6.1.2 Background

To demonstrate capabilities of satellite InSAR in the field of landslide analysis, the Lake Sarez case study was selected. Area of Lake Sarez is a particularly relevant site, being (potentially) affected by different hazard (seismic, landslide, flood) and for cascading effects. Located in the Rushan and Murgab districts of Gorno-Badakhshan Autonomous Oblast (Pamirs, Tajikistan) along the Murghab River, the Usoi dam (Figure 52), is one of the most hazardous situations. The impounded Lake Sarez, with its 500 m of depth, is the world deepest landslide-dammed lake (Costa and Schuster, 1991).

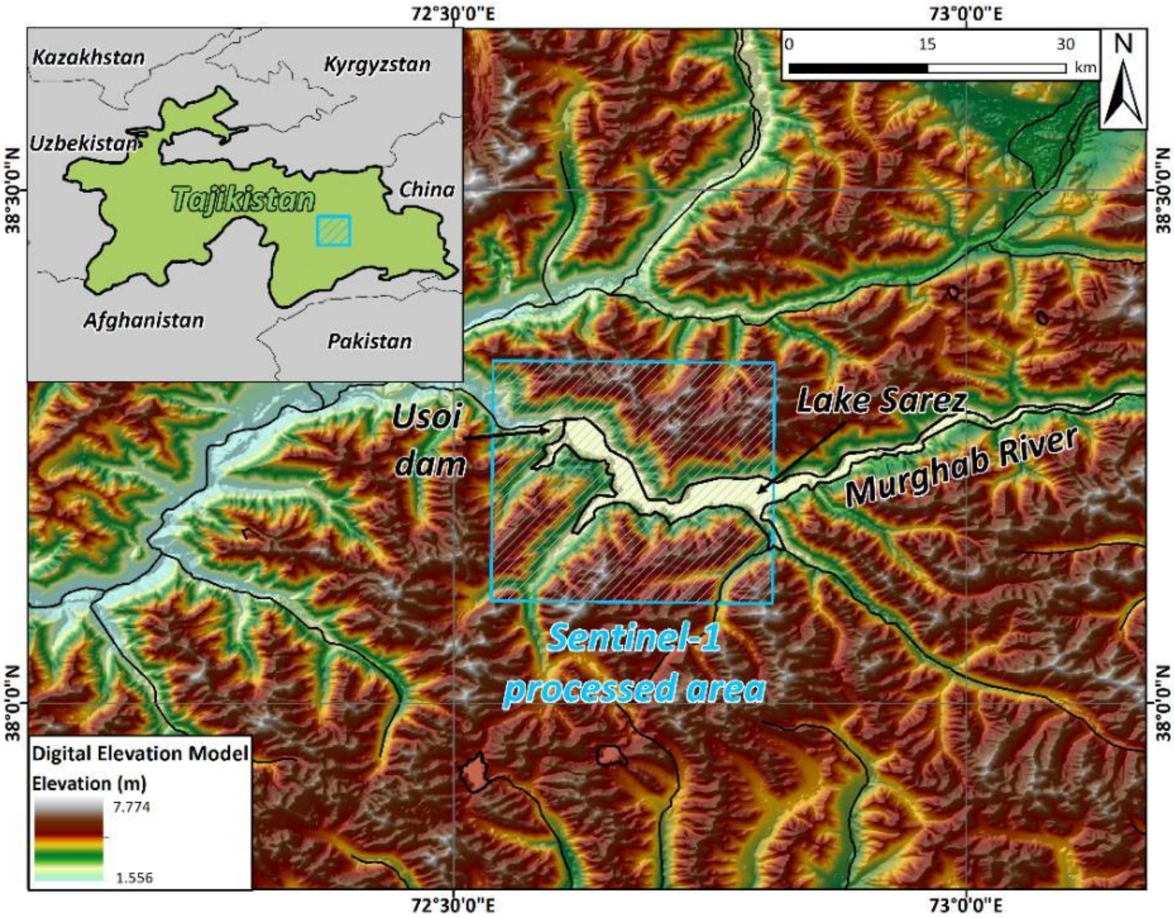

Figure 52. The Usoi dam and the impounded Lake Sarez in Pamirs.

The lake, 60 km long and with a stored volume of about 17 km^3, originated on February 18, 1911, when – triggered by a M_W 7.7 earthquake – a giant wedge-failure of about 2.2 km^3 of rock (mainly quartzite, schist, shale and dolomite) and debris blocked the Murgab River and a tributary valley, forming the 560 m high Usoi dam, impounding Lake Sarez and creating the smaller Lake Shadau. The blockage, named after the small village, that was buried with 54 inhabitants, is 5 km long and 4 km wide and blocks the Murghab River at an elevation of greater than 3,000m. The river was completely blocked without the capability to cut the landslide deposits to create a natural outlet. The water found its way through the landslide deposit in the form of a spring appearing about 140 m below the water level. Seepage water found its way three years later the impoundment, in 1914 (Strom, 2010) and significant filtration from the dam was observed from 1925.

The event drew immediately great attention, and, despite the inaccessibility and remoteness, Russian researchers started preliminary studies The extent of the Usoi catastrophe was not immediately assessed, nor was the time of occurrence of the Usoi landslide with respect to the Sarez earthquake (Шпилько Г.А. 1914). The first expedition of Preobrazhenskiy was sent to Lake Sarez in 1915 to perform mapping, geological and geodetic surveys. They estimated the volume (2.2 km^3) and the mass (6 × 1012 kg) of the landslide and their work 'Usoi avalanche' (Preobrazhenskiy, 1920) was published in 1920. In comparison to the landslide, the Pamir-Sarez earthquake itself attracted less attention from the scientific community until 1915, when Galitzin expressed the idea that there was no earthquake at all and that it was the landslide that was registered on the seismic records (Galitzin, 1915). Based on the data of Preobrazhenskiy (1920), Galitzin (1915) calculated the potential energy released by the landslide and concluded that it would be sufficient to produce the seismic amplitudes recorded on the Pulkova seismic station ∼3800 km away (Kulikova et al., 2016). Investigations became regular during the 1960s (Щеко А.И. and Лехантинов А.М., 1970).

These data remain relevant to the present day and the Usoi dam have received significant attention from the scientific community due to the enormous consequences a possible breach would entail (Papyrin, 2001; Kazakov, 2004; Ischuk, 2006). More recently, a Round Table dedicated to the 110th anniversary of the Sarez earthquake was held under the Government of Tajikistan on February 18th, 2021, in Dushanbe, witnessing the great attention of scientific community and local government. The Round Table discussed the implementation of a refined monitoring system and early warning system for Lake Sarez and proposed solution to minimize the risk for the area.

The lake level is currently rising at an average of 0.2 meters per year (Schuster and Alford, 2004), and approximately 50 to 60 m^3/sec of water leaks through the dam body (Risley et al., 2006), rising to 85 m^3/sec during flood periods when water level increases (UN International Strategy for Disaster Reduction, 2010). Seepage occurs through the uppermost, permeable part of the dam only, and seeping water forms powerful spring appearing about 140 m below the water level and created a canyon in the landslide dam. Secondary landslide occurs within the downstream slope of the blockage and are clearly marked by headscarps (Figure 53). In 1999, the International Decade for Natural Disaster Reduction Secretariat organised and led a mission to Lake Sarez to assess the risk and potential impacts. The field activities at the Usoi dam site and at the right bank of Lake Sarez resulted in several conclusions and practical recommendations.

Figure 53. Satellite view of Lake Sarez and Usoi landslide dam in Tajikistan: on the left view of the Usoi dam with seepage phenomenon in its body. Secondary scarps are also visible within the dam body. On the right location of the named "Right-bank landslide" (from Strom, 2010), whose failure may cause a surge wave in the lake.

While the danger of a general Usoi dam failure caused either by the water pressure, internal erosion or by seepage was found to be low (Ischuk, 2006), the hazard of an overtopping waves from new landslide masses falling into the Lake Sarez was considered more relevant (Strom, 2014 and reference therein). In particular, the "R*ight-bank landslide*", located about 4 km upstream of the dam represents a considerable concern (Figure 53). The landslide has a width along the lake shore of approximately 1 km. Estimated volume ranges from 0,3 to 2,0 km^3 (Schuster and Alford, 2004; State Committee on Emergencies, 1997, 1999). The huge range in the estimate of volume exists both because the thickness of the landslide is very uncertain and because potential movement (single, large, monolithic landslide or smaller individual landslides) is still unclear.

The area is characterized by high seismic activity (Ambraseys and Bilham et al., 2012), potentially leading the landslide slumping into the lake, creating a huge wave that could top over and possibly breach the Usoi dam, creating a destructive flood downstream. On 7 December 2015, an earthquake with a magnitude of 7.2 occurred in Rushon district of Gorno-Badakhshan Autonomous Oblast in Tajikistan, at 12:50 Tajikistan Local Time approximately 10-20 km from Sarez Lake and Usoi Dam in Tajikistan. After this earthquake, four aftershocks have been recorded near the lake.

Along the valley of Murghab River (also known as Bartang from the junction with Ghunda River just below the Sarez Lake) there are several villages along both side of the valley. The Murgab River is a headwater tributary to the Amu Darya River basin. In a worst-case scenario that assumes collapse of the dam (extremely unlikely), a catastrophic outburst flood from Lake Sarez would destroy the villages and infrastructure in the Amu Darya basin between the lake and the Aral Sea, endangering tens or possibly hundreds of thousands of people in the Murgab, Bartang, Panj, and Amu Darya valleys downstream across a distance of over 2000 km.

The people most endangered would be those in the villages and towns along the lower Bartang River in Tajikistan (Barchidiv, Supomji, Shojan, Rushan) and along the Panj River, which forms the Tajik Afghan border, because these mountain valleys are narrow and the people in them would have short warning times. An assessment of flood scenario is presented by Schuster and Alford, 2004. The general evaluation of the dam and the slope stabilities with detailed geotechnical studies and using modern methods and equipment were found necessary. Currently within the Lake Sarez Risk Mitigation Project, the dam and the lake banks are monitored closely.

The monitoring network and the early warning system are expected to protect the villages located along the Murgab and the Bartang rivers and reduce the vulnerability of the population to natural disasters, including the potential outburst of Lake Sarez.

6.1.3 Interferometric satellite analysis

Relying on active radar sensors, interferometric applications, a wide term referring to the exploitation of the SAR signals of at least two complex-valued SAR images (Bamler and Hartl, 1998), currently represent the most consolidated approach to measure and quantify ground deformation induced by landslides occurrence (Scaioni et al., 2014), as they have the unique ability to obtain measurements anytime, regardless of the time of day or season.

Among the several existing approaches, the Small BAseline Subset (SBAS) technique (Berardino et al., 2002) is one of the most used for processing long sequences of SAR imagery (Zhou et al., 2009). SBAS is designed to identify, within the observed scene, a grid of measurement points (MPs) corresponding to single pixel or groups of a few pixels exhibiting a stable radar signature over the entire observation period. MPs usually correspond to manmade objects, rocky outcrops and bare soil, which are characterized by high coherence values and are slightly affected by decorrelation phenomena. For each MPs it is possible to estimate displacement time series along the satellite Line of Sight (LOS) and a set of quality parameters. Common to conventional geodetic networks, all data are differential measurements with respect to a reference point that is assumed to be motionless. LOS deformation rate can be estimated with an accuracy in the order of few mm/year, at least for very stable MPs during a long-time span, while the accuracy of the single measurement in correspondence of each SAR acquisition ranges from few to several mm (Colesanti et al., 2003), depending on the type of adopted approach.

Satellite InSAR has been also widely used since the 1990s (Achache et al., 1996; Fruneau et al., 1996) to measure the spatial extent and the magnitude of surface deformation associated with mass movements (Solari et al., 2020). Multi-temporal approaches (MTInSAR) have demonstrated to be highly valuable in the analysis of a wide range of geological and geomorphological phenomena, including landslide-related events at different stages (Tofani et al., 2013a), becoming one of the most widely adopted and reliable methods for the remote detection of landslide. The ability to make numerous MPs over the landslide body allows the detection and mapping of the actively deforming slopes (Cigna et al., 2013), the characterization of landslide mechanism (Tofani et al., 2013b), the zonation of sectors with different velocities and behavior within the landslide area (Berti et al., 2013), the modeling of large slope instability (Berardino et al., 2003).

Satellite-based InSAR can be used to detect and map landslides in remote areas and in mountainous terrain or in general where deployment of ground-based instruments is not logistically feasible and where in situ activities are challenging. This aspect is important to map landslides without prior knowledge of their location (Bekaert et al., 2020) and stands particularly for areas with permafrost (Singhroy et al., 2007) or seasonally frozen ground (Hao et al., 2019), whose vulnerability to geohazards, including landslides, is expected to increase with rapid warming (Yao et al., 2019; Cui and Jia, 2015).

In the last two decades the use of interferometric applications has been fostered by the launches of several satellite platforms hosting sensors working at specific bands of the microwave domain, corresponding to different wavelengths (λ).

The most used bands in SAR applications are C-band (5–6 GHz, ~5,6 cm wavelength), X-band (8–12 GHz, ~3,1 cm wavelength) and L-band (1–2 GHz ~23 cm wavelength). An exhaustive list of SAR sensors is presented by Wasowski and Bovenga, 2014.

For the analysis of the ground deformation of the Usoi dam and Lake Sarez, the ESA (European Space Agency) Sentinel-1 constellation has been exploited. Launched in April 2014, the Sentinel-1 sensors opened new possibilities for InSAR applications. Developed within the ESA Copernicus initiative, the Sentinel-1 mission is a constellation of two twin satellites, Sentinel-1A and Sentinel-1B. They share the same orbital plane and offer an effective revisiting time of few days (six-day repeat cycle in Europe and other specific areas, globally twelve-days), which is extremely suitable for interferometric applications. With respect to previous SAR satellites, Sentinel-1 data exhibit some favorable characteristics: regional-scale mapping capability, systematic and regular SAR observations and rapid product delivery (typically in less than 3 hours from data acquisition). Sentinel-1 SAR products are freely accessible, thus providing the scientific community, as well as public and private companies, with consistent archives of openly available radar data, suitable for monitoring applications.

6.1.4 The GEP and Sentinel EO Browser platforms

The ESA's Geohazard Exploitation Platform (GEP)[12] and the Sentinel Hub EO Browser [13] are web-based platforms that allow users to perform analysis of satellite data via the Internet (Manunta et al., 2016). These platforms host several services to identify, monitor, and assess hazards that are associated with active seismicity, vulcanism, subsidence, or landslides, among others. The GEP platform has been exploited to assess ground deformation in the Lake Sarez area using the P-SBAS service (De Luca et al., 2015), specialized in producing velocity maps of the Earth surface by applying one specific advanced InSAR algorithm. The Sentinel Hub EO Browser was used to obtain Sentinel-2 satellite multispectral images representing the study area (Figure 54, Figure 57). The optical data represents the true colour study areas with a 10 meters resolution in the visible spectrum.

6.1.5 Results

To retrieve a ground deformation map for the Lake Sarez area, the images archive of the ESA Sentinel-1 C-band images (centre frequency 5.405 GHz and wavelength 5.6 cm) was acquired. Details of the Sentinel-1 datasets employed for the processing step are reported in the table included as inset in Figure 55.

The Sentinel-1 coverage was achieved by using track number 5 along descending geometry. The datasets used for the processing step included Sentinel-1A and 1B images, with an acquisition frequency of twelve days. Sentinel 1 images have been processed with the P-SBAS algorithm within the GEP platform as described above. The obtained ground deformation map is shown in Figure 55. MPs were detected and classified according to their mean annual velocities. Each measurement temporally and spatially refers to a unique reference image and a stable reference point.

[12] https://geohazards-tep.eu/#!

[13] https://www.sentinel-hub.com/explore/eobrowser/

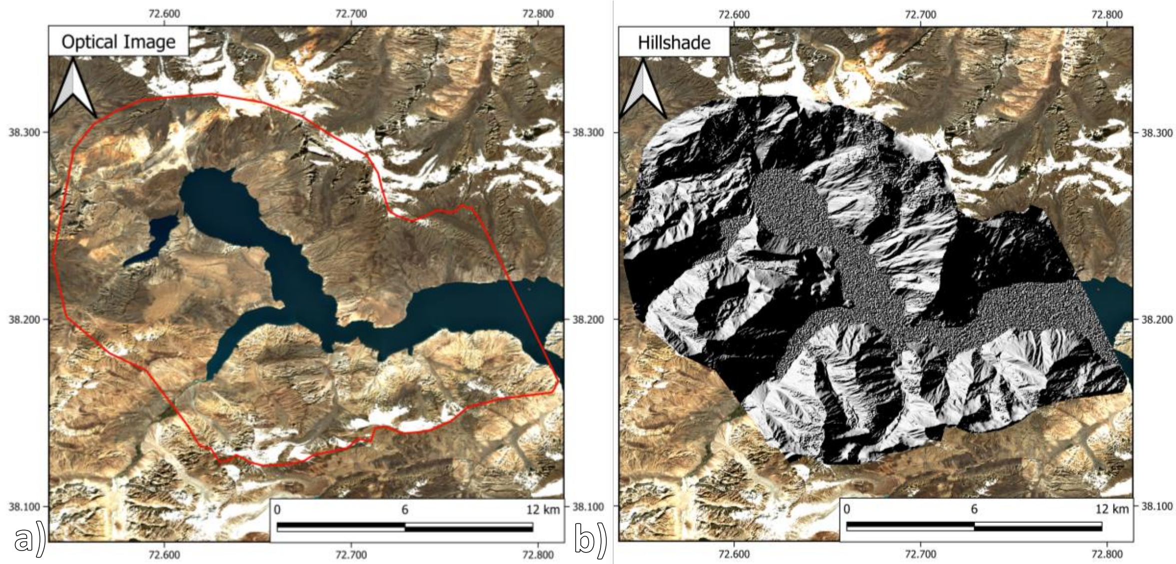

Figure 54. Sentinel-2 optical image (a) and WorldDEM hillshade (b) of the Area of Interest (AoI=346 m²).

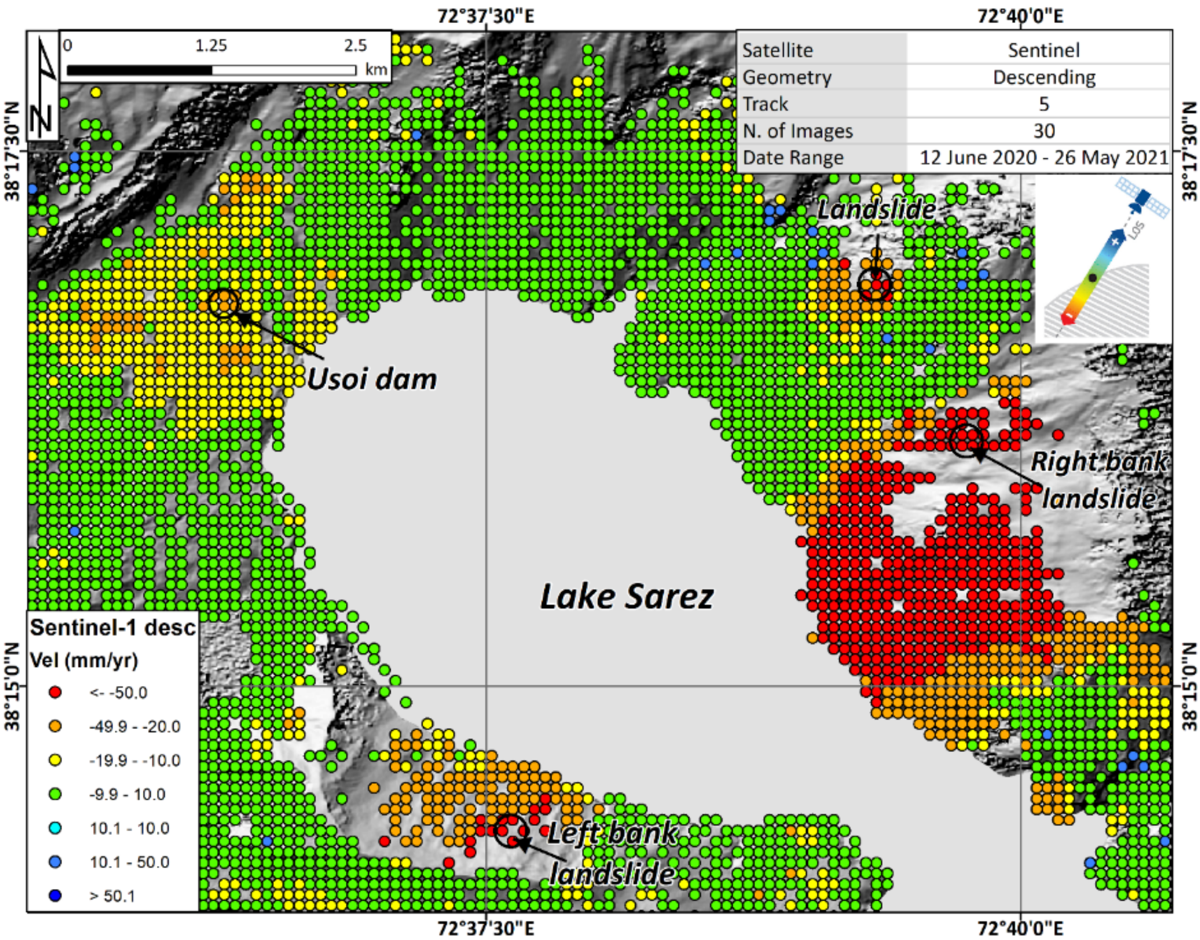

Figure 55. Sentinel-1 ground deformation map for the Usoi dam and the banks of the Lake Sarez. Active deformation can be spotted on both side of the lake banks and on the dam body. Black circle indicates MPs whose time series are reported in Figure 56. Red to yellow points (negative values) mean movements away from the satellite sensor, green means stable points, pale blue to blue points (positive values) mean movements towards the satellite sensor.

For each MP it is possible to estimate movements (and displacement time series) along the satellite LOS. This means that common to any radar application, satellite interferometry can measure only a component of the real movement, *i.e.*, its projection along the line of sight. Therefore, estimated velocity (classified with a colour scale in the map of Figure 55) resulted from the combination of geometry of acquisition of satellite and geometry of the slope (slope and aspect). In other words, as satellite InSAR is capable of tracking only the component of the movement vector projected along the sensor-target direction, a favourable orientation of the slope is required: the true entity of the displacements can be obtained when the slope moves exactly parallel to the LOS (approximately along east-west direction), whereas there is no sensitivity with respect to slopes that move perpendicular to the LOS (approximately along north-south direction). With several thousand of MPs, this map includes information that can be exploited to scan wide areas, flag unstable zones, and reconstruct the deformation histories of observed areas back to the first image of the time interval. P-SBAS results, covering the time interval of one year from June 2020 to June 2021, highlight the presence of active deformation areas affecting lake banks and, with minor magnitude, the dam body. Deformation data are consistent with the occurrence of gravitational movements. A geomorphological analysis using the World DEM with a 12 m resolution confirmed the presence of landslide phenomena.

The highest deformation rates (red points in Figure 56) were recorded in the right bank of the Lake Sarez, in correspondence of the landslide already detected and described by Strom, 2014 and Schuster and Alford, 2004. Here, velocity values range from -50 to -105 mm/yr. Negative values are related to measurement points that are moving away from the sensor, whilst positive velocities are corresponding to measurement points moving towards the satellite sensor. Measurement points with recorded velocities ranging from -10 mm/year to 10 mm/year are considered stable. In the upper part of the slope, NW of the “Right-bank landslide”, another smaller landslide is visible (ranging from -30 to -60 mm/year). Values of deformation are consistent with the south-westward movement of the slope. Also, a sector of the left bank is affected by active movement (ranging from -20 to -60 mm/year) related to landslide phenomena. It is worth highlighting that the landslide dam body is also affected by deformation, though of minor magnitude with respect to right and left bank (in the order of -15 mm/year). Here the deformation may be related to both secondary landslide’s occurrence (whose presence is marked by headscarps as highlighted by Strom et al., 2010) or to consolidation related to piping/seepage (whose evidence is visible in the form of water springs in Figure 53). In addition to the simple use of mean annual LOS velocities, landslide analysis can frequently benefit from the information provided by the deformation time series (TS) of each MP, in which ground movements are recorded with millimetric precision, acquisition by acquisition (Figure 56). TS represent the most advanced P-SBAS product and provide a deformation history over the observed period; they are fundamental for studying the kinematics of a given phenomenon and highlighting any changes that may have occurred during the monitoring period, such as sudden accelerations prior to a landslide failure.

In summary, P-SBAS results obtained within the GEP platform and covering the time interval from June 2020 to June 2021, highlight the presence of active deformation affecting both banks of the Lake Sarez and, though with minor magnitude, the Usoi dam body.

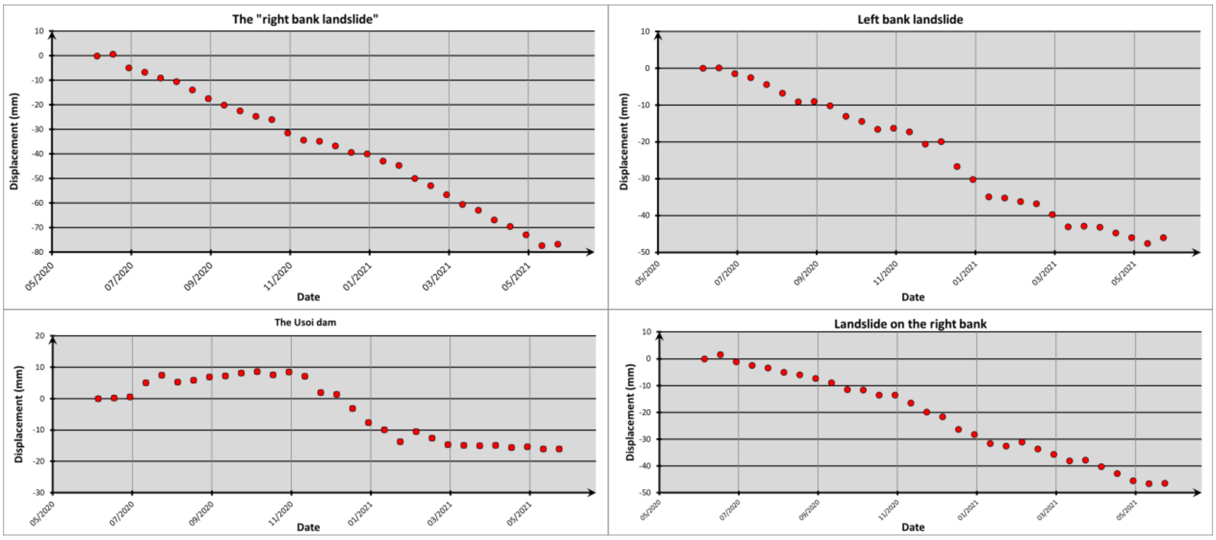

Figure 56. Displacement time series for MPs indicated in Figure 55.

Considering the characteristics of the processing, including the reduced time interval, image under-sampling with a 90 × 90 m of ground resolution and the unsupervised nature of the elaboration itself, obtained results can be valuable for detection and mapping ground deformation, though the estimation of the displacement can suffer from the above-mentioned limitations.

By using Sentinel-2 data it was possible to obtain a soil moisture index map to integrate the interpretation of the slope deformation data obtained by means of the Sentinel-1 SAR images (Figure 57).

Soil moisture maps were computed taking advantage of the Sentinel-2 multispectral data and the NSDSI index developed by Yue et al. (2019). The soil moisture index is based on a normalized difference ratio of SWIR region wavelengths (SWIR1: 1550nm-1750nm; SWIR2: 2100nm-2300nm) according to the following equation:

$$(B_{SWIR1} - B_{SWIR2})/B_{SWIR2}$$

The index takes advantage of different soil reflectance as a function of soil water content. Nevertheless, the index proved to be effective in the remote sensing of soil moisture for soils less than <50% saturated (Yue et al., 2019). The index output therefore represents soil moisture based on soil reflectance. From the image analysis it is clear how there is an ongoing seepage occurring in the Usoi Dam, which could justify the deformation rates measured by the SAR sensor. Alternatively, these latter could be caused by the settlement of the dam incoherent material.

The performed analysis indicates that satellite radar data, systematically acquired over large areas with short revisiting time (as those provided by Sentinel-1), could be used not only as a tool for mapping unstable areas, but also for landslide monitoring. Large-scale displacement monitoring can become a valuable tool for assessing the stability of slopes, particularly when the difficult accessibility of the site or the lack of clear indicators of instability make specific monitoring not feasible or look as not necessary.

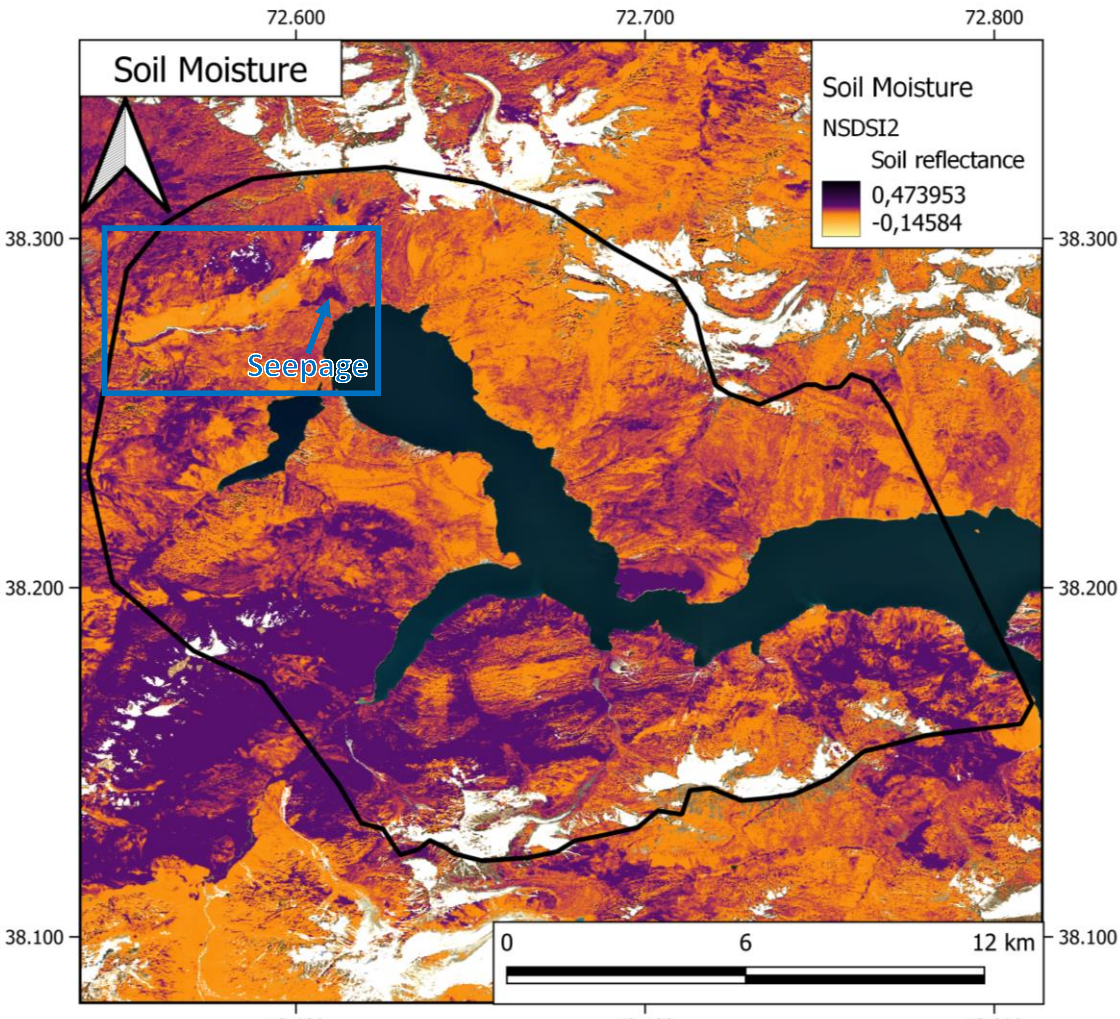

Figure 57. Map of the soil moisture index obtained by Sentinel-2 data.

6.2 Mailu Suu Valley (Kyrgyz Republic)

6.2.1 Background

The aim of this study was investigating the recent behaviour of selected landslides along a 115 km^2 sector of the Mailuu-Suu-Valley and outlining the involvement of risk elements, as roads, buildings and nuclear tailings using the GPP model (Section 6.2.2). The Mailuu-Suu Valley is mainly mountainous with peaks reaching 4400 m a.s.l., with 530 km^2 catchment area between 600 m a.s.l and 4400 m a.s.l, and it is characterized by semi-arid climatic conditions and land cover is mixed woodland-grass (Piroton et al., 2020). The Valley is situated in the north of Fergana Basin (Schlogel et al., 2011) (Figure 58a) and is characterized by a moderate to high seismic hazard (Abdrakhmatov et al., 2003). The central part of the valley is made up by core of the open anticline are made of soft siltstone and sandstone (Cretaceous rocks) overlain by alternating Paleogene to Neogene claystone and limestone; the Paleogene limestone was exploited mainly for mining uranium deposits (Schlogel et al., 2011). On the basis of the available inventories, within the Mailuu Suu area 190 landslides were detected (Havenith et al., 2015a) (Figure 58a, b).

Several studies and field observations confirmed that landslides are generally located within soft sediments composed of clay material or loess overlying the limestone layers (Paleogene-Neogene) (Schlogel et al., 2011, Piroton et al., 2020). Along the Mailuu-Suu Valley the number of large landslides clearly increased from 1950 (0.5 km^2, almost 1%) to 2003 (4.7 km^2 almost 10%), after the start of uranium mining activities in 1946, causing, in some cases, significant damages and victims. The link between the mining and landslide can be explained by consequent abandonment of mines in 1968. In fact, many slope failures were induced by: 1) collapse of underground galleries; 2) possible rise of ground water (Havenith et al., 2006).

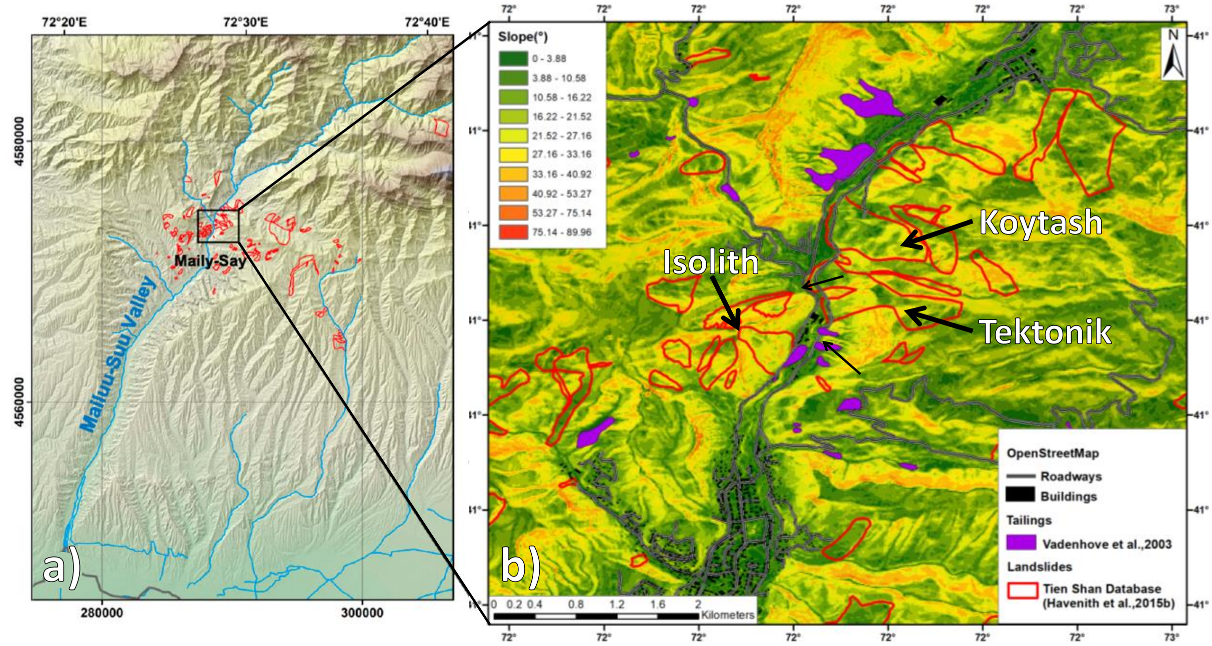

Figure 58. Location of the target area within the Mailuu-Suu Valley on the TanDEM-X hillshade (spatial resolution: 12 m; after Piroton et al., 2020). Study area setting: landslide inventories after Havenith et al., 2015a (red polygons), uranium tailings after Vandenhove et al., 2003 (purple polygons), roadways (grey lines) and housing from the Streetview database (grey polygons).

During the 1990, three of the largest landslides of the Mailuu-Suu Valley (Koytash, Tektonik and Isolith) located near core of the central anticline, displaced more than 5 million m^3 of material, representing the greatest threat for the destabilization of some nuclear waste uranium tailings (Havenith et al., 2017; Torgoev et al., 2012) (Figure 58b). The most recent and most intense activation occurred in spring 2017 with more of hundreds of landslides have been triggered or reactivated with estimated total volume of more than 82 million m^3. The recurrent activation of mass movements is mainly observed during the spring season, in combination between geological and climatic factors (Piroton et al., 2020). The types of landslides that are most detected are fresh earth flows, debris flows, and debris falls (Schlogel et al., 2011). Previous studies identified the Mailuu-Suu Valley as one of the regions of the Central Asia particularly prone to slope instabilities (Aleshin and Torgoev, 2014). In the past, landslides have often blocked the main Mailuu-Suu River and some of its tributaries (Havenith et al., 2006). Furthermore, the population growth also provides more pressure on the fragile landscape and makes the study area more vulnerable to landslide (Li et al., 2021) (Figure 58b). Therefore, it is essential to monitor landslides and to analyze related mechanisms in order to reduce and prevent the negative socioeconomic impacts linked to these natural hazards (Piroton et al., 2020).

6.2.2 GPP model

The intensity of the impact of potential earth flows was assessed using the Gravitational Process Path model (GPP) by Wichmann, 2017. It is an open-source code working in a SAGA-GIS environment. The GPP model simulates the path of gravitational processes, for instance debris flows, avalanches and rockfalls, or snow avalanches. This model combines several approaches to estimate and simulate the movement of a mass point from an initiation site (source area) to the deposition area on a Digital Terrain Model (DTM), by integrating components for process path determination, run-out calculation and sink filling. For each of these components, several algorithms modelling are implemented. This makes it possible to concatenate modelling approaches as required to simulate the behavior of a certain geomorphological process or to use suitable approaches with regarding to the available input data.

In detail the GPP model consists of stochastic models (Random walk, Markov chain, Monte Carlo simulation), physically based models and empirical approaches. The currently implemented modelling approaches are not entirely physically-based, but are built on empirical and basic principles to simulate typical macroscopic characteristics of mass movements. Nowadays, several physically based numerical simulation models are available with a very high level of precision, but requiring many geotechnical parameters, while, some modelling approaches, included in the GPP model, are based on minimum of input data and it is their complex interaction which permits the delineation of the extent of gravitational process areas. The model can be used especially for susceptibility mapping on regional scales.

Depending on the scale detail, the model considers different input data: same terrain parameters, source area and a DTM. For example, for a simple case, only a digital terrain model and a friction angle can be used. Based on the type of event and the characteristics to be outlined, the model and consequently the parameters are chosen. In general, three types of models describe the gravitational process evolution: 1) Process path modelling with Maximum slope (O'Callaghan and Mark 1984) and Random walk (Gamma, 2000); 2) Run-out modelling with Geometric gradient (Heim, 1932), Fahrboeschung principle (Heim, 1932), Shadow angle (Hungr and Evans, 1988) or Mono-bi parametric model (Scheiddeger, 1975; Perla, 1980); 3) Deposition modelling with Sink filling (Gamma, 2000); On Stop (Wichmann, 2017); Slope and-or velocity based (Gamma, 2000). The various modelling approaches and components adopted make it possible to apply this procedure to different geomorphological aspects and processes, predicting multiple event scenarios.

6.2.3 Calibration

The Gravitational Process Path (GPP) should be calibrated on one well-known landslide with source area and deposition area. The model through successive iterations affords to approximate the gravitational process, by deriving some parameters which can be the cause of the trigger of mass movement. These parameters are: i) the slope threshold below which divergent flow is allowed; ii) an exponent for divergent flow, which controls the degree of divergence; iii) a persistence factor, which can be used to preserve the direction of movement. Therefore, from the modelling of a well-known landslide, it is possible to retrieve some values to apply in other areas with conditions of potential instability. Two landslides have been chosen to calibrate the GPP: Tektonik and Koytash. Both of them are well-studied and their activity is controlled by many factors, such as the loess cover in the upper part, and the natural groundwater conditions that can make them unstable (Havenith et al., 2006, Schlogel et al., 2011, Giorgio et al., 2015, Piroton et al., 2020). Both landslides involve soft siltstone and sandstone (Cretaceous rock). Tektonik is a complex (multirotational) and flow-like landslide, while the Koytash landslide is characterized by a roto-translational movement; its landslide body slides along Paleogenic limestone basement with slope steeper than the ground surface. Some translational sliding occurs above the limestone along the internal Paleogenic clay layers, while the base of the landslide is more than 50 m deep (Piroton et al., 2020). Piroton et al. (2020) demonstrated that the number of landslides in the valley is increasing, with predominance of the reactivation and enlargement of existing landslides. Significant concentration of rain and the sudden snowmelt can contribute to the water saturation, increasing the pore pressure and thus the mobility of the sediments. Furthermore, the landslides are located on steep slopes with overhanging mountains from where surface runoff also flows after the snow melts and intense rainfall (Figure 59; Piroton et al., 2020).

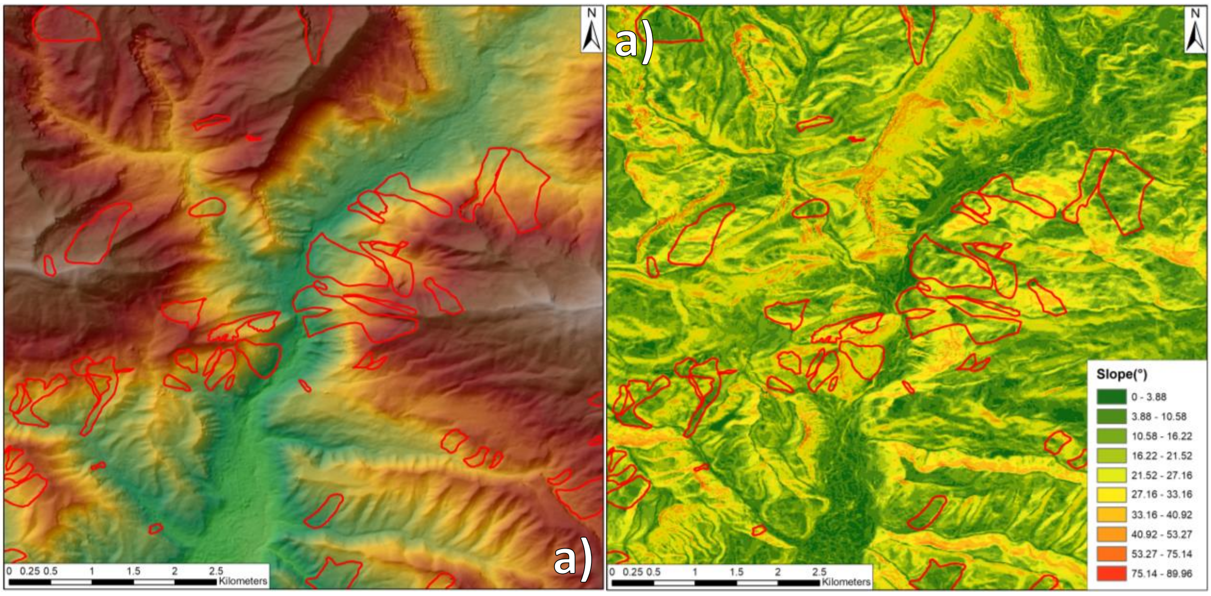

Figure 59. Study area morphological features using WorldDEM products: elevation (a) and slope (b) maps.

For these reasons, two different scenarios have been chosen for the GPP model (Table 13,

Random walk – First case scenario	Value
Slope threshold	**35 (°)**
Exponent of divergence	2 (-)
Persistence factor	2 (-)

Fahrböschung	Value
Friction angle	18 (°)

Table 14):

- First scenario: for which a friction angle of 18° obtained by literature (Havenith et al., 2005) was considered;
- Second "worst case" scenario: considering a very low residual friction angle value for clayey material (13°)

The model used to derive the process area and stopping position is the Random Walk, for the run-out (allowing to get the maximum velocity in m/s) the adopted method was Fahrboeschung. These algorithms outline the process path, deposition area and an estimate of the maximum velocity in m/s of the surface material only, respectively.
The model provides three products in a raster cell format:

- Process area: number of the run-out passing on each cell
- Maximum velocity: maximum velocity observed in each cell (m s^{-1})
- Stopping positions: showing cells in which the run-out length has been reached.

Table 13. Model calibration parameters for the first case scenario.

Random walk – First case scenario	Value
Slope threshold	**35 (°)**
Exponent of divergence	2 (-)
Persistence factor	2 (-)
Fahrböschung	Value
Friction angle	18 (°)

Table 14. Model calibration parameters for the second case scenario.

Random walk – Second case scenario	Value
Slope threshold	27 (°)
2.0 - 8.4	3
Persistence factor	1.5
Fahrböschung	Value
7.0 - 8.3	13 (°)

6.2.4 Results

By using the landslide susceptibility maps it is possible to identify landslide-prone pixels. The resolution of these latter is based on the resolution of the MERIT Dem, which is ideal for regional studies, but not for local applications. We believe that showing the open source GPP code, that is capable of modelling the runout of active known landslides can be useful in the field of land use-planning and emergency management (e.g., to relocate housings in areas at risk). The process area product shows that for the first scenario only the Isolith landslide (which is located in a steep valley flank, with slopes up to 40°) can have an impact on the elements at risk (a tailing on the valley floor, as well as the roadway and some buildings; white arrow in Figure 60). While in the second scenario both Tektonik and Koytash could reach the valley floor road (but impacting no buildings); furthermore, two landslides located about 1 km north-east of the Koytash landslide can impact the roadway and get very close to some housings, without impacting on them (white arrows in Figure 61). In the first case scenario the maximum reached velocity is 43 m/s in correspondence of the Isolith landslide (Figure 62), while in the second scenario the Tektonik landslide could involve the valley floor roadway with over 50 m/s (Figure 63). In conclusion, in all the carried-out simulations it seems how only the Isolith can impact on a small uranium tailing, while for the second worst case scenario other landslides, including Tektonik and Koytash, can impact the road and some buildings.

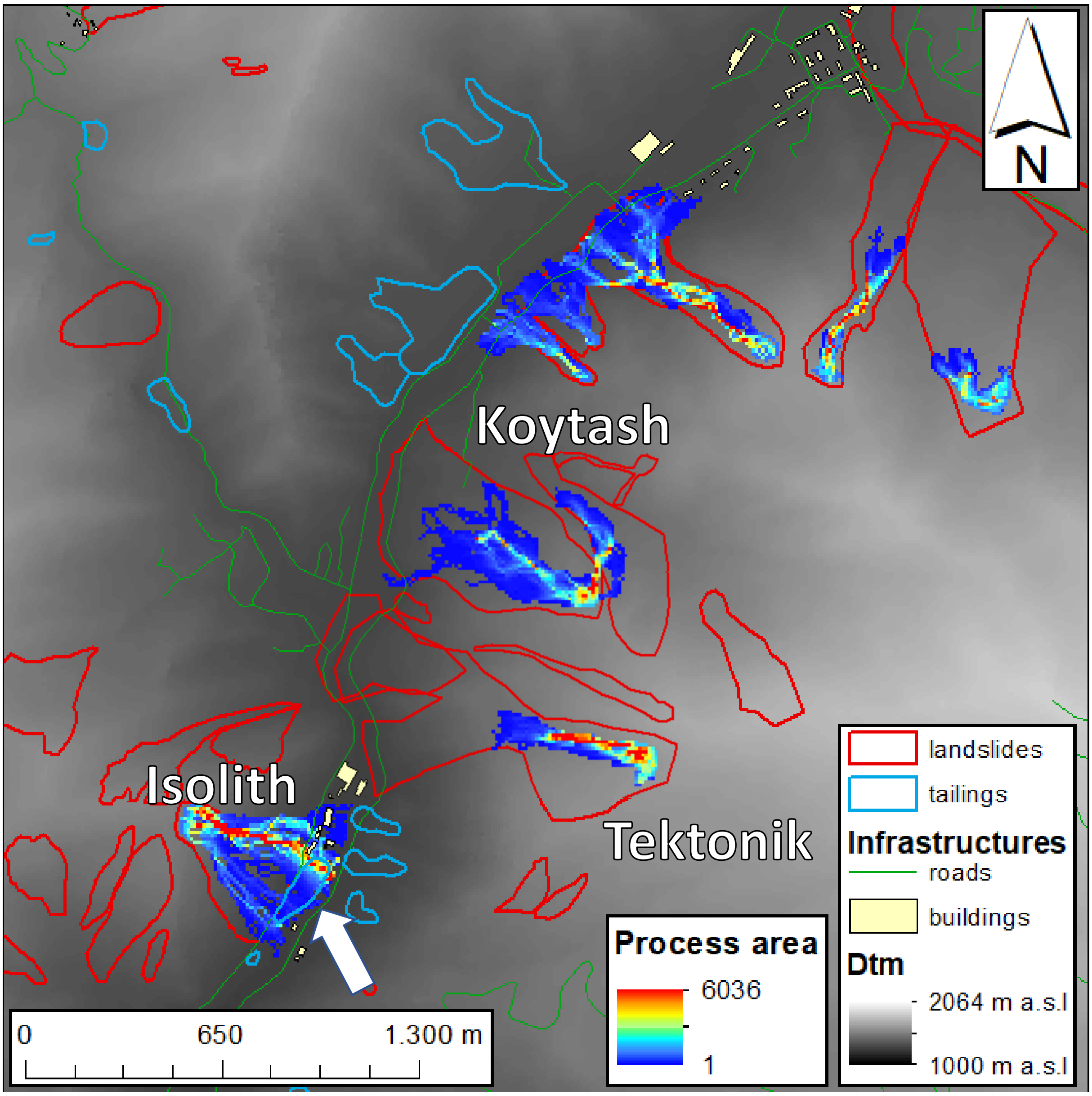

Figure 60. Map of the number of the flow occurrence run-out on each DEM cell for the first scenario.

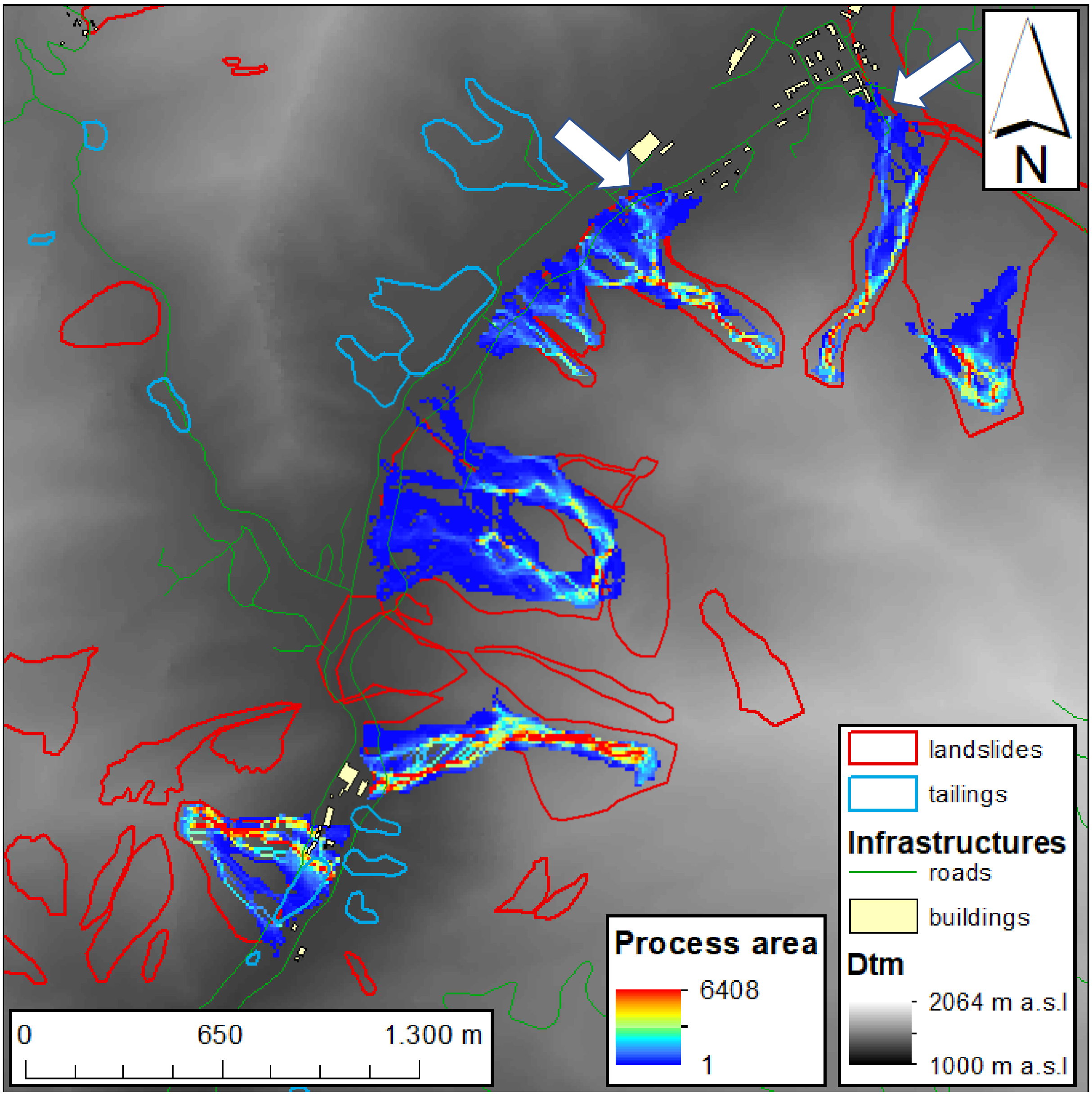

Figure 61. Map of the number of the flow occurrence run-out on each DEM cell for the second scenario.

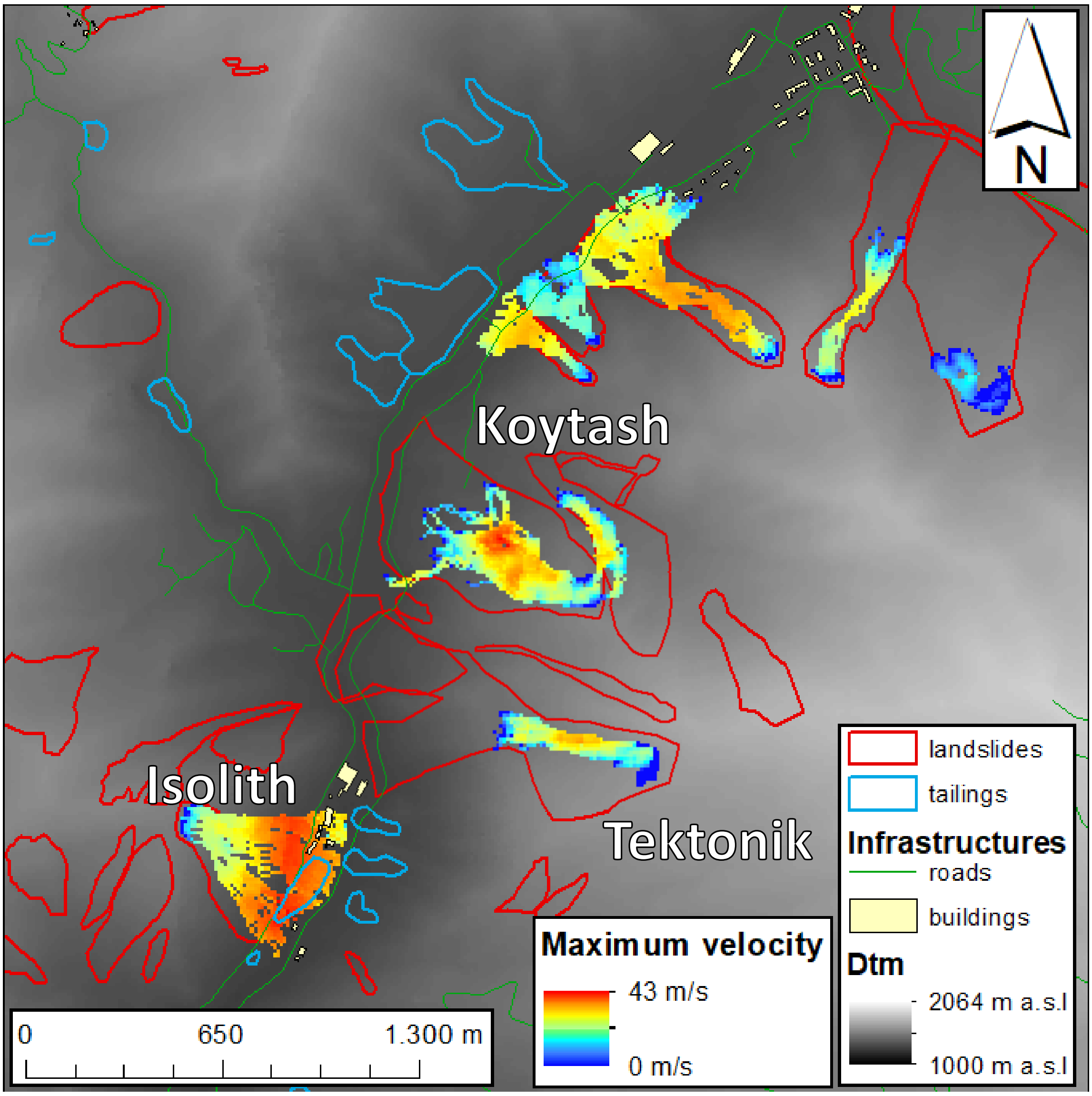

Figure 62. Map of the number of the Maximum velocity of the flow occurrence for the first scenario.

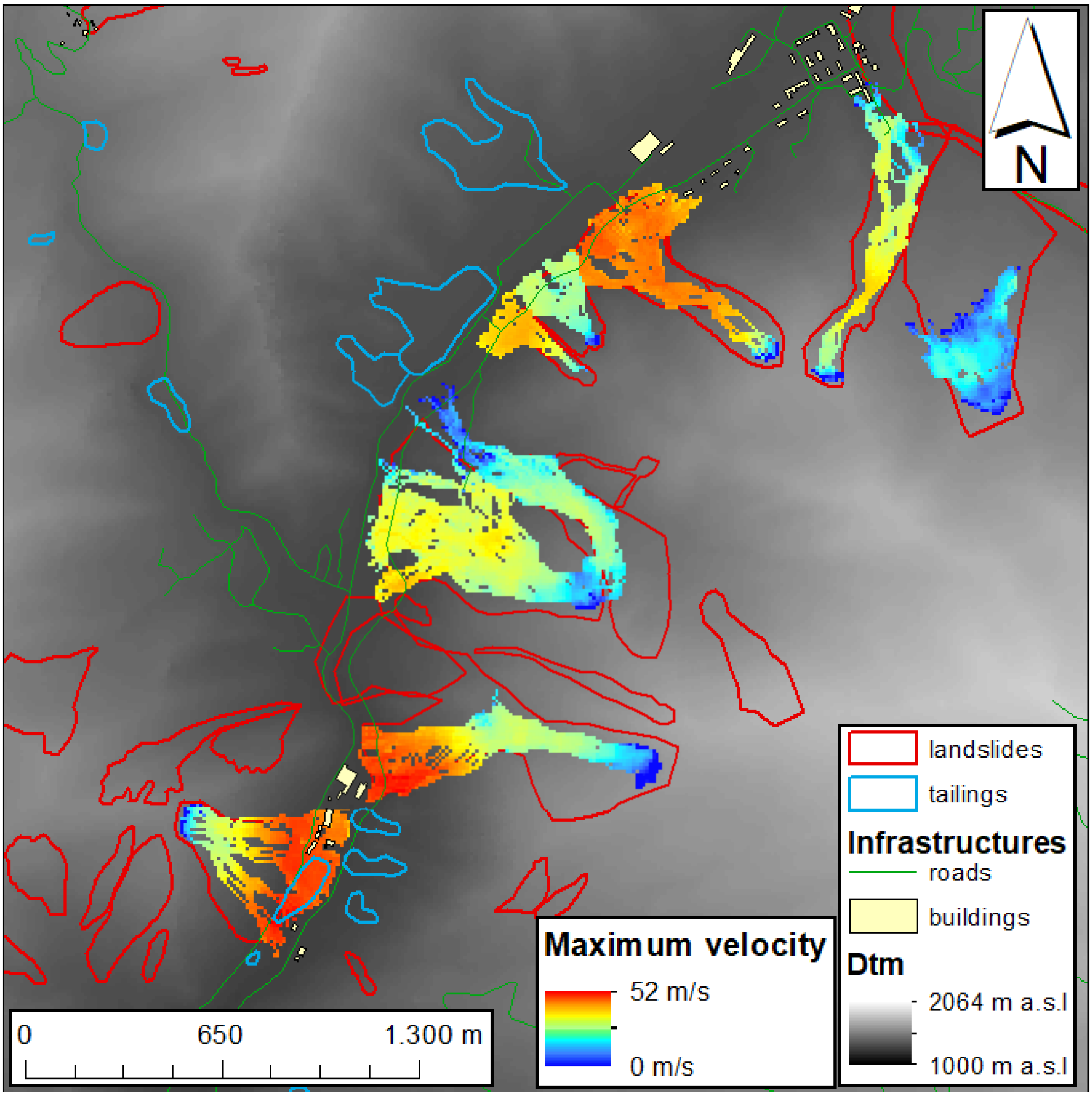

Figure 63. Map of the number of the Maximum velocity of the flow occurrence for the second scenario.

6.3 Osh-Bishkek Highway (Kyrgyz Republic)

6.3.1 Background

Many landslides are derived from or related to road networks (Seutloali, and Beckedahl, 2015); in particular, mountain roads are the most prodigious source of landslide sediments of all widespread land uses (Sidle et al., 2011). Cutting into hillsides and then removal of the toe of slopes or filling slopes to widen and reinforce roads both effectively reduce the slope cohesion and strength, and contribute to slope failures (Zhao et al., 2018).

Moreover, road construction interrupts surface drainage, ditches, and culverts, and alters subsurface water movement, changes the distribution of mass, and increases erosion because of road-related deforestation and construction activities (Banerjee and Ghose, 2016). All the above factors could facilitate landslides during and after road construction (Figure 64).

In Central Asia the road network is highly susceptible to avalanches, landslides, flooding, and erosion; damage by natural causes and the consequent cost of repair is higher than damage caused by traffic. Only in Tajikistan, 331 individual locations were identified and inspected across more than 2,000 km of the road network, highlighting hazards including flooding, landslides, avalanches, rockfalls and mudflows (WB and GFDRR, 2021). Landslides are a major threat for linear infrastructures in Kyrgyzstan; the Osh-Bishkek EM-02 Highway in particular, in the recent years since its completion has suffered several life losses, damage and transport interruptions due to landslides, especially in its mountainous sector. Traffic volumes along this highway are estimated to be 2500 to 3000 vehicles per day following completion of rehabilitation in 2003 (World Bank, 2008). This highway in particular may be used to illustrate the potential costs due to delays and interruptions which may result from geohazard impacts causing shutting of the road and requiring repairs: the annual cost of landslide or mudflow disruption could be of the order of 3.5 million USD (World Bank, 2008).

For these reasons in this section have as study area the Osh-Bishkek (EM-02) highway in Kyrgyz Republic, which, with a length of 672 km, is one of the most important highway corridors in Kyrgyz Republic (Figure 65).

Figure 64. Typical road-induced landslides: fillslope failure (FSF) and cutslope failure (CSF). The CSF with excavation signs always located above and adjacent roads with steep slope, and the FSF always locate under and adjacent roads with relative high slope (after Zhao et al., 2018).

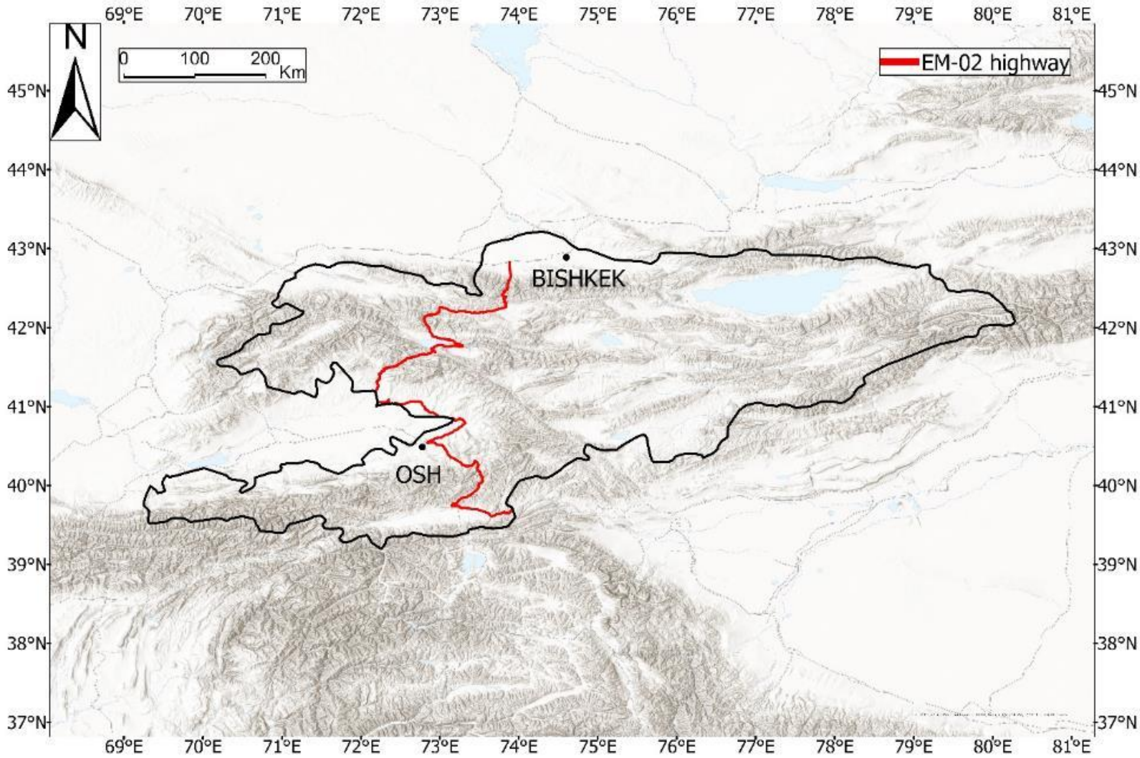

Figure 65. Location of Osh-Bishkek highway (red line).

6.3.2 Methodology and results

The activities focused on determining the length of the highway sections located in landslide areas and the analysis of their susceptibility. All the computed procedures were implemented in a GIS environment by using spatial and statistical analyses. A 100 m buffer was created on the highway sections. Regarding the susceptibility analysis the roadway transect was divided in 1 km-length transects. The obtained susceptibility frequency distribution report that the most frequent values range within 0-0.05 (Figure 66). Concentrating only on landslide-affected highway sections the frequency distribution shift towards higher values, as is shown in Figure 67. Regarding these latter, the most populated range of susceptibility ranges 0.60-0.65. To facilitate the understanding of the susceptibility distribution, these have been divided in the five class, as shown in Section 3.4.

The distribution of the abovementioned landslide susceptibility classes is reported in a pie chart (Figure 68), which clearly highlights that the most frequent class in EM-02 transects is High. Concerning the only transects in landslide areas, the results show that the sections values range in the intervals greater than 0.5 represent the 78% respectively, of the EM-02 transects, proving that this highway is located in an area of high susceptibility. The landslide susceptibility map of EM-02 highway is showed in Figure 69.

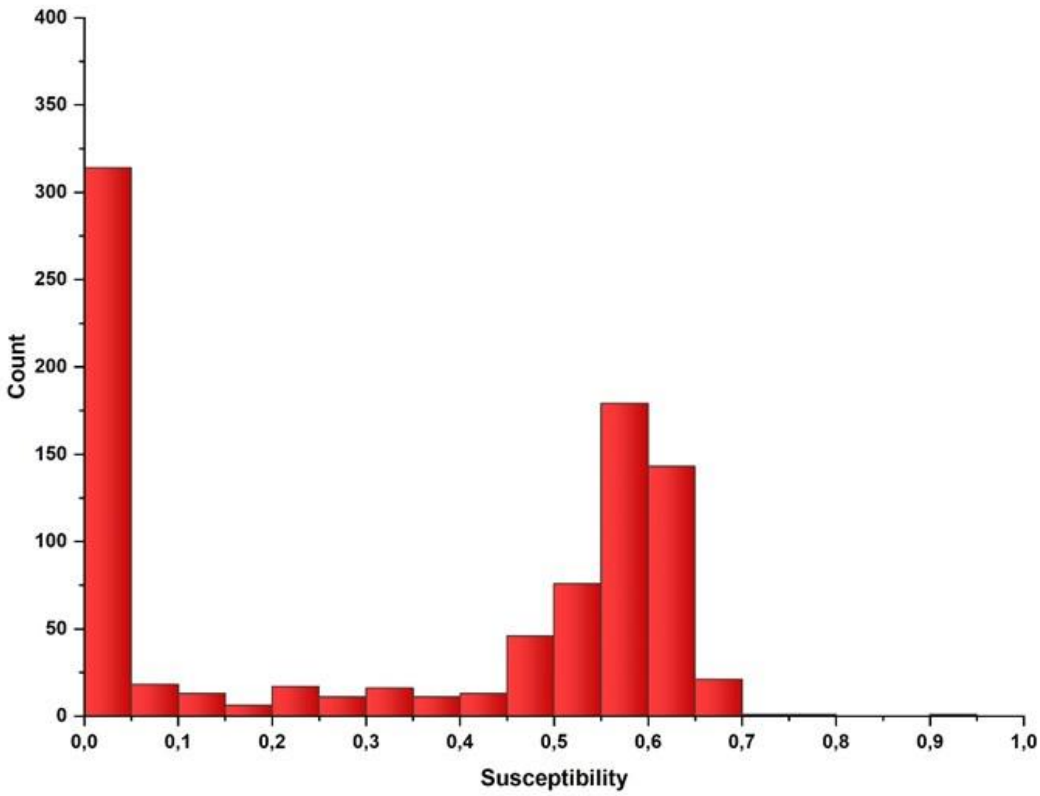

Figure 66. Frequency distribution of landslide susceptibility in the whole Osh-Bishkek highway length.

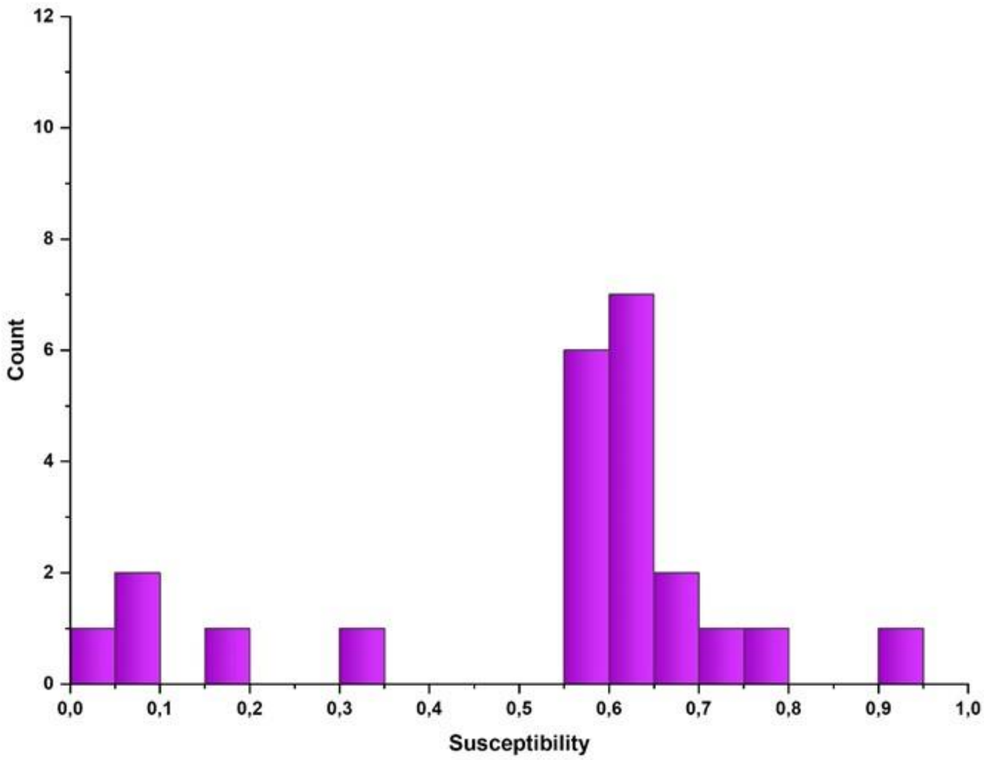

Figure 67. Frequency distribution of susceptibility in landslide-affected highway transects.

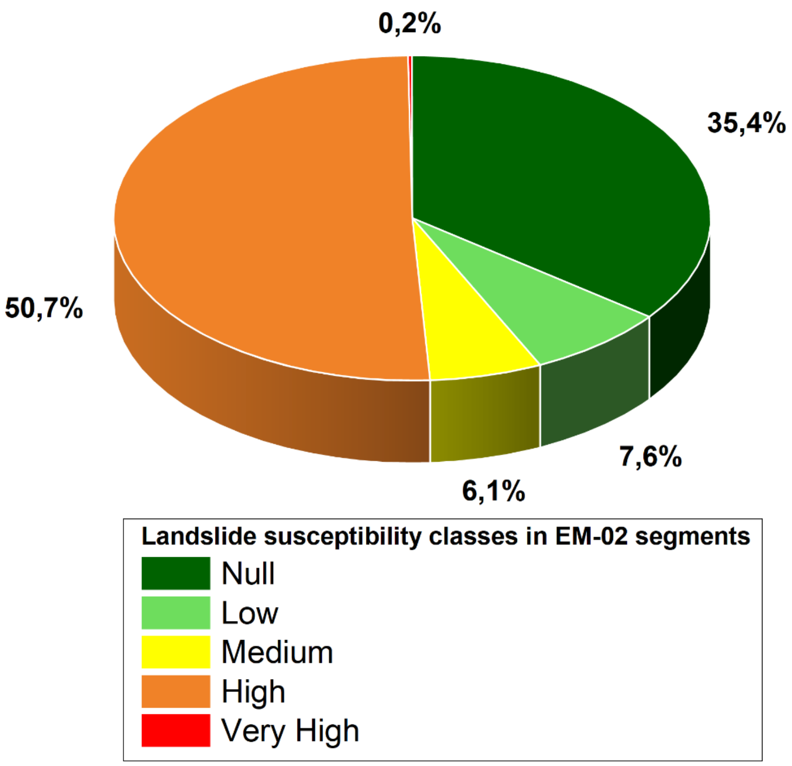

Figure 68. Pie chart of landslide susceptibility distribution in EM-02 segments

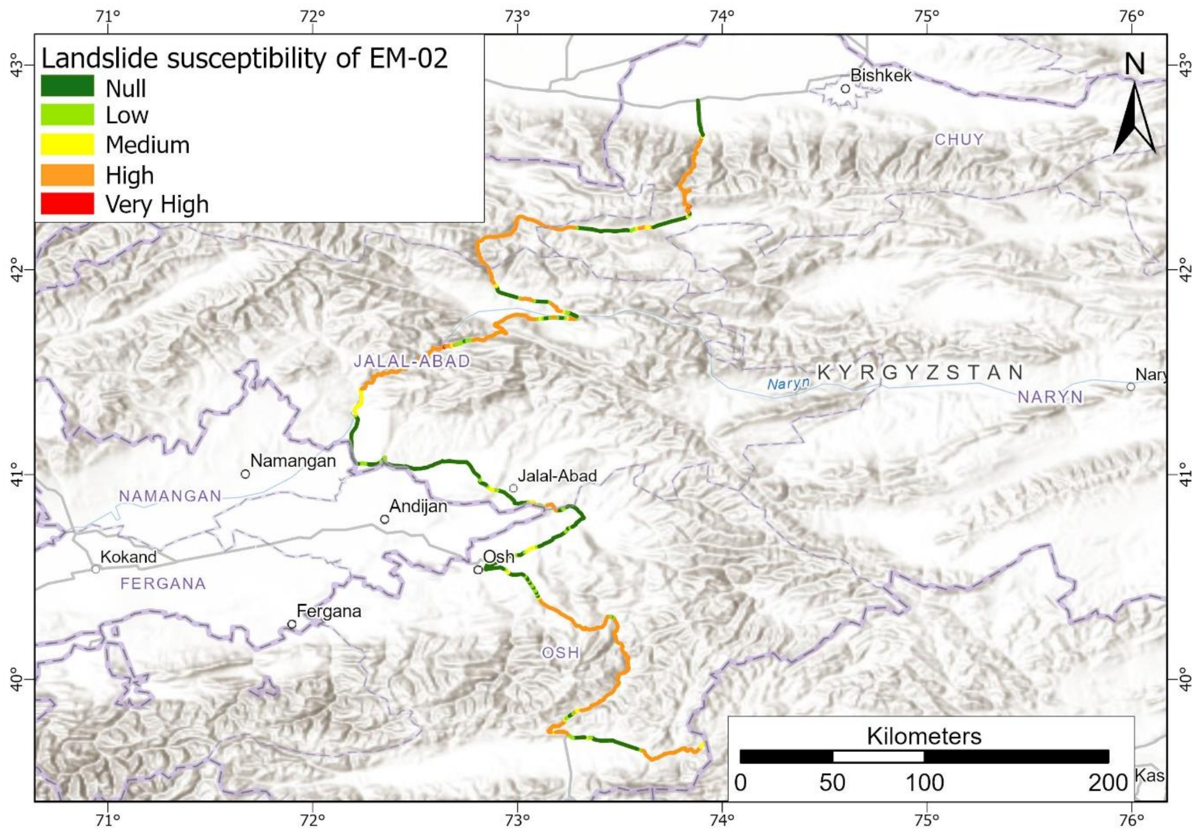

Figure 69. Landslide susceptibility map in EM-02 highway.

6.3.3 Road-landslide risk index

A risk index for the landslide affecting the EM-02 highway is proposed in this section. The approach is based on the employment of the available landslide inventories; in some case these present overlapping mapped polygons, based on the different interpretation of the surveyor. To adopt an approach as cautionary as possible, the largest mapped landslide was employed in the implemented procedure. A landslide-roadway risk index ranking was assessed by combining the length of the impacted highway transect and the landslide volume intersecting the highway, based on the area obtained from the adopted inventories, and using for the volume the equation:

$$V=0.0844 \times A^{1.4324}$$

from Guzzetti et al., 2009 introduced in Section 5.

These parameters were evaluated in a GIS environment by intersecting the road linear shapefile with the landslide shapefile polygons. On this basis, three classes were obtained using the GIS natural breaks classification, for both length (L) and volume (V) (Table 15):

Table 15. The obtained length and volume classes.

Length (m)	Volumes (m^3)
L1 (< 135 m)	V1 <65×10^6 m^3)
L2 (135 <L< 359 m)	V2 (65<V<120 $\times10^6$ m^3)
L3 (> 359 m)	V3 (> 120 $\times10^6$ m^3)

This approach resulted in an overestimation of the calculated volumes: this can be explained since the mapped phenomena are mainly represented by large and very large landslides, which in turns could include prehistoric non-active landslides. Furthermore, not all the volumes of the mapped landslides will impact the roadway in case of failure.

To obtain more accurate volumes, a GPP runout simulation was performed on a mountainous highway sector affected by two large landslides, which could be source areas for potential debris avalanches impacting the roadway (Figure 70). This area is characterized by important elevation drops, ranging in height from 3600 m a.s.l. to about 2100 m a.s.l., due to a paleozoic limestones and crystalline intrusive bedrock, while slope maximum values can exceed 50° (Figure 71). As the previous Mailuu Suu case study, two different scenarios were simulated:

- A first scenario using a friction angle of 32° based on literature data (Havenith et al., 2005), considering Palaeozoic intrusive and sedimentary rocks (Figure 71b)
- A second "worst case scenario" using a low friction angle of 22°, which could be proper for a weathered slope eluvial cover involved by the debris avalanche.

A value of 50° for slope angle and 1.5 for exponent of divergence and 2 for persistence factor, respectively, were used to complete the calibration.

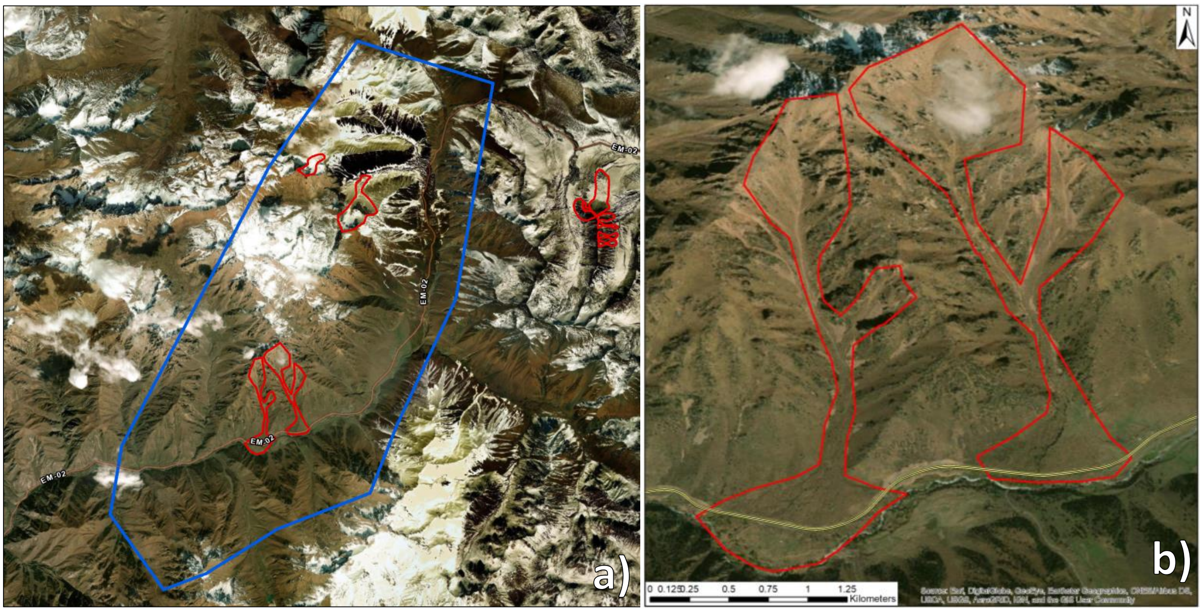

Figure 70. ESRI ArcGIS reference imaging showing analysed EM-02 transect falling within the study area (blue polygon; a), with a close-up on the two landslides which toe was probably cut for the highway construction (b).

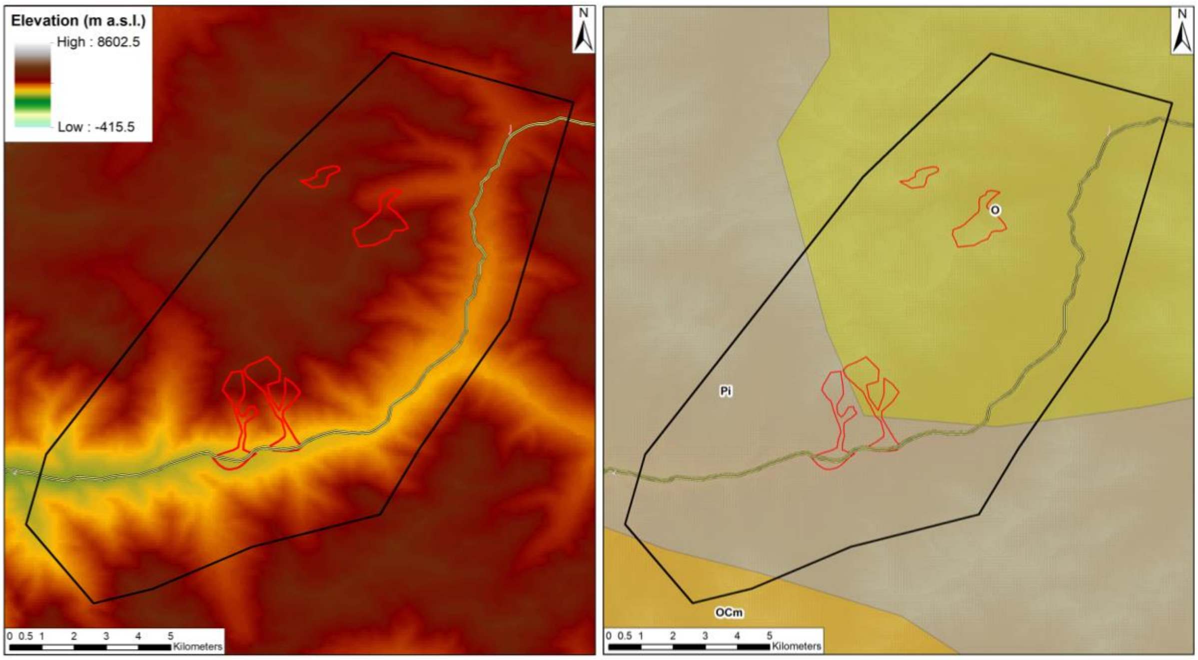

Figure 71. SRTM DEM elevation map (a) and geology from the USGS database (b) O=Ordovician; Pi=Paleozoic intrusive rocks; OCm Ordovician-Cambrian.

As shown in the simulations, the potential flow in the first scenario does not reach the highway (Figure 72a, Figure 73a, Figure 74a), while in the second scenario road transects ranging in length from 350 to 150 m are impacted by the possible debris avalanche, with velocities up to 68 m/s due to the very steep slope (Figure 72b, Figure 73b, Figure 73a). On the basis of the material stopping position the volume of the obstructing material was calculated (landslide toe in Figure 74b) using the equation from Guzzetti et al., 2009: these range from 1.7×10^6 m^3 (Toe L1) to 0.6×10^6 m^3 (Toe L2). Considering that it was generated by a debris avalanche-flows produced by two landslides with volumes of 34 $\times 10^6$ m^3 (Landslide L1) and 45 $\times 10^6$ m^3 (Landslide L2) respectively, this means that the calculated volumes with the adopted procedure and classified for the purpose of the risk index (Table 15) are overestimated by at least one order of magnitude. This can be explained since they were calculated merely on the landslide surface, are not representative of real cases (such as debris-mud flows-avalanches generated by landslide areas).

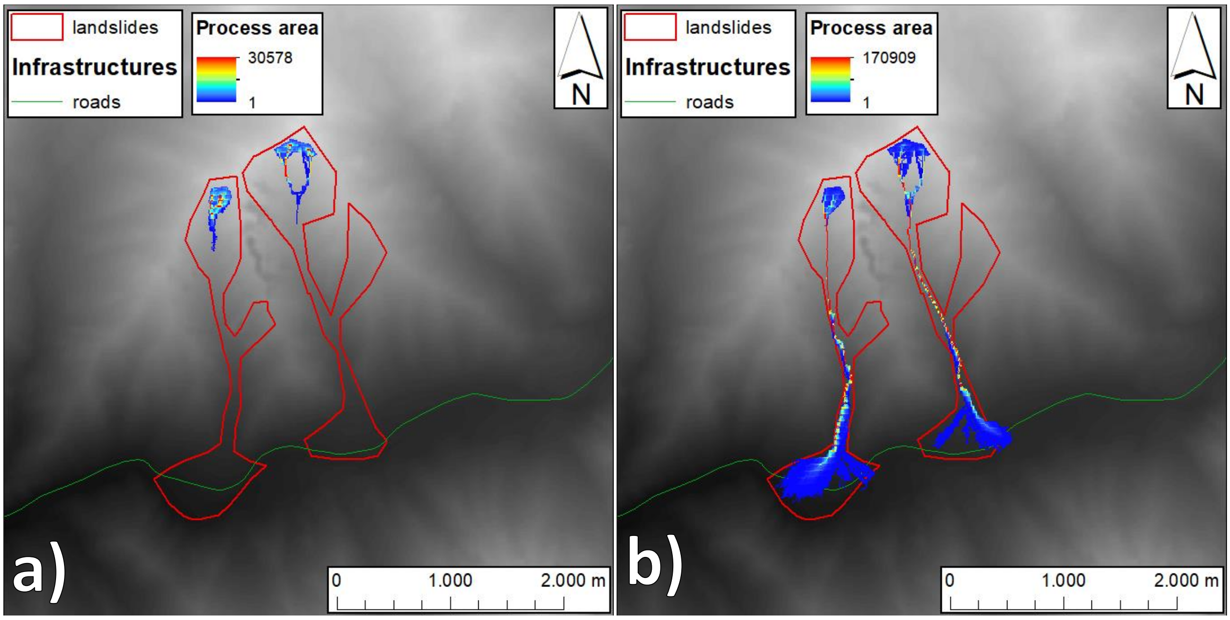

Figure 72. GPP "process area" for the first (a) and second (b) scenarios.

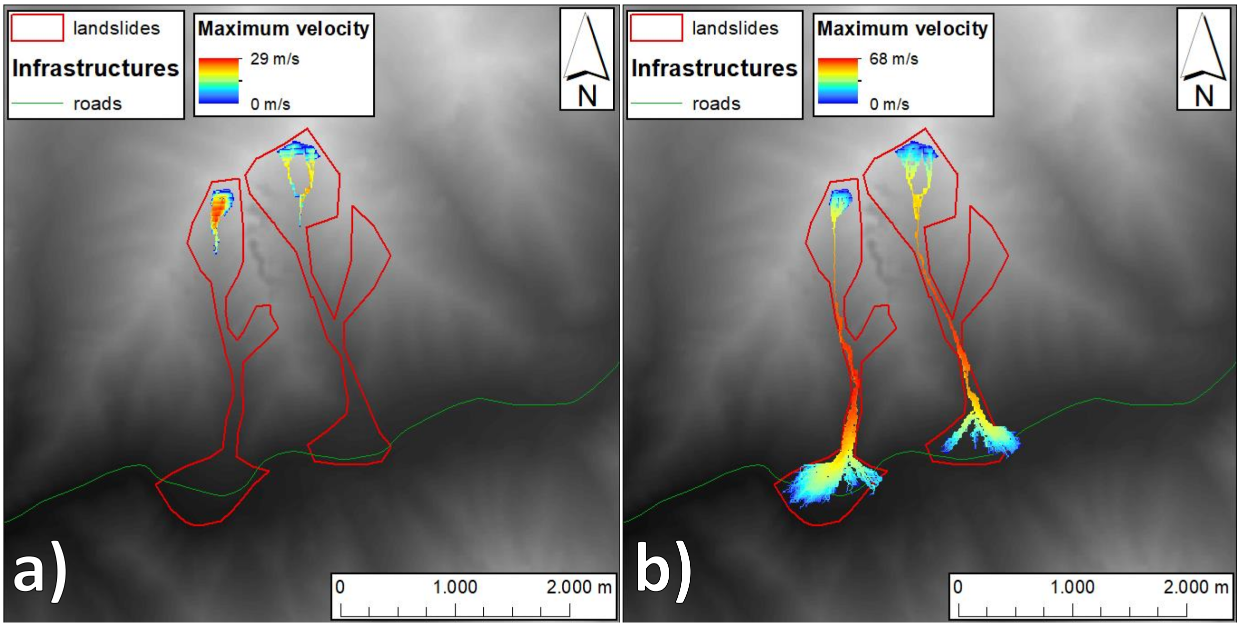

Figure 73. GPP Maximum velocity for the first (a) and second (b) scenarios.

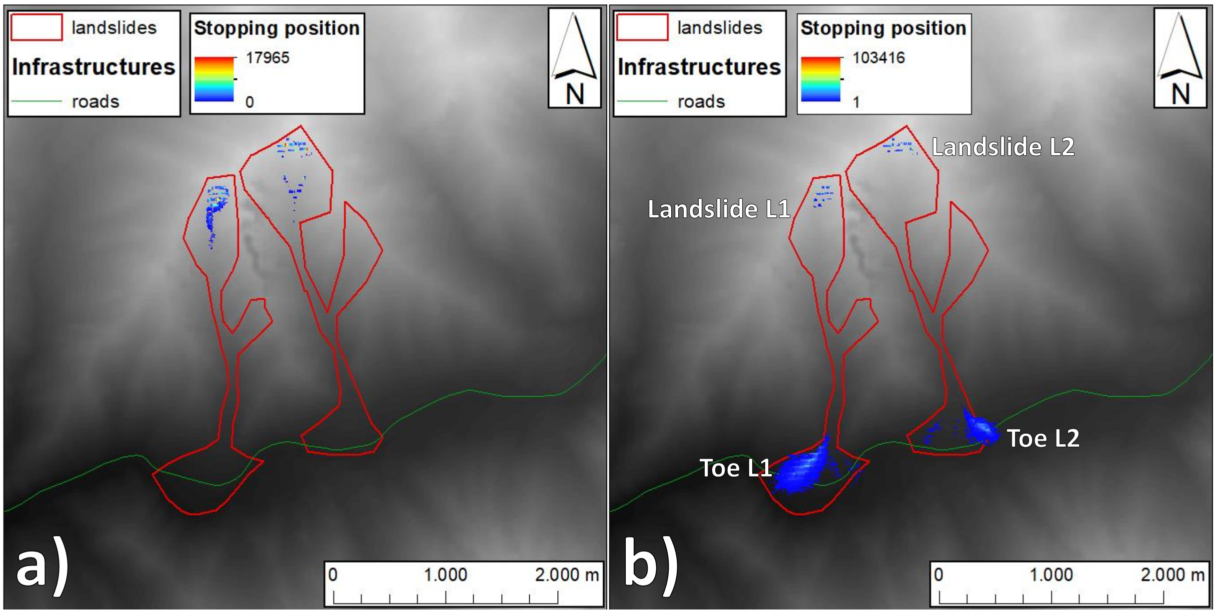

Figure 74. Stopping position for the first (a) and second (b) scenarios.

Bearing this in mind, the volume classes reported in Table 15 should be reduced by one order of magnitude (Table 16):

Table 16. The obtained length and the new volume classes.

Length (m)	Volumes (m^3)
L1 (< 135 m)	V1 ($V<6.5\times10^6$ m^3)
L2 (135 <L< 359 m)	V2 ($6.5<V<12\times10^6$ m^3)
L3 (> 359 m)	V3 ($>12\times10^6$ m^3)

Finally, based on the work of the World Bank (2008) a landslide-roadway risk index was obtained (Table 17) (Figure 75).

Table 17. Risk Index matrix.

Volume / Length	V1	V2	V3
L1	**R1**	**R2**	**R3**
L2	**R2**	**R2**	**R3**
L3	**R3**	**R4**	**R4**

Considerations on the duration of the landslide interruptions and the involved costs to restore the traffic transportations cannot be defined with this input data. In fact, with the available landslide inventories, even performing runout simulations of single landslides, it is only possible to assess landslide volumes impacting on the highway transects in the order of magnitude of million cubic meters. This is due to the nature of the large landslides affecting this territory, but also to the lack of much more specific and accurate inventories reporting smaller phenomena (e.g., with volumes having an order of magnitude of 1,000-10,000 cubic meters at least).

Furthermore, accurate field inspections to validate the outcomes for a correct calibration of the defined volume classes should be carried out. In this perspective, this case scenario could be the starting point for an accurate landslide risk assessment along the Em-02 Highway: a collaboration with the project partners would be mandatory to obtain more accurate inventories with new information about area, volumes, landslide location, type, state of activity, date of occurrence.

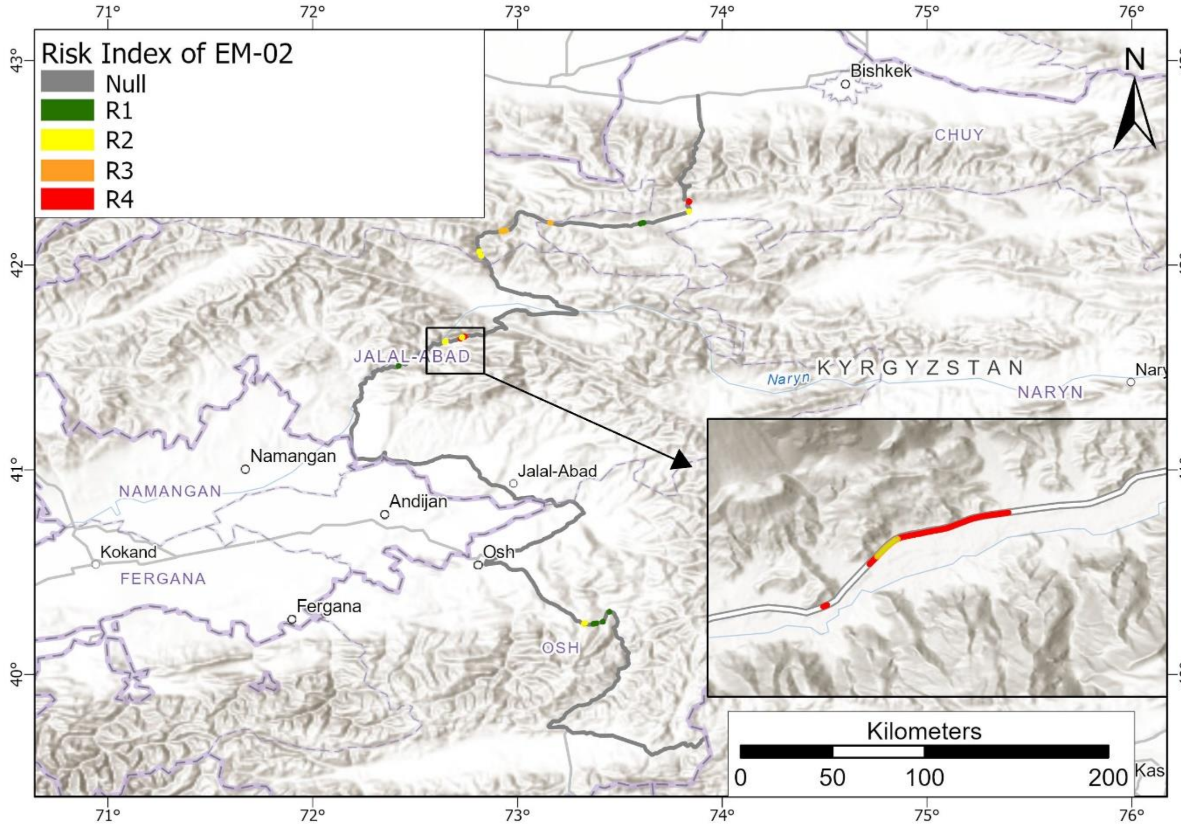

Figure 75. Map of the 22 transects of the EM-02 at risk.

6.4 Upper Pskem river valley (Uzbekistan)

6.4.1 Background

The Pskem river basin is one of the main tributaries of the Tcharvak Lake in Uzbekistan. This artificial lake is central for the local economy for its functions as reserve for fishing and water, for fluvial transports, as well as a source of hydroelectric energy and because of that various villages arise around it and downstream. The formation of a natural obstruction and an upstream impoundment in the Pskem basin could be a serious threat due to the possible instability of the earth dam and for the possible catastrophic cascade effects that its collapse could have downstream on the artificial basin and its concrete dam.

6.4.2 Methodology

With a careful observation of the zoom of the map of Damming Predisposition by landslides reactivation in the lower Pskem basin in an area of 443 km^2 (Figure 76), some of the identified landslides should be the target of future study.

Landslides named A, B, C, D and E in Figure 76, if reactivated, will cause an obstruction of the main river section of the Pskem with unpredictable consequences. As shown in Table 18, the volumes of all these landslides are bigger than the boundary volume of Non-Formation and Formation from Figure 77 and Figure 78 computed using the aforementioned mapping method (see Section 5.1). Even if not visible from the map in Figure 76, it is important to notice that the body of landslide A is cut by the current riverbed, meaning that in the past it had probably already dammed the river in that point.

Table 18. Landslides volumes and damming parameters W_v, V'_l, V''_l of the landslides in Figure 76 computed using the described method.

Landslide	V_l - Landslide volume (m^3)	W_v – River Width (m)	V'_l - Volume of Non-Formation (m^3)	V''_l - Volume of Formation (m^3)
A	200.000.000	300	2.600.000	16.200.000
B	12.000.000	235	1.500.000	10.000.000
C	34.000.000	318	3.000.000	18.200.000
D	73.000.000	513	10.100.000	47.400.000
E	61.000.000	575	13.500.000	60.000.000

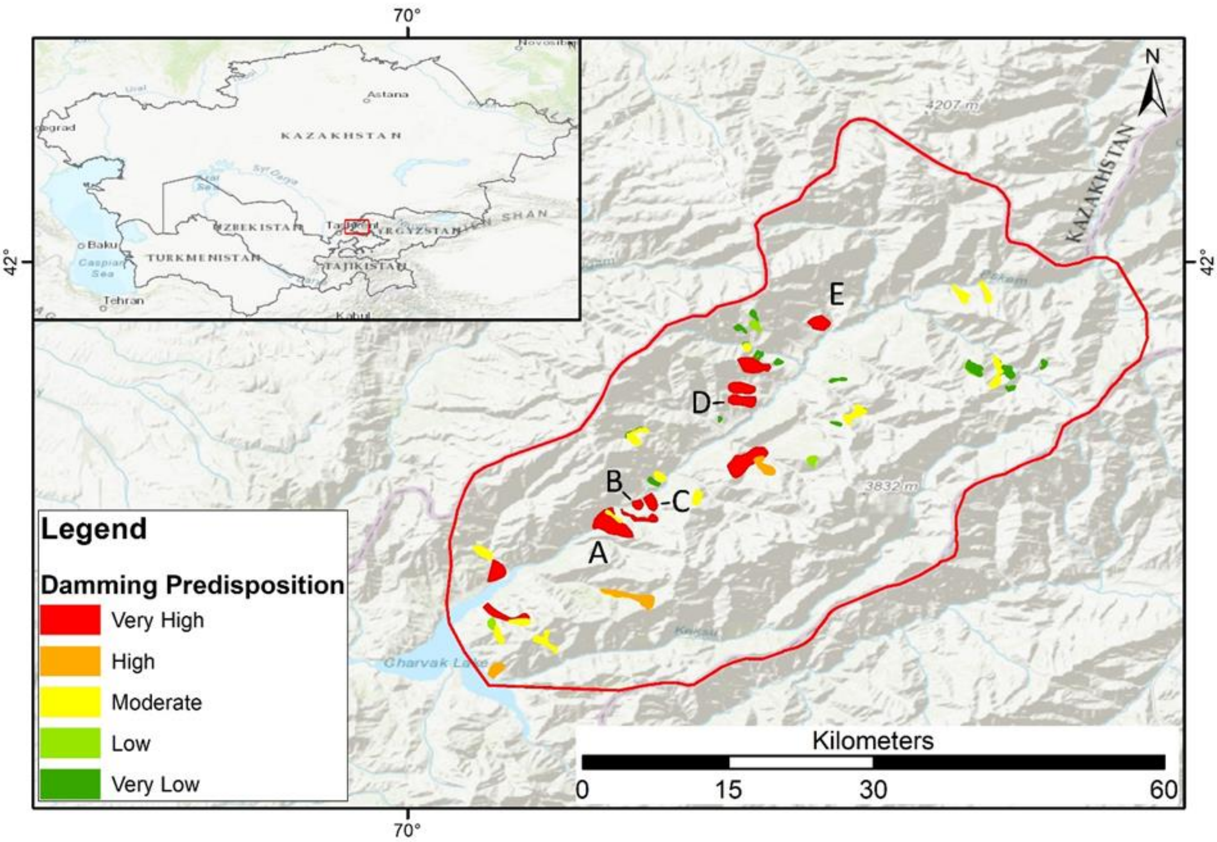

Figure 76. Map of Damming Predisposition by landslides reactivation in the lower Pskem basin.

The obstruction of the Pskem river by one of these landslides would cause an upstream impoundment with a surface from 2 to 10 km^2 or more, depending on the dam height. The dam collapse could release a catastrophic flooding wave with destructive effects in the downstream areas. In the worst scenario, even the concrete dam located a few kilometers downstream could be seriously damaged with unpredictable effects. Since the reliability of this mapping method is strictly correlated to the quality of the input data, when the used DEM has a coarse resolution, in similar cases of possible risk to people's life it is always advisable to do a second "manual check" even using some free satellite imaging services such as Google Earth (GE). In fact, when the DEM resolution is too rough, the GIS tool used in this methodology to evaluate the extension of the riverbed morphologic unit can produce inconsistent and incorrect results, causing improper damming susceptibility evaluations. The results of the measurements on Google Earth orthophotos in Table 19 show that the difference between the river width values calculated with the mapping method and measured on Google Earth can, in some cases, be substantial, although, in this case, they do not modify in any case the final classification of the five landslides, which remain with a Very High predisposition value.

Table 19. Damming parameters W_{vGE}, V'_{lGE}, V''_{lGE} of the landslides in Figure 76 computed with Google Earth observation.

Landslide	W_{vGE} – River Width (m)	V'_{lGE} - Volume of Non-Formation (m^3)	V''_{lGE} - Volume of Formation (m^3)
A	415	6.000.000	31.000.000
B	310	2.800.000	17.300.000
C	260	1.800.000	12.100.000
D	530	11.000.000	50.000.000
E	450	7.300.000	36.500.000

The river network of the upper Pskem valley have been also classified producing the maps of Damming Susceptibility of Non-Formation and Formation (Figure 77 and Figure 78 respectively). Concerning the Damming Susceptibility Map of Non-Formation (Figure 77), the most frequent are Low and Moderate classes with 65.1% and 22.6% respectively, followed by Very Low class with 11.1%. Only just 1.3% have been classified as High and 0.0% as Very High. For the Damming Susceptibility Map of Formation (Figure 78) most of the rivers fall into Very Low and Low classes with 69.8% and 27.7%, followed by Moderate class with 2.1%. Only 0.4% have been classified as High and 0.0% as Very High. The general damming susceptibility of the valley is low, but a singular river stretch classified with High susceptibility in both maps should be carefully evaluated. This river part is clearly noticeable in the middle of the area along the main river path, a bit upstream from the landslides named B and C. The high classification values mean that geographically, in that point, the valley width undergoes a shrinkage and, for this reason, even a relatively small landslide generated from the surrounding slopes can create an obstruction.

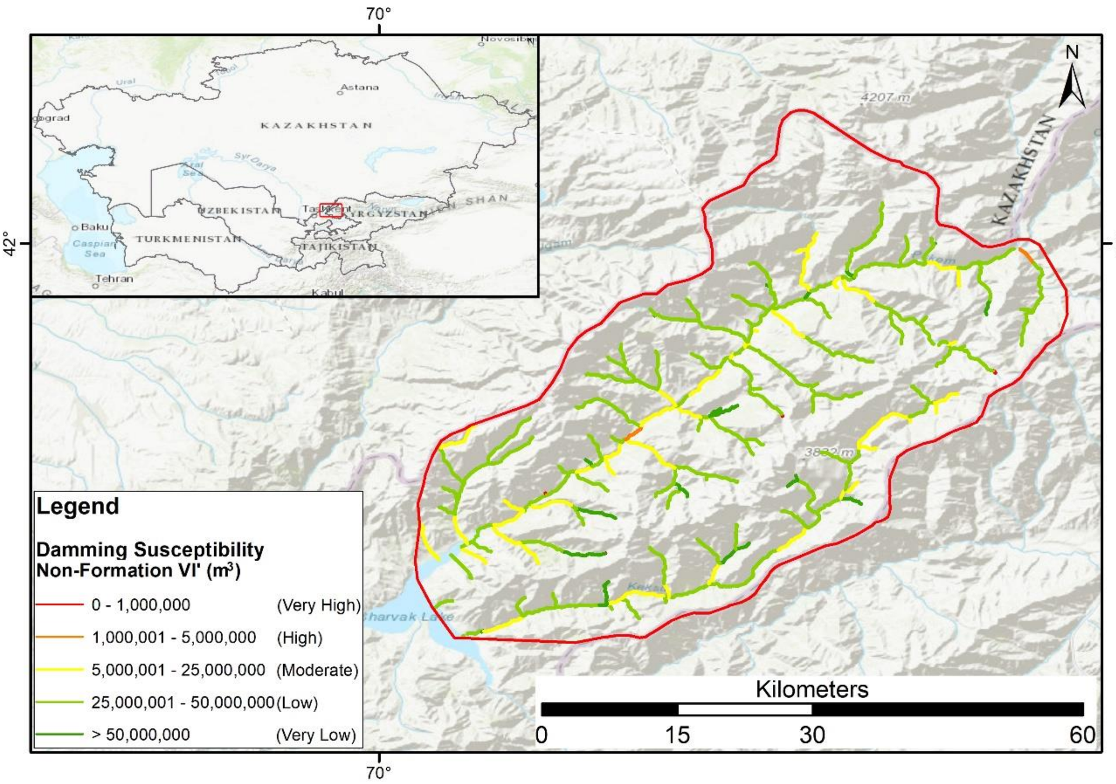

Figure 77. Damming Susceptibility Map of Non-Formation of river stretches by new landslides in the lower Pskem basin.

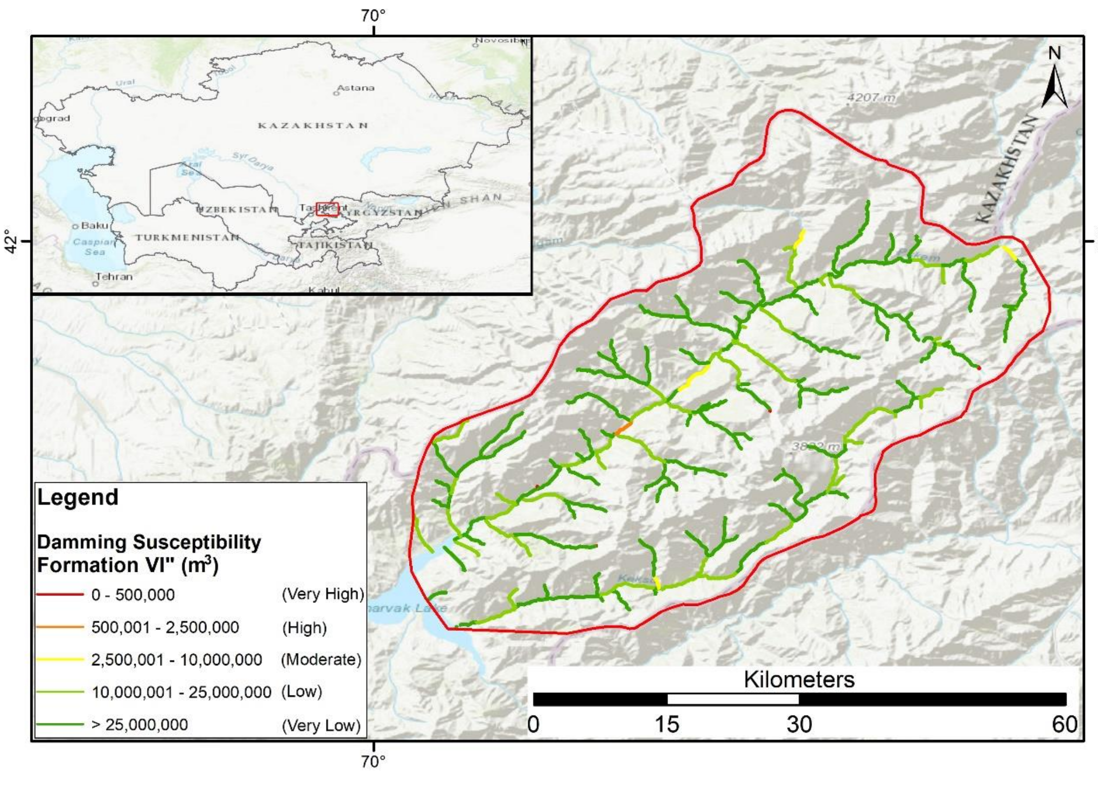

Figure 78. Damming Susceptibility Map of Formation of river stretches by new landslides in the lower Pskem basin.

6.5 The Fergana valley mountainous rim (Tajikistan-Kyrgyz Republic-Uzbekistan)

6.5.1 Background

The Fergana valley spreads across eastern Uzbekistan, southern Kyrgyz Republic and northern Tajikistan. It is an intermountain depression in Central Asia, between the mountain systems of the Tien-Shan in the north and the Gissar-Alai in the south. Into the valley flow two main rivers, the Naryn and the Kara Darya, which unite to form the Syr Darya.

In this area landslides represent one of the major natural hazards due to their frequent (seasonal) occurrence across large areas: in fact, they are particularly concentrated in a range of altitudes between 700 and 2000 m along the topographically rising rim below its transition into higher mountainous terrain (Roessner et al., 2000, 2004, 2005; Behling et al., 2014, 2016). This region is quite densely populated, and landslides lead almost every year to damage of settlements and infrastructure and loss of human life (Schloegel et al., 2011; Piroton et al. 2020). In this area landslide activity is caused by complex interactions between tectonic, geological, geomorphological and hydrometeorological factors (Havenith et al., 2015a, b).

In the Fergana valley rim mass movements are often characterized by deep and steep scarps, mobilize weakly consolidated sediments of Tertiary or Quaternary age, including loess deposits (Piroton et al., 2020). These kinds of landslides are particularly deadly, and can be triggered by a combination of long-term slope destabilization factors (e.g., rainfall and snowmelt) and short-term triggers (Danneels et al., 2008). Slope landslide susceptibility and river damming susceptibility were analyzed in this area using the previously mentioned methodologies.

6.5.2 Landslide susceptibility

Figure 79 shows the detail of the landslide susceptibility map obtained for the Fergana Valley. Instead, Figure 80 shows the histogram of the area occupied by each susceptibility class about the particular of the catchment area of the Fergana Valley. It can be observed that the most frequent susceptibility class in the Fergana Valley area is the Null class, which covers an area of about 20,753 km^2, that is 38,2% of the national territory. The Low class occupies an area of 2,814 km^2, namely 5,2% of the total. The Medium class instead extends for about 14,087 km^2, that is 26% of the total. The High class instead extends for about 16,467 km^2, that is 30,3% of the total and finally, the remaining 0.3% of the national territory, that is about 154 km^2, is classified in the Very High class.

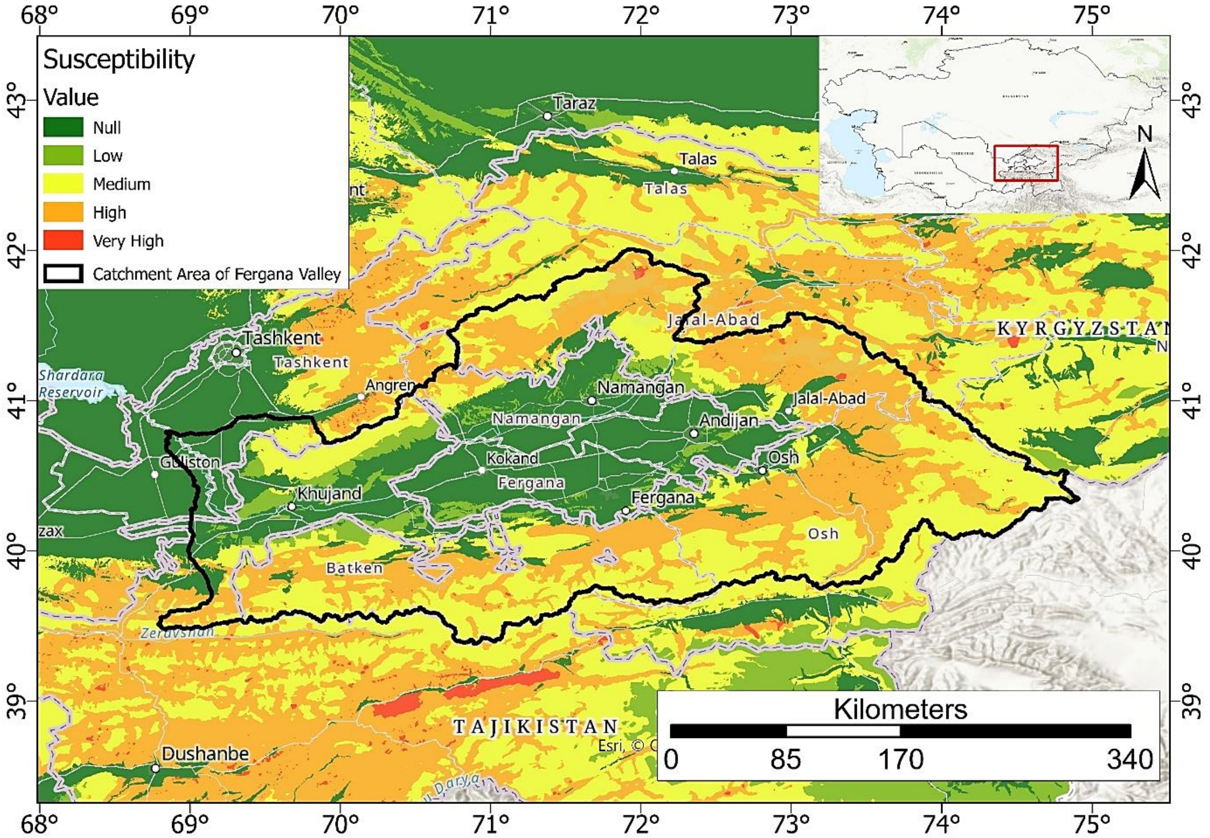

Figure 79. Detail of the landslide susceptibility map obtained for the Fergana Valley.

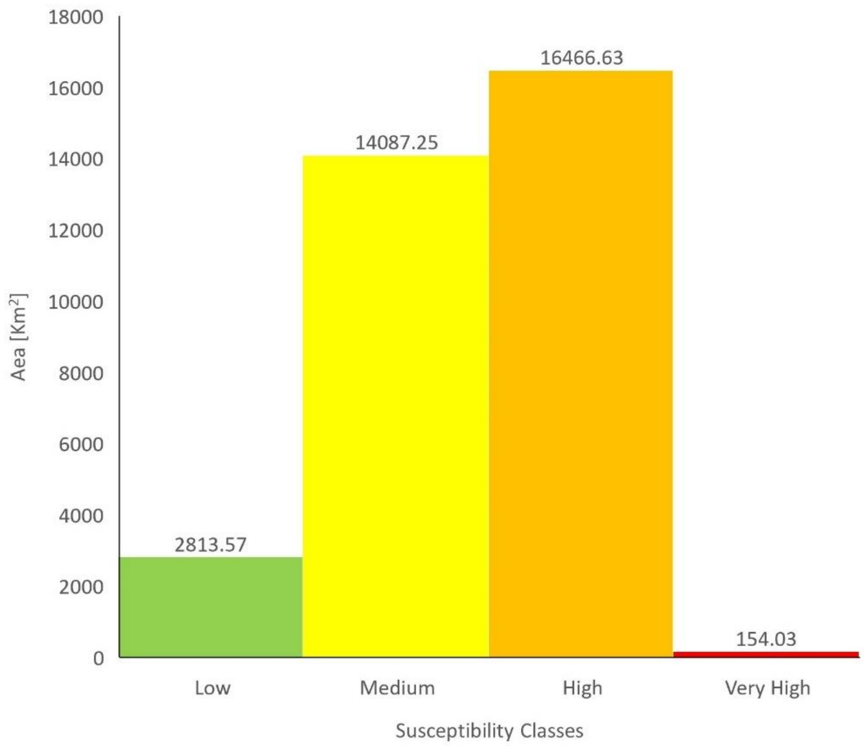

Figure 80. Frequency histogram of susceptibility classes obtained for the Fergana Valley mountainous rim; on each bar the corresponding area in km² is reported ("Null class" was not included to emphasize other classes).

6.5.3 Landslide damming

The mapping methodology have been applied to the Fergana valley and a total of 3370 landslides, coming from various data sources have been classified as shown in Figure 81. Comparably to the classification result of the entire inventory (Figure 38), most of the cases (93.7%) have a Very Low damming predisposition, followed by Moderate and Very High (with 3.6% and 1.5% respectively) as reported in Table 20. Just very few landslides fall into Low and High classes (with 0.8% and 0.4% respectively). For the classification of the river network of the Fergana valley, the maps of Damming Susceptibility of Non-Formation and Formation have been produced (Figure 82 and Figure 83 respectively). As a method with a multi-scale approach, in such large areas, this damming susceptibility method is suitable to provide territorial planning suggestions rather than indications on single interventions at local scale. The overall damming susceptibility of the Fergana valley is quite low, even if there are few landslides (83) classified with Very High damming predisposition which should be studied with more attention through localized analysis of damming susceptibility to ensure that downstream areas are not at risk and therefore require monitoring.

Table 20 reports the distribution of the percentages of the damming susceptibility classes of those river stretches that are not running in flat areas, since these lowland rivers represent 53.6% of the total. Concerning the Damming Susceptibility Map of Non-Formation (Figure 82), the most frequent are Low and Moderate classes with 53.4% and 36.2% respectively, followed by Very Low class with 7.0%. Only just 2.1% and 1.3% have been classified as Very High and High. For the Damming Susceptibility Map of Formation (Figure 83) most of the rivers fall into Very Low and Low classes with 54.5% and 38.1%, followed by Moderate class with 5.2%. Only 1.9% and 0.2% have been classified as Very High and High respectively.

As a method with a multi-scale approach, in such large areas, this damming susceptibility method is suitable to provide territorial planning suggestions rather than indications on single interventions at local scale. The overall damming susceptibility of the Fergana valley is quite low, even if there are few landslides (83) classified with Very High damming predisposition which should be studied with more attention through localized analysis of damming susceptibility to ensure that downstream areas are not at risk and therefore require monitoring.

Table 20. Distribution of Damming Susceptibility classes on existing landslides (Figure 81) and on the river stretches for Non-Formation (Figure 82) and Formation of new landslides (Figure 83).

Damming Susceptibility	Landslides		Non-Formation	Formation
	n.	%	%	%
Very High	51	1.5 %	1.9	1.7
High	15	0.4 %	1.2	0.2
Moderate	120	3.6 %	.7.0	5.3
Low	26	0.8 %	53.2	38.8
Very Low	3158	93.7 %	6.7	54.0

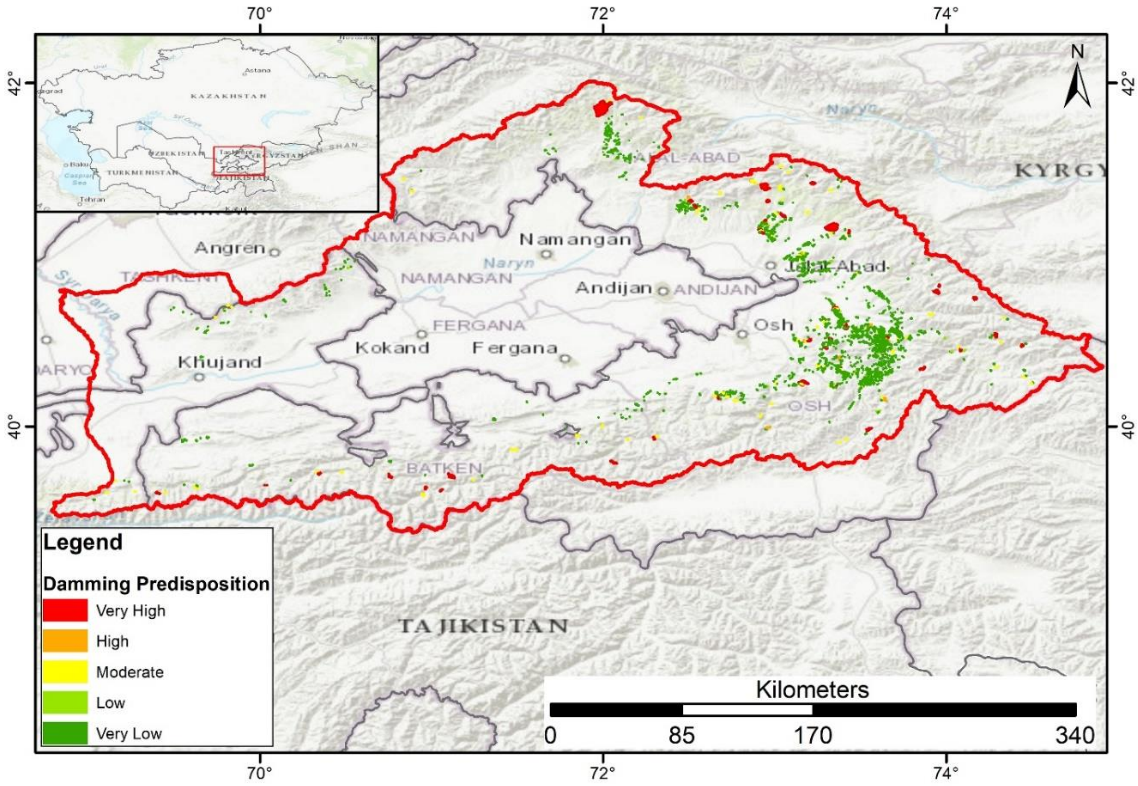

Figure 81. Map of Damming predisposition by landslides reactivation in the Fergana valley and the surrounding mountainous rim.

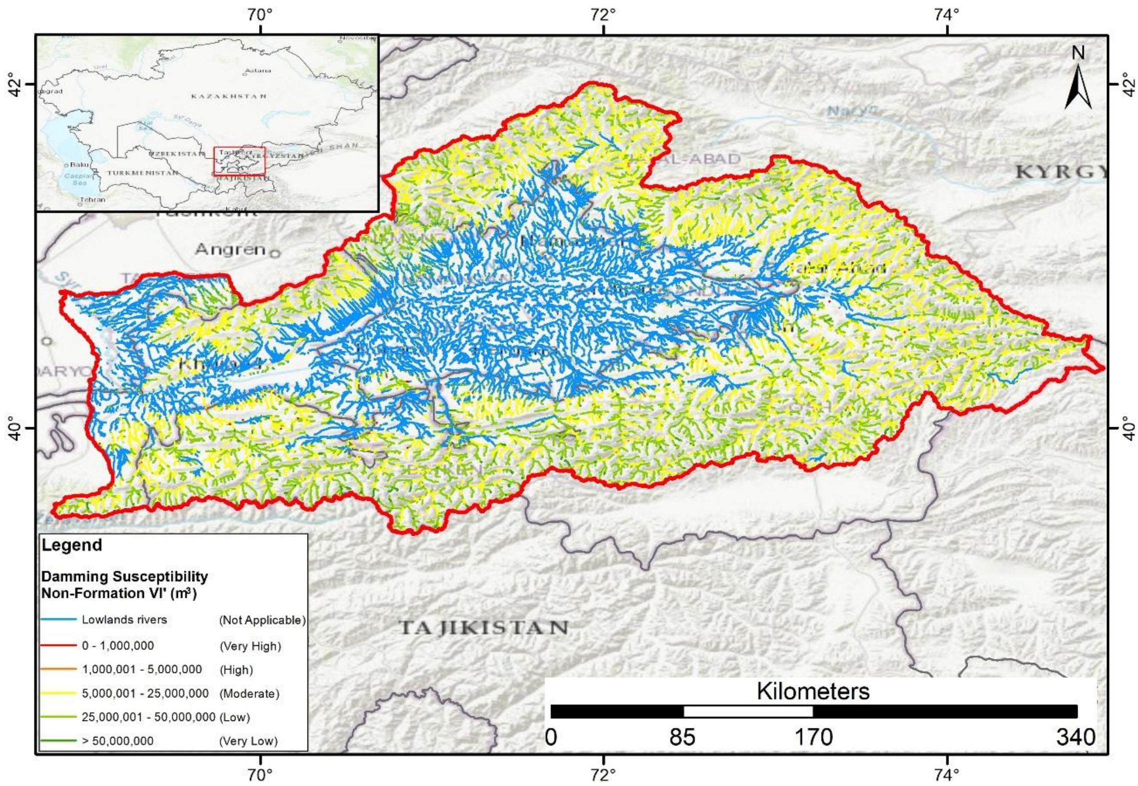

Figure 82. Damming Susceptibility Map of Non-Formation of river stretches by new landslides in the Fergana valley and the surrounding mountainous rim.

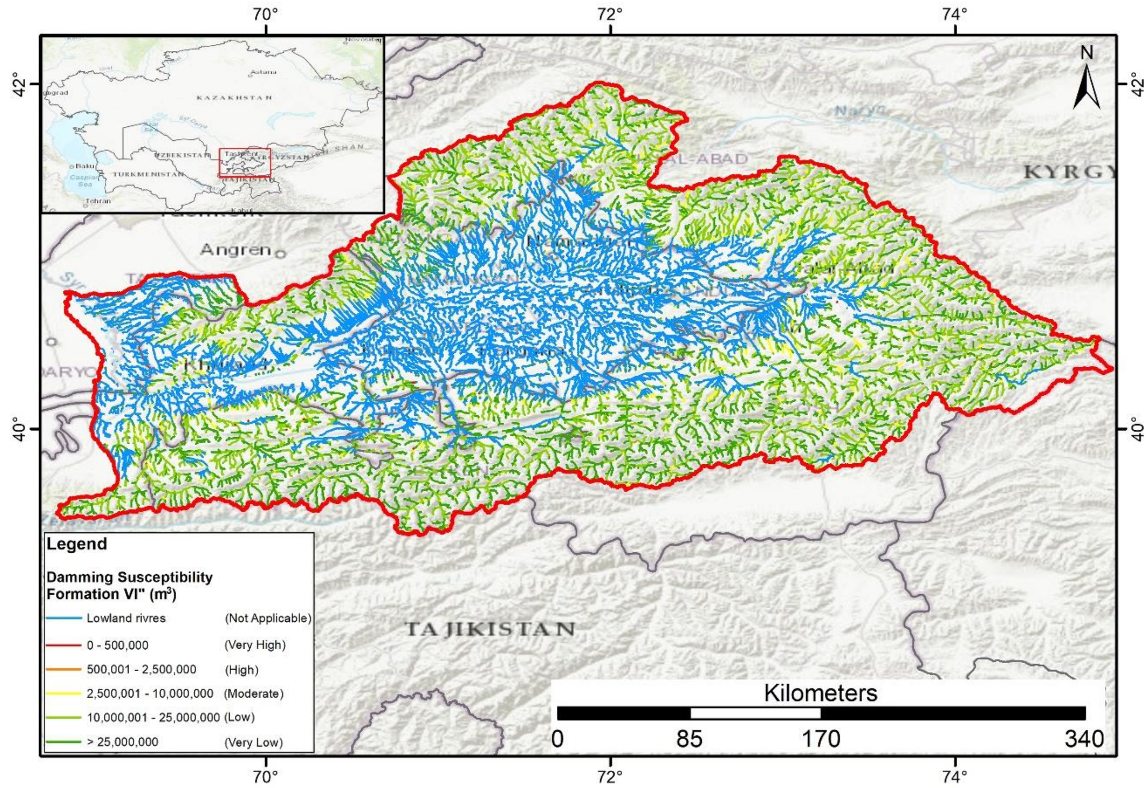

Figure 83. Damming Susceptibility Map of Formation of river stretches by new landslides in the Fergana valley.

7 Challenges, limitations, and future perspectives

Landslide susceptibility

Statistical-probabilistic models for landslide susceptibility can overcome the data gaps and allow to analyse very wide areas (from basin to national scales), by adopting a homogeneous methodology and a harmonized dataset (including global and local data sources). Landslide susceptibility maps provide landslide scientists, practitioners, and administrators with powerful tools for land use-planning and risk reduction strategies. However, landslide hazard assessment is a complex process since it needs accurate knowledge of the topic and appropriate input data (historical inventories).

The main issue affecting the used random forest model is the need of an adequate training dataset to properly calibrate the predictor model. The first step of the work has been the homogenization of the landslide data. The used landslide inventory was created starting from different sources, hence, with quite non-homogeneous data (e.g., in some cases the whole landslide perimeter was available, in other cases only a point representing the source area of each landslide was provided, without information about the landslide dimension or propagation distance; more in general there were few or no data about the landslide type or triggering causes). The lack of some data about the landslides, or the partial or complete lack of landslides as in Kazakhstan and Turkmenistan, could lead to underestimate the real landslide hazard of the studied countries, since some points could have been wrongly classified (e.g., they have been considered as no landslide areas, but it was possible that a not reported landslide was present). Furthermore, the general absence of information about the landslide types led to the creation of a general landslide susceptibility map, where all the types of landslides are considered. The created maps have been validated only using the available landslide dataset, providing good results and highlighting the good prediction capability of the model. Anyway, an in-situ validation in some sample areas can help to verify the quality of the results.

Landslide susceptibility and elements at risk

The obtained results are greatly influenced by the input data (i.e., the susceptibility maps and the elements at risk databases). The buffering procedures on roads and railways had surely overestimated or underestimated the susceptibility distribution in some cases, likewise the analysis at 1-km^2 resolution on population and buildings led to an exaggeration in the assessment of elements distribution in each class of landslide susceptibility. Nevertheless, the adopted approaches represented the only way to obtain an analysis as much accurate as possible with respect to the input databases. In this perspective, the detail of analyses could be improved focusing both on the refinement of the analysis resolution (e.g., population and buildings) and on the elements at risk that are not located in flat areas, where the landslide susceptibility is surely 0 or NULL.

Landslide river damming

The main issue encountered was the extremely wide study area, the amount of data and the processing time required. The adopted mapping methodology, based on the MOI equations, was originally designed to assess the damming susceptibility at basin/regional scale (Tacconi Stefanelli et al., 2016), where the morphological parameters must be found to have the correct river width required in the MOI equations. Although the best results with this method are obtained at basin scale, this time-consuming phase have been optimized to be applied to such a large area changing the working area from basin to national scale and combining the results into the whole Central Asia territory.

Furthermore, the results quality is directly proportional to the resolution of the input DEM, which on the other hand is inversely proportional to the processing time. A further criticality of this process is the reliability on the landslides volumes assessment method, since a higher quality of landslides data (sliding geometry and depth) allows a more accurate volume calculation and therefore a better final result.

Case studies

The assessment of landslide scenarios in Central Asia is particularly complex, due to the heterogeneity of the geomorphological and geological background, which generates different landslide phenomena. In this context the anthropic pressure can only exacerbate the landslide hazard. The reported case studies represent an attempt to evaluate landslide scenarios in Central Asia: more landslide data (e.g., type, area, volume, state of activity, displacement, geotechnical characteristics of the involved material) should be collected in collaboration with local experts. The methods presented here serve as examples as to the application of earth observation to assess landslide hazard and risk across large-scale areas, to complement site-specific research, and inform national and regional level risk management.

References

Abdrakhmatov, K., Havenith, H.B., Delvaux, D., Jongmans, D., Trefois, P. (2003) Probabilistic PGA and Arias Intensity Maps of Kyrgyz Republic (Central Asia). J. Seismol.

Akgun, A. A comparison of landslide susceptibility maps produced by logistic regression, multi-criteria decision, and likelihood ratio methods: A case study at İzmir, Turkey. Landslides 2012, 9, 93–106.

Aleshin, Y., and Torgoev, I. (2014). Slope Dynamic Geomorphology of the Mailuu-Suu Area, Aspects of Long-Term Prediction. In Landslide Science for a Safer Geoenvironment (pp. 339-343). Springer, Cham.

Banerjee, P. and Ghose, M. K. Spatial analysis of environmental impacts of highway projects with special emphasis on mountainous area: an overview. Impact Assessment & Project Appraisal 1–15 (2016).

Behling, R., Roessner, S., Golovko, D., Kleinschmit, B., 2016. Derivation of long-term spatiotemporal landslide activity—A multi-sensor time series approach. Remote Sens. Environ. 186, 88–104.

Behling, R., Roessner, S., Kaufmann, H., Kleinschmit, B., 2014. Automated spatiotemporal landslide mapping over large areas using rapideye time series data. Remote Sens. 6, 8026–8055.

Behling, Robert; Roessner, Sigrid (2020): Multi-temporal landslide inventory for a study area in Southern Kyrgyz Republic derived from RapidEye satellite time series data (2009 – 2013). V. 1.0. GFZ Data Services. https://doi.org/10.5880/GFZ.1.4.2020.001

Brabb, E. E.: Innovative approaches to landslide hazard mapping, in: Proceedings 4th International Symposium on Landslides, Toronto, 1, 307–324, 1984.

Breiman, L. Random forests. Mach. Learn. 2001, 45, 5–32.

Brenning, A. Spatial prediction models for landslide hazards: Review, comparison and evaluation. Nat. Hazard Earth Syst. 2005, 5, 853–862.

CAC DRMI (Central Asia and Caucasus Disaster Risk Management Initiative). 2009. Risk assessment for Central Asia and Caucasus: desk study review.

Carrara, A. Multivariate models for landslide hazard evaluation. J. Int. Assoc. Math. Geol. 1983, 15, 403–426.

Casagli, N., Catani, F., 2020. Sviluppo della conoscenza e supporto tecnico scientifico per la valutazione degli scenari di pericolosità idrogeologica e vulcanica.

Catani, F., Casagli, N., Ermini, L., Righini, G., Menduni, G., 2005. Landslide hazard and risk mapping at catchment scale in the Arno River basin. Landslides 2, 329–342.

Catani, F., Lagomarsino, D., Segoni, S., Tofani, V., 2013. Landslide susceptibility estimation by random forests technique: sensitivity and scaling issues. Nat. Hazards Earth Syst. Sci. 13, 2815.

Cascini L. (2008) - Applicability of landslide susceptibility and hazard zoning at different scales. Eng. Geol., 102 (3-4):164–177.

Corominas J., Copons R., Vilaplana J.M., Altimir J. and Amigó J. (2003) - Integrated landslide susceptibility analysis and hazard assessment in the principality of Andorra. Nat. Hazards, 30 (3): 421–435.

Chen L., Van Westen C.J., Hussin H., Ciurean R.L., Turkington T., Chavarro-Rincon D. and Shrestha, D.P. (2016) - Integrating expert opinion with modelling for quantitative multi-hazard risk assessment in the Eastern Italian Alps. Geomorphology, 273 (15):150–167.

Daniell J.E., Schaefer A.M. [2014] "Eastern Europe and Central Asia Risk Profiling for Earthquakes", World Bank ECA Region Office, Washington D.C., USA.

Duman, T.Y.; Can, T.; Gokceoglu, C.; Sonmez, H. Application of logistic regression for landslide susceptibility zoning of Cekmece Area, Istanbul, Turkey. Environ. Geol. 2006, 51, 241–256.

Emberson, R., D. Kirschbaum, and T. Stanley. 2020. "New global characterisation of landslide exposure." Natural Hazards and Earth System Sciences, 20 (12): 3413-3424. doi:10.5194/nhess-20-3413-2020

Ermini, L.; Catani, F.; Casagli, N. Artificial Neural Networks applied to landslide susceptibility assessment. Geomorphology 2005, 66, 327–343.

Erokhin, S. A., Zaginaev, V. V., Meleshko, A. A., Ruiz-Villanueva, V., Petrakov, D. A., Chernomorets, S. S., Viskhadzhieva, K., D., Tutubalina O., V. and Stoffel, M. (2018). Debris flows triggered from non-stationary glacier lake outbursts: the case of the Teztor Lake complex (Northern Tian Shan, Kyrgyzstan). Landslides, 15(1), 83-98.

ESCAP, 2019. Population Data Sheet.

European Commission Humanitarian Aid, Civil Protection, U.N.I.S. for D.R.R., 2006. Disaster Risk Reduction 20 Examples of Good Practice From Central Asia.

Galitzin, B. (1915). On the earthquake of 18th February 1911. Proc. Imperial Acad. Sci. Ser. VI, 9(10), 991-998.

GFDRR (Global Facility for Disaster Reduction and Recovery), 2009. Disaster Risk Management Notes for Priority Countries 2009-2015. Eur. Asia 48–49.

GFDRR (Global Facility for Disaster Reduction and Recovery), 2016. Europe and Central Asia-Country Risk Profiles for Floods and Earthquakes. 144 pg.

Giorgio, H.-Ö., Markus, K., Wolfhart, P., Nedim, R. (2015) The "Tektonik" Landslide at Mailuu Suu, Kyrgyz Republic. In Engineering Geology for Society and Territory—Volume 2; Springer International Publishing: Cham, Switherland, 2015; Volume 2, pp. 1055–1059.

Golovko, 2015. Development of multi-temporal landslide inventory information system for southern Kyrgyz Republic using GIS and satellite remote sensing. PFG 2015, 157–172.

Guzzetti F., Ardizzone F., Cardinali M., Rossi M., Valigi D. (2009) Landslide volumes and landslide mobilization rates in Umbria, central Italy, Earth and Planetary Science Letters, vol. 279, 222–229.

Havenith, H. B., Strom, A., Jongmans, D., Abdrakhmatov, A., Delvaux, D., and Tréfois, P. (2003). Seismic triggering of landslides, Part A: Field evidence from the Northern Tien Shan. Natural Hazards and Earth System Sciences, 3(1/2), 135-149.

Havenith, H.B., Strom, A., Cacerez, F., Pirard, E., 2006a. Analysis of landslide susceptibility in the Suusamyr region, Tien Shan: statistical and geotechnical approach. Landslides 3, 39–50.

Havenith, H.B., Torgoev, I., Meleshko, A., Alioshin, Y., Torgoev, A., Danneels, G., 2006b. Landslides in the Mailuu-Suu Valley, Kyrgyz Republic—hazards and impacts. Landslides 3, 137–147.

Havenith, H.B., Strom, A., Torgoev, I., Torgoev, A., Lamair, L., Ischuk, A., Abdrakhmatov, K., 2015a. Tien Shan geohazards database: Earthquakes and landslides. Geomorphology 249, 16–31.

Havenith, H.B., Torgoev, A., Schlögel, R., Braun, A., Torgoev, I., Ischuk, A., 2015b. Tien Shan geohazards database: Landslide susceptibility analysis. Geomorphology 249, 32–43.

Havenith, H. B., Torgoev, A., Braun, A., Schlögel, R., and Micu, M. (2016). A new classification of earthquake-induced landslide event sizes based on seismotectonic, topographic, climatic and geologic factors. Geoenvironmental Disasters, 1(3), 1-24.

Havenith, H.B.B., Umaraliev, R., Schlögel, R., Torgoev, I., Ruslan, U., Schlogel, R., Torgoev, I. (2017) Past and Potential Future Socioeconomic Impacts of Environmental Hazards in Kyrgyz Republic. In Kyrgyz Republic: Political, Economic and Social Issues; Olivier, A.P., Ed.; Nova Science Publishers, Inc.: Hauppauge, NY, USA; pp. 63–113.

Hong, Y., Adler, R., and Huffman, G. 2007, Use of satellite remote sensing data in the mapping of global landslide susceptibility. Nat. Hazards, 43, 23–44.

Hungr, O., and Evans, S. G. (2004). Entrainment of debris in rock avalanches: an analysis of a long run-out mechanism. Geological Society of America Bulletin, 116(9-10), 1240-1252.

Ishihara, K., Okusa, S., Oyagi, N., and Ischuk, A. (1990). Liquefaction-induced flow slide in the collapsible loess deposit in Soviet Tajik. Soils and foundations, 30(4), 73-89.

Ischuk, A. R. (2006). Usoy natural dam: Problem of security; Lake Sarez, Pamir Mountains, Tadjikistan. Italian Journal of Engineering Geology and the Environment, (special issue 1), 189-192.

Juliev, M., Pulatov, A., and Hubl, J. (2017). Natural hazards in mountain regions of Uzbekistan: A review of mass movement processes in Tashkent province. International Journal of Scientific and Engineering Research, 8(2), 1102.

Kalmetieva, Z.A., Mikolaichuk, A. V, Moldobekov, B.D., Meleshko, A. V, Janaev, M.M., Zubovich, A. V, 2009. Atlas of earthquakes in Kyrgyz Republic.

Kirschbaum, D., Stanley, T., and Zhou, Y. (2015). Spatial and temporal analysis of a global landslide catalog. Geomorphology, 249, 4-15.

Kulikova, G., Schurr, B., Krüger, F., Brzoska, E., and Heimann, S. (2016). Source parameters of the Sarez-Pamir earthquake of 1911 February 18. Geophysical Journal International, 205(2), 1086-1098.

Kazakov N. 2004 Russian Geologists on Lake Sarez A collection of the publications related to the lake Sarez and Usoy avalanche. Available at: http://www.nikzdaru.com/, last accessed 21 January 2022

Lagomarsino, D.; Tofani, V.; Segoni, S.; Catani, F.; Casagli, N. A tool for classification and regression using random forest methodology: Applications to landslide susceptibility mapping and soil thickness modeling. Environ. Model. Assess. 2017, 22, 201–214.

Li, F., Torgoev, I., Zaredinov, D., Li, M., Talipov, B., Belousova, A., Kunze, C., Schneider, P. (2021) Influence of Earthquakes on Landslide Susceptibility in a Seismic Prone Catchment in Central Asia. Appl Sci, 11, 3768.

Lee, S. Application of logistic regression model and its validation for landslide susceptibility mapping using GIS and remote sensing data. Int. J. Remote Sens. 2005, 26, 1477–1491.

Manzo, G.; Tofani, V.; Segoni, S.; Battistini, A.; Catani, F. GIS techniques for regional-scale landslide susceptibility assessment: The Sicily (Italy) case study. Int. J. Geogr. Inf. Sci. 2013, 27, 1433–1452.

Medeu, A. R., and Blagovechshenskiy, A. R. Seismogenic landslide risk zoning in the surrounding areas of Almaty City, Kazakhstan. Vestnick, 6, 121.

Mohadjer, S., Ehlers, T.A., Bendick, R., Stübner, K., Strube, T., 2016. A Quaternary fault database for central Asia. Nat. Hazards Earth Syst. Sci. 16, 529–542. https://doi.org/10.5194/nhess-16-529-2016

Nadim, F., Kjekstad, O., Peduzzi, P., Herold, C., and Jaedicke, C. (2006). Global landslide and avalanche hotspots. Landslides, 3(2), 159-173.

Niyazov, R. A., and Nurtaev, B. S. (2013). Evaluation of Landslides in Uzebekistan Caused by the Joint Impact of Precipitation and Deep-focus Pamir-Hindu Earthquakes. In Landslides: Global Risk Preparedness (pp. 253-265). Springer, Berlin, Heidelberg.

Niyazov R.A. (2020). Uzbekistan landslides, Uzbekistan landslide service, Technical report.

Niyazov, R., Nurtaev, B., Bimurzaev, G., and Tashpulatov, M. (2020b, November). Flow Slides in Uzbekistan: Overview and Case Studies. In Workshop on World Landslide Forum (pp. 59-65). Springer, Cham.

Oldham, R.D., 1923. The Pamir Earthquake of 18th February, 1911. Q. J. Geol. Soc. 79, 237–245. https://doi.org/10.1144/GSL.JGS.1923.079.01-04.15

Piroton, V., Schlögel, R., Barbier, C., Havenith, H.B. (2020) Monitoring the recent activity of landslides in the Mailuu-suu valley (Kyrgyz Republic) using radar and optical remote sensing techniques. Geosciences, 10 (5), p. 164

Pittore, Massimiliano; Ozturk, Ugur; Moldobekov, Bolot; Saponaro, A., 2018. EMCA landslide catalog Central Asia.

Pollner, J., Kryspin-Watson, J., Nieuwejaar, S., 2010. Disaster Risk Management and Climate Change Adaptation in Europe and Central Asia. World Bank 1–53.

Pusch, C., 2004. A comprehensive risk management framework for Europe and Central Asia. Disaster.

Preobrazhenskiy, I. A. (1915). Usoy Avalanche.

Reichenbach, P.; Rossi, M.; Malamud, B.D.; Mihir, M.; Guzzetti, F. A review of statistically-based landslide susceptibility models. Earth Sci. Rev. 2018, 180, 60–91.

Roessner, S., H.-U. Wetzel, H. Kaufmann, W. Kornus, M. Lehner, P. Reinartz and R. Mueller, (2000), "Landslide Investigations in Southern Kyrgyz Republic Based on a Digital Elevation Model Derived from MOMS-2P Data," IAPRS, Vol. 33, Part B7, Amsterdam, pp. 1259 -1266.

Roessner, S. Wetzel, H.-U. Kaufmann, H. Sarnagoev, A. (2004), "Satellite Remote Sensing and GIS Based Analysis of Large Landslides in Southern Kyrgyz Republic NATO Advanced Research Workshop: Security of Natural and Artificial Rockslide Dams", Bishkek, Kyrgyz Republic 2004.

Roessner, S. Wetzel, H.-U. Kaufmann, H. Sarnagoev, A. (2005), "Potential of Satellite Remote Sensing and GIS for Landslide Hazard Assessment in Southern Kyrgyz Republic (Central Asia)", Natural Hazards, Vol. 35, No. 3, pp. 395 -416.

Saponaro, A., Pilz, M., Wieland, M., Bindi, D., Moldobekov, B., Parolai, S., 2014. Landslide susceptibility analysis in data-scarce regions: the case of Kyrgyz Republic. Bull. Eng. Geol.

Environ. 74, 1117–1136.

Saponaro, A., Pilz, M., Bindi, D., and Parolai, S. (2015). The contribution of EMCA to landslide susceptibility mapping in Central Asia. Annals of Geophysics, 58(1).

Schlögel, R., Torgoev, I., De, Marneffe, C., Havenith, H.B. (2011) Evidence of a changing size-frequency distribution of landslides in the Kyrgyz Tien Shan, Central Asia. Earth Surf Process Landf 36(12):1658– 1669. doi:10.1002/esp.2184

Segoni S., Tofani V., Rosi A., Catani F. and Casagli N. (2018) - Combination of rainfall thresholds and susceptibility maps for dynamic landslide hazardassessment at regional scale. Front Earth Sci., 6: 85.

Seutloali, K. E. and Beckedahl, H. R. A review of road-related soil erosion: an assessment of causes, evaluation techniques and available control measures. Earth Sciences Research Journal 19(1), 73–80 (2015).

Sidle, R. C., Furuichi, T. and Kono, Y. Unprecedented rates of landslide and surface erosion along a newly constructed road in Yunnan, China. Natural Hazards 57(2), 313–326 (2011).

Stanley, T., Kirschbaum, D.B., 2017. A heuristic approach to global landslide susceptibility mapping. Nat. Hazards 87, 145–164. https://doi.org/10.1007/s11069-017-2757-y

Sternberg R., 2006. Damming a river: a changing perspective on altering nature. Renewable Sustainable Energy Rev 10:165–197

Strom, A.L., Korup, O., 2006. Extremely large rockslides and rock avalanches in the Tien Shan, Kyrgyz Republic. Landslides 3, 125–136.

Strom, A. (2010). Landslide dams in Central Asia region. Journal of the Japan Landslide Society, 47(6), 309-324.

Strom, A., Abdrakhmatov, K., 2017. Large-Scale Rockslide Inventories: From the Kokomeren River Basin to the Entire Central Asia Region (WCoE 2014–2017, IPL-106-2, in: Workshop on World Landslide Forum. Springer, Cham, pp. 339–346.

Strom, A., Abdrakhmatov. K., 2018. Rockslides and rock avalanches of Central Asia: distribution, morphology, and internal structure. Elsevier, 441pg. ISBN: 978-0-12-803204-6.

Styron, R., and Pagani. M. 2020 "The GEM Global Active Faults Database." Earthquake Spectra, vol. 36, no. 1_suppl, Oct. 2020, pp. 160–180, doi:10.1177/8755293020944182.

Swanson FJ, Oyagi N, Tominaga M (1986). Landslide dams in Japan. In: Schuster RL (ed) Landslide dams: processes, risk and mitigation. Geotech Sp, vol 3. ASCE, New York, pp 131–145.

Tacconi Stefanelli C, Segoni S, Casagli N, Catani F (2016). Geomorphic indexing of landslide dams evolution. Eng Geol 208, 1–10. https://doi.org/10.1016/j.enggeo.2016.04.024.

Tacconi Stefanelli, C., Vilímek, V., Emmer, A., and Catani, F. (2018). Morphological analysis and features of the landslide dams in the Cordillera Blanca, Peru. Landslides, 15(3), 507-521.

Tacconi Stefanelli, C., Casagli, N., Catani, F., 2020. Landslide damming hazard susceptibility maps: a new GIS-based procedure for risk management. Landslides 1–14.

Thurman, M., 2011. Natural Disaster Risks in Central Asia: A Synthesis. UNDP BCPR.

Tiranti D., Nicolò G. and Gaeta A.R. (2019) - Shallow landslides predisposing and triggering factors in developing a regional early warning system. Landslides 16 (2): 235–251.

Torgoev, I., Abdrakhmatov, K., Kasymbek, S.U., Strom, A.L., Kristekova, M., Havenith, H., Korup,

O. (2012) Prevention of Landslide Dam Disasters in the Tien Shan, Kyrgyz Republic; NATO: Brussels, Belgium.

Trigila, A., Frattini, P., Casagli, N., Catani, F., Crosta, G., Esposito, C., Spizzichino, D., 2013. Landslide susceptibility mapping at national scale: the Italian case study, in: Landslide Science and Practice. Springer, Berlin, Heidelberg, pp. 287–295.

United Nations (UN) 2007. Dam Safety in Central Asia: capacity building and regional cooperation.

UN ISDR (United Nations International Strategy for Disaster Reduction) 2009. Risk assessment for Central Asia and Caucasus: desk study review, CAC DRMI 2009, Risk Management Working Paper Series No. 9. The World Bank.

Vandenhove, H.; Quarch, H.; Sweeck, L.; Sillen, X.; Mallants, D. Remediation of Uranium Mining and Milling Tailing in Mailuu-Suu District of Kyrgyz Republic; Tacis Project N_ SCRE1/N_38; SCK CEN: Mol, Belgium, 2003.

Wood J (2009). Geomorphometry in LandSerf. In: Hengl, T. and Reuter, H.I. [Eds.]: Geomorphometry: Concepts, Software, Applications. Dev Soil Sci, Elsevier, Vol.33, 333-349.

World Bank (WB) 2006. Natural Disaster Hotspots: Case Studies. Disaster Risk Management Series No. 6.

World Bank (WB) 2008. Investigation and Analysis of Natural Hazard Impacts on Linear Infrastructure in Southern Kyrgyz Republic Desk and Field Studies Report. Report 68669

World Bank, 2020. The Global Landslide Hazard Map: Final Project Report. Appendix A.

World Bank and Global Facility for Disaster Risk Reduction, 2021. Assessment of economic impacts from disasters along key corridors: Final report, May 2021.

Yaning, C. (1992). Landslide-debris flow and its prevention in Kazakhstan. Arid Land Geography.

Yilmaz I. (2009) - Landslide susceptibility mapping using frequency ratio, logistic regression, artificial neural networks and their comparison: a case study from Kat landslides (Tokat—Turkey). Computers and Geosciences, 35 (6): 1125-1138.

Yue, J., Tian, J., Tian, Q., Xu, K., and Xu, N. (2019). Development of soil moisture indices from differences in water absorption between shortwave-infrared bands. ISPRS Journal of Photogrammetry and Remote Sensing, 154, 216-230.

Zhao, Y., Huang, Y., Liu, H., Wei, Y., Lin, Q., and Lu, Y. (2018). Use of the Normalized Difference Road Landside Index (NDRLI)-based method for the quick delineation of road-induced landslides. Scientific reports, 8(1), 1-10.

Ниязов Р.А. (2009) Оползни Узбекистана (тенденции развития на рубеже XXI века). Ташкент: ГИДРОИНГЕО, 208 с.

Шпилько Г.А. (1914). Землетрясение 1911 года на Памирах и его последствия. Изв Туркест. ОРГО, т. X, вып. I.

Щеко А.И., Лехантинов А.М. (1970). Современное состояние Усойского завала и задачи дальнейших исследований // Мат-лы науч.-техн. совещ. по вопросам методики изучения и прогноза селей, обвалов и оползней, Душанбе, С. 219-223.

Appendix A - List of acronyms

AFEAD: Active Fault for Eurasia and Adjacent regions

AUC: Area Under Curve

BMBF: German Federal Ministry of Research and Technology (German: Bundesministerium für Bildung und Forschung)

CA: Central Asia

CAC DRMI: Central Asia and Caucasus Disaster Risk Management Initiative

CAIAG: Central Asian Institute for Applied Geosciences

CSF: Cutslope Failure

DEM: Digital Elevation Model

DSM: Digital Soil Map

DSMW: Digital Soil Map of the World

DTM: Digital Terrain Model

EMCA: Earthquake Model of Central Asia

EO: Earth Observation

ESA: European Space Agency

ESRI: Environmental System Research Institute

FN: False Negative

FP: False Positive

FSF: Fillslope Failure

GDP: Gross Domestic Product

GE: Google Earth

GEP: Geohazard Exploitation Platform

GFDRR: Global Facility for Disaster Reduction and Recovery

GIS: Geographic Information System

GLC: Global Landslide Catalog

GLOF: Glacial lakes outburst flood

GPP: Gravitational Process Path model

HECCA: Harmonized Catalogue for Central Asia

IPL: International Programme on Landslides

IS: Institute of Seismology

ISASUZ: Institute of Seismology of the Academy of Science of Uzbekistan

ISDR: International Strategy for Disaster Reduction

ISNASKR: Institute of Seismology of Kyrgyz Republic

IWPHE: Institute of Water Problems, Hydropower Engineering and Ecology

LADATSHA: Landslide Dam disasters in the Tien Shan

LOS: Line of Sight

LSM: Landslide susceptibility map

MAP: Mean Annual Precipitation

MERIT: Multi-Error-Removed Improved-Terrain

MOI: Morphological Obstruction Index

MPs: Measurement Points

NASA: National Aeronautics and Space Administration

NATO: North Atlantic Treaty Organization

NE: Northeast

NSDSI: Normalized Shortwave-infrared Difference SM Indices

NW: Northwest

OGS: Istituto Nazionale di Oceanografia e di Geofisica Sperimentale

OOBE: Out-of-Bag Error

OSM: Open Street Map

PGA: Peak Ground Acceleration

PROGRESS: Potsdam Research Cluster for Georisk Analysis, Environmental Change and Sustainability

QGIS: Quantum GIS

RED: Risk Engineering + Development

RF: Random Forest

ROC: Receiver Operating Characteristic

SAGA GIS: System for Automated Geoscientific Analyses GIS

SAR: Synthetic Aperture Radar

SBAS: Small BAseline Subset

SE: Southeast

SFRARR: Strengthening Financial Resilience and Accelerating Risk Reduction in Central Asia

SPI: Stream Power Index

SRTM: Shuttle Radar Topography Mission

SWIR: Shortwave-Infrared

TIPTIMON: Tian Shan-Pamir Monitoring Program

TN: True Negative

TP: True Positive

TPI: Topographic Position Index

TS: Time Series

TSTU: Tashkent State Transport University (former TashIIT)

TWI: Topographic Wetness Index

UN: United Nations

UNESCO: United Nations Educational, Scientific and Cultural Organization

USD: United States Dollar

USGS: United States Geological Survey

WB: World Bank